

**Q-SWITCHED AND MODE-LOCKED PULSE
GENERATION WITH ORGANIC DYES BASED
SATURABLE ABSORBER**

RAWAN M S SOBOH

**FACULTY OF ENGINEERING
UNIVERSITY OF MALAYA
KUALA LUMPUR**

2021

**Q-SWITCHED AND MODE-LOCKED PULSE
GENERATION WITH ORGANIC DYES BASED
SATURABLE ABSORBER**

RAWAN M S SOBOH

**THESIS SUBMITTED IN FULFILMENT OF THE
REQUIREMENTS FOR THE DEGREE OF DOCTOR OF
PHILOSOPHY**

**FACULTY OF ENGINEERING
UNIVERSITY OF MALAYA
KUALA LUMPUR**

2021

UNIVERSITY OF MALAYA
ORIGINAL LITERARY WORK DECLARATION

Name of Candidate: Rawan M S Soboh

Matric No: KVA180072

Name of Degree: Doctor of Philosophy

Title of Thesis (“this Work”): Q-Switched and Mode-Locked Pulse Generation
With Organic Dyes Based Saturable Absorber

Field of Study: Photonic (Electronics and Automation)

I do solemnly and sincerely declare that:

- (1) I am the sole author/writer of this Work;
- (2) This Work is original;
- (3) Any use of any work in which copyright exists was done by way of fair dealing and for permitted purposes and any excerpt or extract from, or reference to or reproduction of any copyright work has been disclosed expressly and sufficiently and the title of the Work and its authorship have been acknowledged in this Work;
- (4) I do not have any actual knowledge nor do I ought reasonably to know that the making of this work constitutes an infringement of any copyright work;
- (5) I hereby assign all and every rights in the copyright to this Work to the University of Malaya (“UM”), who henceforth shall be owner of the copyright in this Work and that any reproduction or use in any form or by any means whatsoever is prohibited without the written consent of UM having been first had and obtained;
- (6) I am fully aware that if in the course of making this Work I have infringed any copyright whether intentionally or otherwise, I may be subject to legal action or any other action as may be determined by UM.

Candidate’s Signature

Date: 23/8/2021

Subscribed and solemnly declared before,

Witness’s Signature

Date: 23/8/2021

Name:

Designation:

Q-SWITCHED AND MODE-LOCKED PULSE GENERATION WITH ORGANIC DYES BASED SATURABLE ABSORBER

ABSTRACT

The manifold applications of pulsed fiber lasers are an evidence of the importance of laser technology in science and engineering. Saturable absorbers (SA) play a key role in the generation of pulsed laser, whether passive Q-switched or passive mode-locked, without using the modulators. In this thesis, two saturable absorbers (SAs) based on organic materials were fabricated, characterized, and successfully incorporated into the erbium-doped fiber laser (EDFL) and the Ytterbium-doped fiber laser (YDFL) cavities to produce both Q-switched and mode-locked pulsed lasers. Zinc Phthalocyanine (ZnPc) SAs were constructed in three different ways; by embedding ZnPC in the polyvinyl alcohol (PVA) film to obtain embedded ZnPc:PVA, by casting ZnPC onto the PVA film to get casted ZnPc/PVA, and by spin-coating ZnPc onto the film to produce spin-coated ZnPc:PVA. The three samples of the ZnPc-SA were inserted one by one between the two fiber ferrules to form a fiber compatible Q-switch, and were placed in an EDFL cavity. Stable Q-switched pulse trains operating at the central wavelengths of 1561.4 nm, 1560.4 nm, and 1559.5 nm were produced by the SAs formed from embedded ZnPc:PVA, casted ZnPc/PVA, and spin-coated ZnPc/PVA thin films, respectively. The maximum achieved pulse energies for these Q-switched laser pulses were 71 nJ, 32 nJ, and 50 nJ. For Q-switched operation in the EDFL cavity, the shortest pulse width was 3.6 μ s and the maximum repetition rate was 48 kHz, obtained with the use of the embedded ZnPc:PVA SA. By integrating the fabricated ZnPc:PVA SA inside the ring cavity, soliton EDFL mode-locked pulses with a pulse width of 1.83 ps, pulse energy of 2.1 nJ, and a peak power of 1.15 kW were also obtained. When the ZnPc:PVA SA was placed in a YDFL cavity, Q-switched pulses were generated with the minimum pulse width of 2.2 μ s,

maximum repetition rate of 63 kHz, pulse energy of 91 nJ, and an average output power of 5.7 mW. In addition, successful generation of mode locked YDFL pulses using the ZnPc/PVA SA, at a fixed repetition rate of 3.3 MHz with a picosecond pulse width, were also demonstrated. The highest pulse energy for mode locked YDFL by using ZnPc/PVA SA was 1.36 nJ. Finally, an SA made of a lawsone film was successfully prepared and tested in generating a passive Q-switched EDFL, realizing the highest pulse energy of 53.7 nJ and the shortest pulse width of 1.7 μ s. The results indicate that both ZnPc and Lawsone thin films have great potential as alternative SA materials for Q-switched and mode-locked pulse generation.

Keywords: Q-switch, Mode-lock, Saturable Absorber, Organic optical material, Erbium doped fiber laser, Ytterbium-doped fiber laser.

Q-SWITCHED DAN MODE-LOCKED PULSE GENERATION DENGAN PEWARNA ORGANIK BERASASKAN PENYELESAIAN

ABSTRAK

Laser serat berdenyut telah diaplikasi di pelbagai tempat dan ini membuktikan kepentingan teknologi laser dalam sains dan kejuruteraan. Penyerap tepu (SA) memainkan peranan penting dalam penghasilan laser berdenyut, sama ada secara pasif Q-switched atau pasif mode-lock, tanpa menggunakan modulator. Dalam tesis ini, dua penyerap tepu berdasarkan bahan organik dibuat, dicirikan, dan berjaya dimasukkan ke dalam rongga laser serat erbium (EDFL) dan rongga laser serat Ytterbium (YDFL) untuk menghasilkan kedua-dua Q-switched dan laser berdenyut mod-terkunci. Zinc Phthalocyanine (ZnPc) SA dibina dalam tiga cara yang berbeza - dengan memasukkan ZnPC ke dalam polivinil alkohol (PVA) to lm untuk mendapatkan ZnPc: PVA tertanam, dengan membuang ZnPC ke filem PVA untuk mendapatkan cast ZnPc / PVA, dan dengan lapisan berputar ZnPc ke filem untuk menghasilkan ZnPc: PVA bersalut berputar. Ketiga-tiga sampel ZnPc-SA dimasukkan satu demi satu di antara dua serat serat untuk membentuk suis Q yang serat, dan ditempatkan dalam rongga EDFL. Kereta api nadi Q-switched stabil yang beroperasi pada panjang gelombang pusat 1561.4 nm, 1560.4 nm, dan 1559.5 nm dihasilkan oleh SA yang terbentuk dari ZnPc: PVA, ZnPc / PVA yang dilekatkan, dan filem nipis ZnPc / PVA yang dilapisi putaran, masing-masing. Tenaga nadi maksimum yang sesuai untuk ketiga SA adalah 71 nJ, 32 nJ, dan 50 nJ. Untuk operasi Q-switched di rongga EDFL, lebar nadi terpendek adalah 3.6 μ s dan kadar pengulangan maksimum adalah 48 kHz, diperoleh dengan penggunaan ZnPc: PVA SA yang tertanam. Dengan menyatukan fabrikasi ZnPc: PVA SA di dalam rongga cincin, pulsa terkunci mod EDFL soliton dengan lebar nadi 1.83 ps, tenaga nadi 2.1 nJ, dan daya puncak 1.15 kW juga diperoleh. Apabila ZnPc: PVA SA diletakkan di rongga YDFL, denyutan Q-

switched dihasilkan dengan lebar denyut minimum $2.2 \mu\text{s}$, kadar pengulangan maksimum 63 kHz, tenaga nadi 91 nJ, dan daya output purata 5.7 mW. Di samping itu, kejayaan menghasilkan denyut YDFL terkunci mod menggunakan ZnPc / PVA SA, pada kadar pengulangan tetap 3.3 MHz dengan lebar nadi picosecond, juga ditunjukkan. Tenaga nadi tertinggi ialah 1.36 nJ. Akhirnya, SA yang diperbuat daripada filem lawas berjaya disiapkan dan diuji dalam menghasilkan EDFL berpindah Q pasif, menyedari tenaga nadi tertinggi 53.7 nJ dan lebar nadi terpendek $1.7 \mu\text{s}$. Hasilnya menunjukkan bahawa kedua-dua filem nipis ZnPc dan Lawsonsone berpotensi besar sebagai bahan SA alternatif untuk penjanaan denyut secara Q-switch dan mode-lock.

Kata kunci: Q-switch, Mode-lock, Saturable Absorber, Organic optical material, Erbium doped fiber laser, Ytterbium-doped laser.

ACKNOWLEDGEMENTS

First and foremost, Alhamdulillah, all thanks and praise is due to the most gracious Allah for granting me the required good health guidance, spiritual comfort and steadfastness throughout my research journey. A big thank you to my main supervisor PROF. DR. SULAIMAN WADI HARUN for his invaluable support, guidance, encouragement, intellectual input and friendship towards me in conducting this research to its success. A special gratitude is also extended to my co-supervisor PROF. DR. HAMZAH AROF and DR. AHMED ALMASOODI for making my PhD program a truly fruitful experience. Their helpful suggestions and advices on various aspects of my research work have certainly been very constructive. I thank the UNIVERSITY OF MALAYA, especially the staff of the Electrical Department for their continuous support.

I am extremely grateful to MY PARENTS for their love, prayers, caring and sacrifices for educating and preparing me for my future. I am very much thankful to MY HUSBAND (Fuad) and MY SONS (karam and Aghyad) for their love, understanding, prayers and continuing support to complete this research work. Also, I express my thanks to MY SISTERS (Reem, Iman and Tasneem) and BROTHERS (Ayman and Alaa) for their support and valuable prayers.

RAWAN M S SOBOH

TABLE OF CONTENTS

Abstract	iii
ABSTRAK	v
Acknowledgements.....	vii
Table of Contents.....	viii
List of Figures.....	xi
List of Tables.....	xiv
List of Symbols and Abbreviations	xv
CHAPTER 1: INTRODUCTION.....	1
1.1 Background	1
1.2 Motivation of Research.....	2
1.3 Principle Objectives of the Dissertation	5
1.4 Research / Dissertation Outline	6
CHAPTER 2: LITERATURE REVIEW: FIBER LASER SYSTEMS	8
2.1 Short History of Optical Fiber.....	8
2.2 Optical Fibers	9
2.3 Light Propagation in Optical Fiber	12
2.3.1 Dispersion in Optical Fibers	15
2.3.1.1 Chromatic Dispersion.....	15
2.3.2 Normal and Anomalous Dispersion.....	17
2.3.3 Polarization Dispersion	18
2.4 Self-Phase Modulation.....	18
2.5 Interaction of Dispersion and Nonlinearity.....	21
2.6 Fundamentals of Optical Fiber Laser.....	24

2.6.1	Population Inversion	24
2.6.2	Fiber Laser Amplifier.....	25
2.6.3	Erbium-Doped Fiber	26
2.6.4	Ytterium-Doped Fiber.....	28
2.7	Pulse Formation in Fiber Laser Cavity	30
2.7.1	Q-Switching.....	32
2.7.2	Mode-Locking	33
2.8	Saturable Absorber (SA).....	35
2.9	Organic Material.....	38
2.9.1	Zinc Phthalocyanine.....	38
2.9.2	Lawsone Dye	41

CHAPTER 3: PREPARATION AND CHARACTERIZATION OF ORGANIC MATERIAL BASED SATURABLE ABSORBERS..... 43

3.1	Introduction	43
3.2	The Preparation and Characterization of Zinc Phthalocyanine Thin Film Based SA 43	
3.2.1	Preparation of the SA Films.	45
3.2.2	Characterization of the SA films.	46
3.3	The Preparation and Characterization of Lawsone Dye Material-Based SA.....	52
3.4	Summary	58

CHAPTER 4: ZINC PHTHALOCYANINE THIN FILM AS SATURABLE ABSORBER TO GENERATE Q-SWITCHED AND MODE-LOCKED PULSES IN ERBIUM DOPED FIBER LASER CAVITY 59

4.1	Introduction	59
4.2	ZnPc Thin Film as Saturable Absorber for Q-switched Pulse Generation	60

4.2.1	Q-switched EDFL Setup	60
4.2.1.1	Results and Discussion	61
4.3	ZnPc Thin Film as Saturable Absorber for Picosecond Soliton Pulse Generation	66
4.4	Summary	71
CHAPTER 5: ZINC PHTHALOCYANINE THIN FILM AS SATURABLE ABSORBER TO GENERATE Q-SWITCHED AND MODE-LOCKED PULSES IN YTTERBIUM DOPED FIBER LASER CAVITY		72
5.1	Introduction	72
5.2	Passively Q-switched YDFL Using ZnPc Thin Film as Saturable Absorber	72
5.3	Passively Mode-Locked YDFL Using ZnPc Thin Film as Saturable Absorber ...	77
5.4	Summary	80
CHAPTER 6: LAWSONE THIN FILM AS SATURABLE ABSORBER FOR Q-SWITCHING AND MODE-LOCKING APPLICATION		82
6.1	Introduction	82
6.2	Lawsone Dye Material as Potential SA for Q-Switched EDFL	82
6.3	Lawsone Dye Material for Mode-Locking	87
6.4	Summary	91
CHAPTER 7: CONCLUSION AND FUTURE WORK.....		92
7.1	Conclusion.....	92
7.2	Recommendation for future work.....	96
	References	98
	List of Publications and Papers Presented	112

LIST OF FIGURES

Figure 2.1: Cross-section view of an optical fiber and illustration of its refractive index profile.	11
Figure 2.2 Normal and anomalous dispersion in a standard single-mode optical fiber. (Agrawal, 2000).....	17
Figure 2.3. Chirp induced by SPM in an optical pulse. (G. P. Agrawal, 2007).....	21
Figure 2.4. Energy level diagram for Er ³⁺ . Pump transitions are shown in blue, and the specific laser transitions are shown in red.....	28
Figure 2.5. Energy diagram of Yb ³⁺ ions exhibiting sub-level Stark splitting.	29
Figure 2.6. Typical absorption and emission spectra of YDF. (Weber et al., 1983).....	30
Figure 2.7. Process of the formation of Q-switched pulse, depicting cavity gain and loss modulation.....	33
Figure 2.8. The technological evolution of saturable absorber for fiber lasers.	35
Figure 2.9. Crystal structures of the ZnPc polymorphs. For α -ZnPc, projection is shown on (a) [010] plane and (b) [100] plane. For β -ZnPc, the projection is illustrated on (c) [010] plane and (d) [110] plane.	40
Figure 2.10. Q-band absorbance spectra of ZnPc thin film in (a) as-deposited state, and (b) at different annealing temperatures.	40
Figure 3.1. Molecular structures of (a) ZnPc and (b) PVA.....	45
Figure 3.2. Step by step process on fabricating ZnPc:PVA thin film based on embedding technique.	46
Figure 3.3. FTIR of ZnPc:PVA thin film; the black and red numbers are the vibration peaks of PVA and ZnPc, respectively.....	47
Figure 3.4. (a–c) SEM images for different methods of spin-coating ZnPc/PVA, casting Znpc/PVA, and embedding ZnPc:PVA thin films, respectively. (d–f) High magnification SEM of the respective methods.	48
Figure 3.5. (a) Optical absorption spectrum of pure PVA and ZnPc thin films prepared at different methods. (b-d) Tuac's plot for the composite materials of ZnPc and PVA thin films prepared at different methods.....	50
Figure 3.6. Nonlinear optical transmission curve of the embedding ZnPc:PVA thin film SA.	51

Figure 3.7. Molecular structures of (a) lawsone and (b) PVA.	53
Figure 3.8. FTIR spectra of lawsone powder and lawsone: PVA thin film.	54
Figure 3.9. Absorbance spectrum of lawsone: PVA and PVA thin films. An inset figure is the calculated optical band gap of lawsone: PVA thin films obtained by extrapolation to $\alpha = 0$	55
Figure 3.10. The lawsone: PVA thin film SEM image in magnification of (a) 2 K X, and (b) 10 K X.	56
Figure 3.11. (a) The EDX measurement of lawsone: PVA thin film. (b) The used SEM image for EDX measurement.	56
Figure 3.12. Nonlinear optical transmission properties of the lawsone:PVA thin film SA.	57
Figure 4.1. Experimental setup of the passively Q-switched EDFL with insertion of ZnPc film SA.	61
Figure 4.2. Pulse trains recorded at the threshold pump power of (a) 115.8 mW (embedding ZnPc:PVA), (b) 119 mW (Casting ZnPc/PVA), and (c) 109.6 mW (Spin-coating ZnPc/PVA).	62
Figure 4.3. The typical pulse performance of the Q-switched EDFL with embedding ZnPc:PVA, casting ZnPc/PVA, and spin-coating ZnPc/PVA based SA recorded at maximum pump power of 148, 141, and 135 mW (a) Optical spectrum, (b) Pulse train, (c) Single envelope pulse profile, and (d) the RF spectrum.	64
Figure 4.4. Pulse repetition rate and pulse width variation with pump power. (b) Average output power and pulse energy versus pump power.	66
Figure 4.5. The proposed cavity setup for the soliton mode locked EDFL.	67
Figure 4.6. Properties of the mode-locked EDFL. (a) Optical spectrum. (b) Wavelength of the pulse train. (c) Autocorrelation trace. (d) RF spectrum.	69
Figure 4.7. (a) Measured output power as a function of pump power. (b) Pulse energy and peak power against the pump power.	70
Figure 5.1. Experimental setup of Q-Switched YDFL.	73
Figure 5.2. Optical spectrum of Q-switched YDFL with ZnPc:PVA SA at 276.8 mW pump power.	74
Figure 5.3. The typical pulse performance of Q-switched YDFL with embedding ZnPc:PVA based SA. (a) Pulse train at threshold pump power of 246 mW. (b-c) Pulse	

and single envelope pulse at maximum pump power of 276.8 mW. (d) RF spectrum at the maximum pump power of 276.8 mW.	75
Figure 5.4. Q-switched laser performance against pump power utilizing a newly developed ZnPc:PVA based SA. (a) Repetition rate and pulse width. (b) Average output power and pulse energy.....	76
Figure 5.5. YDFL cavity configuration for the mode-locking operation.....	78
Figure 5.6. Characteristics of the mode-locked pulses from YDFL. (a) Wavelength. (b) Time. (c) Frequency domain at maximum pump power.....	78
Figure 5.7. Average power and pulse energy at various pumping power.....	80
Figure 6.1. Experimental configurations of Q-switched EDFL with lawsone film SA..	83
Figure 6.2. Typical oscilloscope traces and single pulse profile of the Q-switched pulse trains with pump powers of (a) 26 mW, (b) 33.6 mW, and (c) 43.3 mW.....	84
Figure 6.3. (a) Optical spectrum of EDFL at pump power of 43.3 mW. (b) The relationships between output power and pump power.....	85
Figure 6.4. (a) Pulse repetition rate and pulse width as function of pump power. (b) Pulse energy and peak power as functions of pump power.....	86
Figure 6.5. (a) Radio frequency spectrum of the Q-switched fiber laser at pump power of 43.3 mW. (b) The broadband RF output spectrum.	86
Figure 6.6. Experimental configuration of mode-locked EDFL with lawsone film SA.	88
Figure 6.7. Stretched-pulse operation characteristics at 43.3 mW pump power. (a) Measured oscilloscope trace with a repetition rate of 3.4 MHz. (b) Output spectrum centered at 1567.5 nm. (c) Autocorrelation trace obtained by 50% output ratio. (d) Measured RF spectrum profile.	90
Figure 6.8. The linear variation of average output power and pulse energy versus injected pump power.....	91

LIST OF TABLES

Table 2.1: Few Rare Earth ions employed in Optical Fiber Lasers and their Output and Pump Wavelength Regions	9
Table 7.1. Comparison of Q-switching and Mode-locking performances.....	95
Table 7.2. Comparison of different organic group result in QS-EDFL.....	96
Table 7.3. Comparison of different organic group result in ML-EDFL.....	96

Universiti Malaya

LIST OF SYMBOLS AND ABBREVIATIONS

1D	:	One-Dimensional
2D	:	Two-Dimensional
A_{eff}	:	Effective area
BP	:	Black Phosphorous
C	:	Carbon
CNTs	:	Carbon Nanotubes
CVD	:	Chemical Vapor Deposition
CW	:	Continuous Wave
D	:	Dispersion
DMF	:	Dimethylformamide
DMS	:	Dimethyl Sulfoxide
Eb	:	Erbium
EDFL	:	Erbium-Doped Fiber Laser
EDX	:	Energy-Dispersive X-Ray
Er^{3+}	:	Erbium ion
ESA	:	Excited State Absorption
FTIR	:	Fourier Transform Infrared Spectroscopy
FWHM	:	Full Width at Half Maximum
FWM	:	Four-Wave-Mixing
GVD	:	Group Velocity Dispersion
Ho^{3+}	:	Holmium ion
I	:	Incident Laser Intensity
I_{sat}	:	Saturation Intensity
LB	:	A Langmuir–Blodgett

L_D	:	Dispersion length
LED	:	Light Emitting Diode
L_{NL}	:	Nonlinear length
NA	:	Numerical Aperture
Na	:	Sodium
NALM	:	Nonlinear Amplifying Loop Mirror
Nd^{3+}	:	Neodymium ion
NFs	:	Noise Figures
NLe	:	Nonlinear effective
NLs	:	Nonlinear Schrodinger
NOLM	:	Nonlinear Optical Loop Mirror
NPR	:	Nonlinear Polarization Rotation
O	:	Oxygen
OC	:	Optical Coupler
OFETs	:	Organic Feld Effect Transistors
OPM	:	Optical power meter
OSA	:	Optical Spectrum Analyzer
OSC	:	Organic Semiconductors
OSC	:	Oscilloscope
P	:	Polarization
P_0	:	Power
PC	:	Polarization Controller
Pcs	:	Phthalocyanines
Pr^{3+}	:	Praseodymium ion
PVA	:	Polyvinyl Alcohol
RF	:	Radio Frequency

RFSA	:	Radio Frequency Spectrum Analyzer
SA	:	Saturable Absorber
SBS	:	Stimulated Brillouin Scattering
SEM	:	Scanning Electron Microscope
SESAM	:	Semiconductor Saturable Absorber Mirror
Sm ³⁺	:	Samarium ion
SMF	:	Single Mode Fiber
SNR	:	Signal to Noise Ratio
SPM	:	Self-Phase Modulation
SRS	:	Stimulated Raman Scattering
SWCNTs	:	Single-Walled Carbon Nanotubes
T ₀	:	Width
T _{rt}	:	Time Round-Trip
TBP	:	Time Bandwidth Product
TIR	:	Total Internal Reflection
TIs	:	Topological Insulators
Tm ³⁺	:	Thulium ion
TMDs	:	Transition Metal Dichalcogenides
T _{NS}	:	Non-Saturable Absorption
TR	:	Transmission Ratio
V _g	:	Group velocity
XPM	:	Cross-Phase Modulation
Yb	:	Ytterbium
Yb ³⁺	:	Ytterbium ion
YDFL	:	Ytterbium-Doped Fiber Laser
ZnPc	:	Zinc Phthalocyanine

ΔT : Modulation Depth

Universiti Malaya

CHAPTER 1: INTRODUCTION

1.1 Background

A consistently progressive development has been witnessed over the past 50 years in development of optical fiber technology used for manufacturing laser light sources and devices. It has acted as a catalyst in boosting the scientific and technological advancements in numerous fields, such as optical communications (Yi, Li, & Liu, 2015), medical diagnostics (Busser, Moncayo, Coll, Sancey, & Motto-Ros, 2018; Ushenko et al., 2016), micromachining (Saxena, Qian, & Reynaerts, 2020), multiphoton imaging (B. Tian et al., 2018), spectroscopy, and microscopy (Fahad et al., 2018). A revolutionary progress has been recorded in the last decade pertaining to the methodological schemes of generating high energy ultrashort optical pulses. The advancements in material sciences have simplified and boosted the developments in fiber lasers. The rare-earth ion doped fiber sitting in a glass host is primarily used as the active medium in producing a short optical pulse while it possesses wide gain bandwidth. Optical pulsed fiber laser stands as state of the art in laser technology and holds a huge promise for robust and portable light sources. The pulsed laser operation in a laser cavity is obtained through Q-switching or mode-locking technique. Q-switching approach possesses the ability to generating the optical pulses with high energy, which has application for micromachining and drilling. This type of laser benefits the electronic and automotive industry (Shinomoto et al., 2016), since many processes such as logo and manufacturing date inscription can be performed. It is also beneficial in the electronic semiconductor manufacturing industry (Jiang et al., 2020), and medical field-especially in the eye and dental surgery (Niemz, 2019; Plamann et al., 2010). The system used for eye surgery is known as laser-assisted in situ keratomileusis (LASIK) (Sandoval et al., 2016). Mode-locking approach has the capability of producing ultrashort pulsed laser of a few nano- / femto-seconds. The laser action depends on the gain medium and the modulation technique. Multiple axial modes

in a laser cavity are locked together leading to the commencement of ultrashort pulsed laser operation. The generated peak powers are higher, many times in magnitude, than the continuous wave (CW) mode peak powers. Such pulsed lasers are useful in many applications such as micromachining, communication, and optical systems (Nizamani, Salam, et al., 2020).

The infrared and near-infrared ($\sim 1.0\text{--}2.0\ \mu\text{m}$) spectral regions are now well addressed by silica glass fiber amplifiers which including active medium doped with ytterbium (Yb) (Soboh, Al-Masoodi, Erman, Al-Masoodi, Yasin, et al., 2021), erbium (Er) (Soboh, Al-Masoodi, Erman, Al-Masoodi, Nizamani, et al., 2021), bismuth (Bi) (Kelleher et al., 2010), and thulium (Tm) (Rusdi et al., 2019). This allows an almost continuous coverage of this wavelength region. This thesis focuses on developing Q-switched and mode-locked fiber lasers operating in $1.5\ \mu\text{m}$ and $1.0\ \mu\text{m}$ region using an Erbium-doped fiber (EDF) and Ytterbium-doped fiber (YDF), respectively, as the gain medium. The Q-switching and mode-locking operation is achieved using an organic material as saturable absorber (SA).

1.2 Motivation of Research

Fiber lasers have received a wide interest in both industry and academic research in recent years as an alternative approach to generate high energy short and ultra-short pulses. They use a rare-earth doped fiber as a gain medium, and thus have many advantages over its solid-state counterparts. The large ratio of the surface area to the volume of the fiber eliminates the need for water cooling of the laser medium. In addition, the waveguide nature of optical fiber enables perfect overlap of the pump and signal in the gain medium, and thus eliminate the need for optical alignment. The single mode properties of optical fiber ensure excellent beam quality. Practically, fiber lasers tend to

be less expensive than solid-state lasers, enabling laser technology to be more widely adopted in various industries.

The generation of optical pulse train can be done via two techniques. One is an active technique, while the other is a passive technique. The passive technique possesses several advantages such as high efficiency, simplicity, compactness, design flexibility, and low cost (Rui et al., 2011; Soboh, Al-Masoodi, Erman, Al-Masoodi, Nizamani, et al., 2021). Different passive approaches have been proposed in the literature, such as non-linear polarization (Radnatarov, Khripunov, Kobtsev, Ivanenko, & Kukarin, 2013), and figure-of-eight cavity design (Jeong, Sahu, Payne, & Nilsson, 2004). These approaches are superior in terms of cost, the achieved pulse width, and overall fiber construction. However, their performance is easily affected by external environmental factors.

Recently, a new approach has been proposed that involves the development of saturable absorber (SA). The optical laser pulse is generated by inserting the SA material into the laser cavity. This technique is preferable because of its performance and simplicity. Therefore, various SAs have been proposed for generation of optical laser pulse in different operation regions. Initially, conventional bulk SAs have been employed for generating optical pulse train; such as color filter glasses (Snitzer & Woodcock, 1966) and ion-doped crystals (Zolotovskaya et al., 2006); however, these materials have limitations such as slow response time, narrow spectral range, and low optical damage threshold (Jiang et al., 2020). Later, researchers proposed semiconductor saturable absorption mirrors (SESAMs) for achieving Q-switched and mode-locked fiber lasers. This has emerged as a mature technology of optical pulse train generation (J. Li et al., 2014; M. Wang, Chen, Huang, & Chen, 2014). The far-reaching implementations of SESAMs have been hindered in recent years because of their high cost. Besides, their operating bandwidth is narrow, fabrication process is complex, and also have high

packaging cost (Soboh et al., 2020). The excellent optical as well as optoelectronic properties of low-dimensional nanomaterials encouraged the researchers to explore them for the purpose of generating optical pulse train (Chernysheva et al., 2017; Du et al., 2017; Mao et al., 2016). For instance, the carbon nanotubes (CNTs) have also been successfully utilized as SAs in fiber lasers. However, their operation is limited to certain wavelengths because of high demanding chirality control or band-gap engineering (Schmidt et al., 2008). Graphene has also been employed as SA for generating fiber laser. It has received considerable attention because of its fast recovery time and broadband saturable absorption (Bao et al., 2009; Serres et al., 2015).

More recently, other 2D nanomaterials such as topological insulators (TIs) and transition-metal dichalcogenides (TMDs) have also proposed and demonstrated as SA for both Q-switching and mode-locking applications (Ares et al., 2016; W. Liu et al., 2020; W. Liu et al., 2018). This is due to their thickness dependent bandgap and unique absorption characteristics. Another type of SA material is metal nanoparticles. In contrast to the 2D materials, it has advantages of larger third-order nonlinear coefficient, and variable surface plasmon resonance peak (X. Tian et al., 2018; Zhao et al., 2012). However, it is important to mention that nanomaterials incur long-term exposure hazards to human health, and hence have raised safety concerns (Yao et al., 2020). Although various SAs have been widely proposed and demonstrated for application in Ytterbium doped fiber laser (YDFL) and Erbium doped fiber laser (EDFL) cavity, finding new SA materials that have broadband saturable absorption, ultrafast recovery time, and high damage threshold is still an active area of research attracting considerable interest of scientists and engineers.

It is of utmost importance to dig for new SA materials which are of low cost, whose fabrication is also simple and cost effective, which should yield low saturation intensity

with appropriate modulation depth and should have high damage threshold. Lately, organic materials that are environmentally friendly and bio-compatible have also been experimented with as SA materials. They are favorable since they do not pose any health risk to human. This thesis focuses on developing Q-switched and mode-locked fiber lasers, operating at 1.5 μm and 1.0 μm wavelength regions, using new organic material as a saturable absorber. The suggested new organic materials are zinc phthalocyanine (ZnPc) and lawsone dye.

1.3 Principle Objectives of the Dissertation

The aim of this work is to develop efficient and low-cost Q-switched and mode-locked fiber lasers operating in the near and mid-infrared regions using two organic materials: ZnPc and lawsone dye. By far, organic material is one of the most promising candidates for many optical and electronic applications because of their many advantageous including fast recovery time, high optical damage threshold, large optical nonlinearity and being environmentally safe. Although there is ample literature that addresses organic saturable absorber, very few studies focus on Q-switching and mode-locking applications in near-infrared region above 1 μm .

Several objectives have been outlined to guide the research direction toward achieving the aim:

1. To fabricate and characterize new passive SAs based on two different organic materials: ZnPc and lawsone dye.
2. To design and optimize Erbium-doped fiber laser (EDFL) cavity to generate Q-switched and mode-locked pulse train in 1.5 μm region using the newly developed ZnPc SA.

3. To design and optimize Ytterbium-doped fiber laser (YDFL) cavity to generate Q-switched and mode-locked pulse train in 1.0 μm region using the newly developed ZnPc SA.
4. To demonstrate Q-switched and mode-locked fiber lasers based on the newly developed lawsone dye SA.

1.4 Research / Dissertation Outline

This thesis contains 7 chapters in which a comprehensive study on Q-switched and mode-locked pulse generations by using the newly developed organic SAs is presented. Chapter presents a background, motivation, and objectives of this study. Chapter 1 is intended to present the brief history of fiber laser technologies and provides details of fundamentals of optical fibers and pulse formation in fiber laser cavities. Characteristic equations are also presented for pulse propagation in optical fiber. This chapter also presents a detailed literature review of new materials used to generate pulses in fiber lasers.

In chapter 3, two new SAs are developed based on ZnPc and lawsone dye materials. The SA thin films were fabricated based on liquid exfoliation technique using PVA as a host polymer. The ZnPc based thin film is prepared in three different methods; ZnPc is embedded into, casted onto and spin-coated onto the PVA film. The lawsone based film is prepared by embedding lawsone material into the PVA film. The physical and optical characterizations of these SAs are also described in this chapter.

Chapter 4 investigates the potential of ZnPc based SAs, for Q-switched and mode-locked pulse laser generation at 1.5 μm region. The developed ZnPc SA is inserted between two optical fiber ferrules in the EDFL cavity to act as a Q-switcher and mode-locker for microsecond and picosecond pulse generation, respectively.

In Chapter 5, ZnPc PVA thin film is proposed and demonstrated as a SA in a YDFL cavity. The Q-switching operation was realized at the center of wavelength of 1036 nm with the minimum pulse width of 2.2 μ s, the highest repetition rate of 63 kHz and the maximum pulse energy of 91 nJ, respectively. A stable and self-starting mode-locked optical pulse train located at 1034.5 nm wavelength is achieved within the pump power range from 246 to 277 mW.

Chapter 6 investigates the potential of lawsone dye-based SA for generating Q-switched and mode-locked pulses in EDFL cavity.

Chapter 7 concludes the thesis and presents a summary of the research findings. Future research directions from this work are also discussed in this chapter.

CHAPTER 2: LITERATURE REVIEW: FIBER LASER SYSTEMS

2.1 Short History of Optical Fiber

To let the fiber guides the light through it, the principle of total internal reflection (TIR) should be fulfilled. The TIR is leveraged based on a cladding material that has lower refractive index than the core. It is the presence of the cladding that ensures the light wave is guided through the core based on the TIR. The optical fiber developed in 1920 had this issue that it had no cladding, and hence no guarantee of guiding the light signal. Subsequent research efforts solved this issue and led to two major developments in the optical fiber technology. The first progress was the realization of optical fibers consisting of cladding made of silica, and this was achieved in 1950s (Hirschowitz, 1961). The silica cladded fibers improved and ensured the optical signal guiding property of the core through the TIR principle. The second milestone was achieved in 1979 and this was the achievement of reduction of loss / attenuation of optical signal through the waveguide (Miya, Terunuma, Hosaka, & Miyashita, 1979).

The optical fiber is made of silica which is a material that contains almost no impurities. This enables the Rayleigh scattering and material absorption to be at the limit of optical loss, at long wavelengths. The lowest attenuation of the optical signal has been observed at 1.55 μm , with the level of attenuation of approximately 0.2 dB/km. This forms the basis of the employment of this wavelength band (1.55 μm) for contemporary telecommunication systems. So, the growth of telecommunications technology has been associated with the development of optical fiber technology, as a part and parcel, and not only this, it also played its role as a catalyst in the invention of optical fiber laser technology in 1960. The consolidation and integration of trivalent rare-earth ions into the glass hosts led to the realization and demonstration of fiber lasers (Hirschowitz, 1961). The rare-earth ions included neodymium Nd^{3+} , erbium Er^{3+} and thulium Tm^{3+} . Following this, fiber cores employing Nd^{3+} ions were fabricated (Koester & Snitzer,

1964), and it was observed Nd^{3+} lasers showed enhanced efficiency at 1.06 μm wavelength of 1.55 μm . At this operating wavelength, the fiber offers the lowest signal loss / attenuation, i.e., ~ 0.15 dB/km, and this is an extremely beneficial factor for the purpose of light wave telecommunication systems. Besides incorporating the above mentioned dopants, to investigate and develop new wavelength bands in silica and fluoride based optical fiber lasers, the use of following dopants / co-dopants have also been explored: praseodymium ions Pr^{3+} (Durteste, Monerie, Allain, & Poignant, 1991), samarium ions Sm^{3+} (Farries, Morkel, & Townsend, 1990). Table 2.1 shows the operating and pump wavelength for few rare-earth doped materials used in fiber lasers.

Table 2.1: Few Rare Earth ions employed in Optical Fiber Lasers and their Output and Pump Wavelength Regions

Doped Ion	Host Material	Output Wavelength (nm)	Pump Wavelength (nm)
Er^{3+}	Silica/Fluoride	Around 1550	1480 and 1980
Nd^{3+}	Silica/Fluoride	1064 to 1088	808
Ho^{3+}	Silica/Fluoride	2874	1064
Tm^{3+}	Silica/Fluoride/ZBLAN	1900 to 2100	793
Yb^{3+}	Silica/Fluoride	1030 to 1100	910 to 975

2.2 Optical Fibers

A circular waveguide made of dielectric material that can carry information through it in the form of light / optical signals is known as an optical fiber. It consists of two parts, the inner core, and the outer cladding. The refractive index of cladding is lower than its core, and it is by virtue of this arrangement that total internal reflection of the guided signal in the core takes place and makes the operation of the optical fiber possible. To achieve this, it is ensured that the incident angle at which the optical signal strikes the core-cladding interface lies in a range that it meets the condition of TIR. In this way, the incident signal gets trapped within the fiber and travels down along the fiber length. Therefore, the two prime factors to achieve wave-guiding property of an optical fiber are:

(1) higher refractive index of core than cladding, (2) Requisite angle of incidence to achieve TIR. In this scenario, it is mandatory for an optical signal to travel from an optically denser medium towards an optically rarer medium. It is to note that the above scenario does not consider the wave nature of the optical signal; rather, it relies on the ray optics theory. The composition of an optical fiber consists of optically transparent materials that include plastics, silica, fluoride, and chalcogenide glasses (Dragic, Cavillon, & Ballato, 2018). However, owing to the extremely low optical losses as well as stable and robust mechanical and chemical properties, it is the silica that primarily wins as a material for optical fiber fabrication. The realization of difference between the values of index of refraction of the core and cladding is achieved by incorporating small amounts of dopants at the time the fabrication process is underway. To name the example dopant materials, boron and fluorine are used, which when added, lower the value of refractive index. Opposite behavior is observed with germanium and phosphor dopants. To ensure the strength of the optical fiber for practical applications, a further coating of a couple of acrylate polymer layers is done around the cladding. Also, various coatings of protective sheath are added to form an optical fiber cable that is robust enough to withstand damages from manhandling as well as environmental changes. Optical fibers are constructed into various configurations, the basic one is known as a step-index fiber. This configuration consists of a core and a cladding that bear constant individual refractive indices, and there is a step decrease of refractive index from core towards cladding. Another configuration consists of graded index profile; however, the easiest and simplest from fabrication point of view is the step-index fiber. Figure 2.1 illustrates the cross-sectional view of an optical fiber.

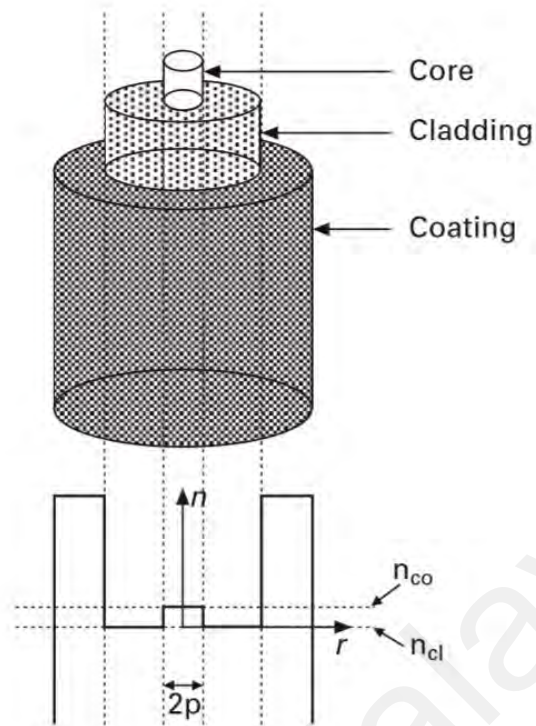


Figure 2.1: Cross-section view of an optical fiber and illustration of its refractive index profile.

To achieve TIR, there is a condition on maximum angle of incidence (α) for the signal to get propagated through the waveguide. This angle is determined by the difference of indices of refraction between the core and the cladding. Besides, determining the acceptance angle of the fiber- the angle at which an optical ray enters the dielectric facet, as depicted in Figure 2.1. The numerical aperture (NA) is defined as the sine of the acceptance angle and is expressed as:

$$NA = \sin \alpha = (n_1^2 - n_2^2)^{1/2} \quad (2.1)$$

where, n_1 represents index of refraction of core material, n_2 is the index of refraction of the cladding material, and α represents critical angle. NA, intuitively, determines the ease of coupling of light signal / ray into the fiber. Quantitatively, it measures the light gathering capability of the fiber.

2.3 Light Propagation in Optical Fiber

As the signal propagates within the dispersive dielectric medium of the optical fiber, the associated non-linear wave phenomena can be understood by the underlying electromagnetic wave propagation theory. To this end, James Clark Maxwell, in 1860, proposed and identified the link between the wave electromagnetics and the ray optics. He presented his findings in terms of four equations. These four equations form the foundations to elaborate and investigate the electromagnetic wave propagation phenomena in free space and within media (Maxwell, 1865). These equations are given below:

$$\nabla \times \mathbf{E} = -\partial \mathbf{B} / \partial t \quad (2.2)$$

$$\nabla \times \mathbf{H} = \mathbf{J} + \partial \mathbf{D} / \partial t \quad (2.3)$$

$$\nabla \cdot \mathbf{D} = \rho_f \quad (2.4)$$

$$\nabla \cdot \mathbf{B} = 0 \quad (2.5)$$

where \mathbf{E} is electric field vector, \mathbf{H} represents magnetic field vector, \mathbf{D} is electric flux density, \mathbf{B} is magnetic flux density, \mathbf{J} represents the current density vector, ρ_f is charge density, and t represents the time coordinate. In a medium where free charges are non-existent, e.g., an optical fiber, $\mathbf{J} = \rho_f = 0$. The propagation of electric (\mathbf{E}) and magnetic (\mathbf{H}) fields inside a medium results in electric and magnetic flux densities (\mathbf{D} and \mathbf{B} respectively). The relationship between the field quantities and their respective flux densities depends on the constitutive parameters, and are expressed as (Diament, 1990):

$$\mathbf{D} = \epsilon_0 \mathbf{E} + \mathbf{P} \quad (2.6)$$

$$\mathbf{B} = \mu_0 \mathbf{H} + \mathbf{M} \quad (2.7)$$

where, P stands for induced electric polarization, M stands for induced magnetic polarization, and ϵ_0 and μ_0 are the vacuum / free space permittivity and permeability, respectively. $M = 0$ when wave propagation occurs in a non-magnetic medium, example being as an optical fiber. To analytically represent the propagation of light within the optical fiber medium, Maxwell's equations with charges (ρf) or currents (J) equal to zero can be employed. B and D can be taken out by taking the curl of Eq. (2.2) and employing equations (2.3), (2.6), and (2.7). What remains is a wave equation represented in terms of E and P , and expressed as:

$$\nabla \times \nabla \times \mathbf{E} = \frac{-1}{c^2} \frac{\partial^2 E^2}{\partial t^2} - \mu_0 \frac{\partial^2 P}{\partial t^2} \quad (2.8)$$

where, c represents the speed of light in vacuum, and the relation $\mu_0 \epsilon_0 = 1/c^2$ has been utilized. The electrons of a medium oscillate in response to the incident oscillating electric field. The oscillations of the electrons occur about their equilibrium position. This oscillation is given scientifically as the dipole moment per unit volume, and is represented by the induced electric polarization (P) of the medium. The relationship between the electric field strength and its induced electric polarization, for a given material, is determined by the material's electric susceptibility tensor (χ). By utilizing the Taylor series expansion, the n^{th} order susceptibility (χ) can be expressed as Equation 2.9 (Tritschler, Mücke, & Wegener, 2003). The P represents polarization, ϵ_0 is the permittivity of free space and E is the electric field.

$$P = \epsilon_0 (\chi^{(1)} \cdot E + \chi^{(2)} \cdot E^{(2)} + \chi^{(3)} \cdot E^{(3)} + \dots) \quad (2.9)$$

The incident field that induces the electric polarization of a material causes oscillations of the dipoles of the material, and this movement of the dipoles in turn create a new radiated field, that propagates with a specific phase delay. As the incident electric field is a vector quantity, and the induced material polarization is also vector in nature; therefore,

the susceptibility is a tensor. The relationship between the direction of the incident electric field and the induced material polarization (which thereby means the new radiated field) is expressed by equation 2.8 (Hocquet, Neauport, & Bonod, 2011). Sufficient information is manifested by this equation to understand the nonlinear response of the material. It considers the incident light's polarization and the light yielded through nonlinearity. With the objective to investigate the nonlinear behaviors and effects shown by the optical fibers, short pulses are propagated into the fiber medium. The duration of these pulses lie in the range of approximately 10 ns to 10 fs, and the nonlinearity and the depressiveness of the fiber medium gets detected by a change in the shape and spectrum of these pulses. The wave propagation in such nonlinear mediums is expressed by nonlinear Schrodinger (NLS) equation, a partial differential equation, and is given as:

$$i \frac{\partial A}{\partial z} - \frac{\beta_2}{2} \frac{\partial^2 A}{\partial T^2} + \gamma |A|^2 A = 0 \quad (2.10)$$

where, $A(z, t)$ represents the amplitude of the pulse envelope, β_2 is the Group Velocity Dispersion (GVD) parameter, and the nonlinear parameter γ is responsible for Self-Phase Modulation (SPM). GVD and SPM are presented in this equation, whereby both dispersive and nonlinear effects have an impact on the shape and spectrum. The Kerr effect is assumed to be instantaneous nonlinear response which results from optical interaction with electrons of the medium, which lead to an intensity dependent refractive index. This depends on the real part of $\chi^{(3)}$ in Eq (2.9) and leads to nonlinear effects such as self-phase modulation (SPM), cross-phase modulation (XPM) and four-wave mixing (FWM). Other effects such as Stimulated Raman Scattering (SRS) and Stimulated Brillouin Scattering (SBS) are also considered in fiber, which are non-instantaneous. The SRS arises from interaction between light and optical phonons, whereas SBS is due to acoustic phonon interaction. Each of these effects can be usefully exploited to achieve a

particular optical function or can manifest as an unwanted source of loss or distortion depending on the application.

2.3.1 Dispersion in Optical Fibers

2.3.1.1 Chromatic Dispersion

The phase velocity of the signal in an optical medium depends on the frequency of the optical signal, and this forms the basis of the dependence of the refractive index of the material on frequency ($n(\omega)$). Such property of the material is known as chromatic dispersion (Okamoto & Marcatili, 1989). When signal passes through the optical medium, absorption of the electromagnetic energy occurs at the characteristic resonant frequencies. Fundamentally, the chromatic dispersion pertains to these absorptions which happen because of the interaction of the signal with the bound oscillating electrons of the medium. For those wavelengths that lie away from the characteristic resonant frequencies of the material, the refractive index approximation is achieved by Sellmeier equation (G. Agrawal, 2007) given as:

$$n^2(\omega) = 1 + \sum_{j=1}^m \frac{B_j \omega_j^2}{\omega_j^2 - \omega^2} \quad (2.11)$$

where, ω_j is frequency of resonance, and B_j is the strength of j^{th} resonant frequency. The summation is obtained over the frequency range that covers all resonant frequencies of the material. The mathematical inclusion of chromatic dispersion is considered based on propagation constant (β). The propagation constant is expanded by Taylor series at the frequency (ω_0) at which light signal is propagating within the medium (Agrawal, 2000). It is expressed as:

$$\beta(\omega) = n(\omega) \frac{\omega}{c} = \beta_0 + \beta_1(\omega - \omega_0) + \frac{1}{2}\beta_2(\omega - \omega_0)^2 + \frac{1}{6}\beta_3(\omega - \omega_0)^3 + \dots \quad (2.12)$$

where

$$\beta_m = \left(\frac{d^m \beta}{d\omega^m} \right)_{\omega=\omega_0} \quad (m = 0,1,2, \dots) \quad (2.13)$$

As the frequency spectrum of narrow pulses is very wide, dispersion impacts the pulsed light quite peculiarly. Propagation velocity of the pulse envelope is termed as group velocity (v_g), and it ties in with the propagation constant of first order as:

$$v_g = \frac{1}{\beta_1} \quad (2.14)$$

The envelope of the optical pulse consists of optical components of different spectral values, and therefore, every spectral component propagates at varied group velocities. The parameter that represents this dispersion of the group velocity is termed as β_2 , and it is because of the various group velocities of the spectral components that the pulse broadening occurs. This behavior manifested by the pulse envelope is called group velocity dispersion (GVD), and the term β_2 (ps²/km) mentioned above is called the GVD parameter. Alternatively, more common representation of the waveguide's GVD is dispersion parameter (D) (ps/nm·km) (Agrawal, 2000) that is expressed as:

$$D = \frac{d\beta_1}{d\lambda} = -\frac{2\pi c}{\lambda^2} \beta_2 \quad (2.15)$$

The term β_3 is called third-order dispersion, and is a vital parameter particularly when both parameters, β_2 and D, are at the wavelength of zeroth order dispersion. Hence it needs to be rigorously included in the dispersion analysis of the fiber. A primary indicator of a fiber's dispersion is its zeroth order dispersion wavelength. The parameter D represents the fiber's nonlinear phenomena.

2.3.2 Normal and Anomalous Dispersion

The nonlinear effects appearing in the optical fiber are of varied behaviors and depend on the sign of the parameter GVD. Therefore, it is extremely important to know the sign of GVD as it qualitatively determines and differentiates between the nonlinear effects. The normal dispersion region of the optical fiber is shown in Figure 2.2, where $\lambda < \lambda_0$ and $\beta_2 > 0$, and it shows that the longer wavelengths (low frequency spectral components) of the pulse travel faster and reach the other end of the fiber in a short span of time (Agrawal, 2000). This implies that the value of D is negative. Likewise, in the anomalous dispersion region of the fiber, where $\beta_2 < 0$ and $\lambda > \lambda_0$, for the positive value of D, longer wavelengths (low frequency spectral components) of the pulse travel slowly and take a relatively longer span of time to arrive at the other end of the fiber. As it is known that the fiber supports solitons in the anomalous region of dispersion and achieves it by reaching an equilibrium between the fiber's nonlinear effects and its dispersion effects; therefore, the study of this region of the fiber becomes of vital importance.

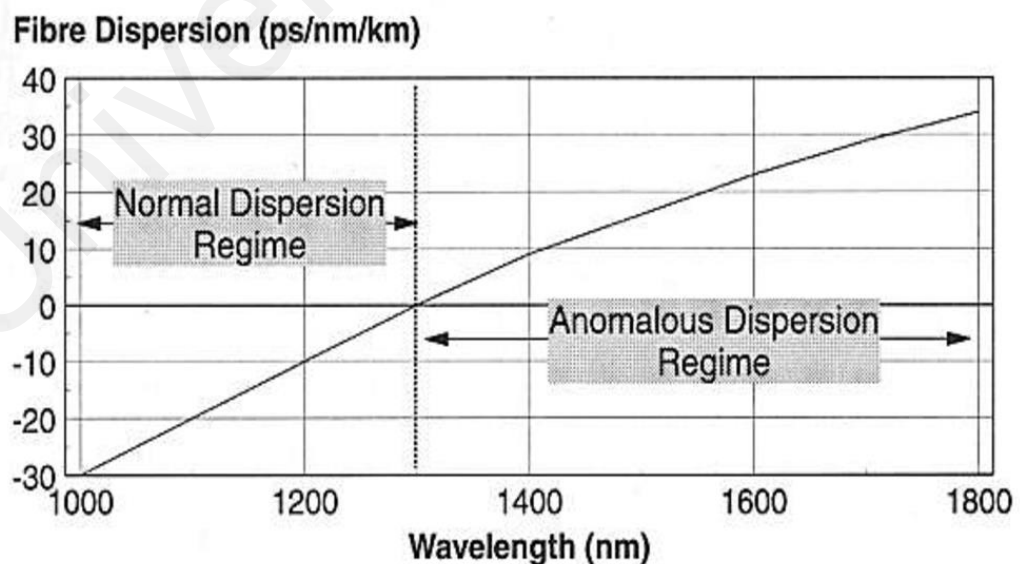


Figure 2.2 Normal and anomalous dispersion in a standard single-mode optical fiber. (Agrawal, 2000)

2.3.3 Polarization Dispersion

A marked optical axis does not exist in an ideal optical fiber, and so does the birefringence phenomenon (S. Yang, Sheng, Zhao, & Li, 2019). This is because the material of which the core and cladding of the fiber is made, is isotropic in its behavior. However, in real applications, the optical fiber undergoes various strains and tensions which can vary its thickness over its length and can accidentally alter the diameter and shape of the core. Under such circumstances, distinguished optical axis can appear, and hence lead to the presence of local birefringence. Therefore, two orthogonal components of the optical ray form and propagate down the optical fiber with varying velocities. These two orthogonal components are termed as ordinary rays and extraordinary rays. Difference between velocities of the two orthogonal rays causes a time changing difference of phase between them while the rays propagate in the fiber. Not only this, it also causes a time changing polarization. Furthermore, the different velocities of the two orthogonal rays cause them to reach the other end of the fiber in different time spans.

2.4 Self-Phase Modulation

There can be severe limitations in the operation of fiber lasers because of the nonlinear effects of the fiber. This becomes extremely problematic in a small core with highly intense optical ray, as well as when the interaction length is long, ranging from few meters to a few tens of meters. The electric field of the light signal in an optical fiber induces an electric dipole moment in the bound electrons of the dielectric material. When the optical pulse is highly intense, its strong electric field causes an inharmonic motion of the bound electrons, and thereby producing a nonlinear behavior of the induced polarization.

Self-phase modulation (SPM) is a phenomenon that originates because of the property that the refractive index depends on the pulse intensity. For the pulses propagating in the optical fiber, this can cause them to have a change in their temporal as well as spectral

consistencies. SPM tantamount to self-focus in temporal domain, where self-focus is the result of intensity-dependent index of refraction in the spatial domain. Looking at this mathematically, the real part of the index of refraction can be given as (G. Agrawal, 2007):

$$n(\omega, I) = n_0(\omega) + n_2 I(t) \quad (2.16)$$

where, I represents optical intensity, n_0 is a linear index, and n_2 has been introduced as a nonlinear index. Its value for silica is $n_2 = 2.74 \times 10^{-20} \text{ m}^2 \text{ W}^{-1}$, and is a quantity that is almost independent of the wavelength (Milam, 1998). Nonlinear effects are addressed using NLS equation (2.10), and given as (G. P. Agrawal, 2007):

$$\gamma = \frac{2\pi n_2}{\lambda A_{eff}} \quad (2.17)$$

where A_{eff} represents effective area of shape of the mode in the optical fiber.

The temporal changes in the intensity of the optical pulses that induce time varying phase appear in the form of self-phase modulation that produces new spectral components. The relative initial positions of various spectral components of a pulse are set because of the original chirp of the optical pulse. Also, the relative positions of the spectral components get altered because of the fiber's GVD while the pulse is propagating down the optical fiber. Consequently, the overall interactions among the fiber's GVD, initial chirp of the pulses, and the SPM dictate the spectrum of the output pulse and its shape. To aid in identifying the various regimes of the fiber's operation, two types of length scales are important to know. One is dispersion length (L_D), and the other is nonlinear length (L_{NL}). The two lengths, for an optical pulse having width T_0 and peak power P_0 , are defined as (Z. Liu, Zhang, Tam, & Tao, 2019):

$$L_D = \frac{T_o^2}{|\beta_2|} \quad (2.18)$$

$$L_{NL} = \frac{1}{\gamma P_o} \quad (2.19)$$

Dispersion length (L_D) is that length scale over which the effect of dispersion becomes significant, while nonlinear length (L_{NL}) is a scale of length over which the nonlinear effects become significant. An optical fiber of length L will not have any significant nonlinear or dispersion effects when $L \ll L_D$ and $L \ll L_{NL}$. The fiber length for which $L \ll L_D$ and $L \approx L_{NL}$, the dispersion effects are significantly high. When $L \approx L_D \approx L_{NL}$, both effects, i.e., dispersion and nonlinearity, are significant for a propagating pulse.

At the center of the pulse at $T = 0$, the maximum phase shift (ϕ_{max}) occurs and is expressed as:

$$\phi_{max} = \frac{L_{eff}}{L_{NL}} = \gamma P_o L_{eff} \quad (2.20)$$

For a fiber having length L and loss α , its effective length L_{eff} is given as:

$$L_{eff} = \frac{1 - e^{-\alpha L}}{\alpha} \quad (2.21)$$

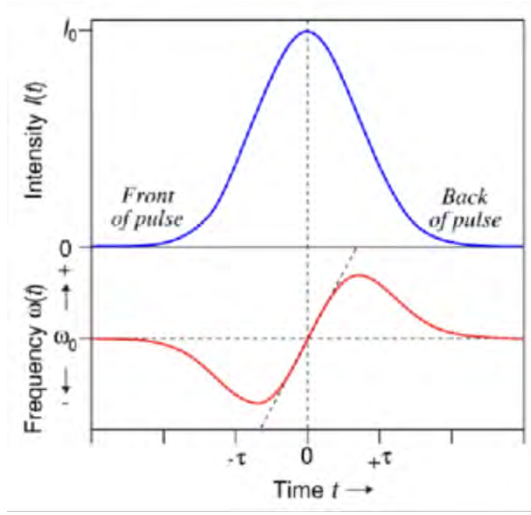


Figure 2.3. Chirp induced by SPM in an optical pulse. (G. P. Agrawal, 2007)

Clearly, the effective propagation distance when $\phi_{max} = 1$ is the nonlinear length. For the case of dispersion, the observation of pulse broadening is done in the time domain, whereas self-phase modulation induces broadening of the spectrum. Figure 2.3 (upper curve) illustrates the shift of self-frequency because of SPM, for an optical pulse that is propagating down a nonlinear medium. The rear of the pulse is shifted in frequency towards higher values, whereas the front of the pulse undergoes a frequency shift towards lower values. The chirp ($\delta\omega(T)$) induced by SPM for a Gaussian type of optical pulse is expressed as:

$$\delta\omega(T) = \frac{2mL_{eff}}{T_0 L_{NL}} \left(\frac{T}{T_0}\right)^{2m-1} \exp\left[-\left(\frac{T}{T_0}\right)^{2m}\right] \quad (2.22)$$

where $m = 1$ for a Gaussian pulse.

2.5 Interaction of Dispersion and Nonlinearity

When an optical pulse propagates in a fiber, its duration and shape can vary because of dispersion. As SPM has its dependence on the intensity of the optical pulse as well as its shape, the GVD influences the SPM. The interplay between SPM and GVD is because they impact the chirp and characteristics of the pulse while it propagates in the fiber. The GVD influences the pulse in a way that it either broadens its spectral components, or it

makes them united. On the other hand, the influence of SPM is such that it brings a red shift at the forward edge of the pulse and a blue shift at its rear edge.

To compare and analyze the influence of SPM and GVD on the propagating optical pulse, it is important to understand and define the dispersion length (L_D) and nonlinearity (L_{NL}) length.

$$L_D = \frac{t_0^2}{|\beta_2|} \quad (2.23)$$

$$L_{NL} = \frac{1}{\gamma P_0} \quad (2.24)$$

Due to GVD, the duration of an optical pulse broadens over its propagation distance. When this broadening gets doubled in duration, the distance the band limited Gaussian pulse travelled is termed as dispersion length. The symbol t_0 represents the half 1/e Gaussian pulse width or half hyperbolic secant pulse width. For a pulse with peak power P_0 , over a certain propagation length, the SPM brings about a phase shift of 1 at the maximum value of the pulse. This length is termed as nonlinear length (G. Agrawal, 2007).

If in a fiber, the nonlinear length is longer than its dispersion length, this means the dispersion in the fiber prevails over the SPM. It also means that SPM meagerly impacts the pulse evolution, and henceforth, the interplay between SPM and GVD is insignificant and can be avoided from consideration. On the other hand, if the dispersion length is same as the nonlinear length, in this case, SPM and GVD both have equal strengths.

The SPM and GVD produce juxtaposed pulse chirps in an optical fiber that have normal dispersion behavior. Because of this, the broadening of pulse is considerably rapid as compared to the scenario without substantial SPM. Eventually, the intensity of the

pulse broadening reduces, and after various dispersion lengths, GVD prevails over the pulse evolution. For the case of an optical fiber that has anomalous dispersion with the chirp caused by SPM and GVD, if its nonlinear length equates to its dispersion length, a close nullification of the chirp occurs by the central part of the Gaussian pulse.

Mathematically, it can be presented that under this scenario, full cancellation takes place, or a hyperbolic secant pulse is produced. As these pulses retain their shape while propagating in the fiber, these are known as optical solitons. As solitons remain stable against minuscule perturbations in an optical fiber that has anomalous dispersion, the solution to the propagation equation is only the solitons. Because of this reason, despite the marginal deviation of the input signal from a soliton, they do evolve while the pulse propagates in an optical fiber with anomalous dispersion.

For an optical fiber, if its nonlinear length becomes smaller than its dispersive length, the SPM prevails over the GVD and induces a chirp on the optical pulse. This generates new frequency components. Nonetheless, as dispersion effects have a dominant impact on the shape of the pulse, the GVD cannot be addressed as a minuscule perturbation because a large frequency chirp is induced by SPM. The chirp induced by SPM for a Gaussian type of optical pulse approaches zero towards its outer edges, while over a significant portion of its central region, it stays linear and positive. In an optical fiber that has anomalous dispersion, the interplay between the fiber dispersion and the central chirp leads to compressing the pulse, eventually evolving into one or various solitons. In fibers with normal dispersion, the chirp induced by GVD bears an identical sign in its central region as the chirp induced by SPM. This consequently causes a more intense stretching by GVD in the central part than the outer edges and forms a pulse that is dominantly rectangular with sharp forward and rear edges. This is achieved through a linear chirp almost over its full pulse width. Additionally, during the pulse stretching, SPM produces

multiple peaks in the center of the spectrum that get altered and mitigated by an extra influence of the GVD.

2.6 Fundamentals of Optical Fiber Laser

To understand and grasp the basic mechanisms of laser fiber working principles, the concept and intuition of the process called population inversion is extremely important. It is identified as a basic method that is leveraged in laser physics, to obtain light amplification and associated photonic oscillations.

2.6.1 Population Inversion

To grasp understanding of the population inversion mechanism, it is vital to highlight the fundamental statistics of the distribution of particles at thermal equilibrium. So, at thermal equilibrium, it is the Boltzmann distribution that is obeyed by the particles that are lying at two non-degenerate energy levels, and is expressed as:

$$N_2 = N_1 \exp \left[-\frac{E_2 - E_1}{K_B T} \right] \quad (2.25)$$

where $E_2 > E_1$. The existence of particles can be in either of the levels. The particle population in level 1 is represented as N_1 , and for level 2, it is represented as N_2 . The total number of the particles is give as:

$$N = N_1 + N_2 \quad (2.26)$$

Fundamentally, when the atomic system is at thermal equilibrium, the population of the lower energy level is more than the higher energy level. The system inherently remains relaxed with no emission of light. Despite increasing the temperature of the system, although the population of higher energy level does increase, it always remains less than the lower energy level. This is elaborated by the Boltzmann distribution equation (Equation 2.25), where it shows that the population of level 1 and level 2 equals only

when the temperature becomes infinite for the system. A non-equilibrium state is necessary to be achieved in order to obtain the optical gain based on stimulated emission. In this state, the population of the lower energy level decreases than the population of the upper energy level, and the condition of the system is termed as population inversion. Such a state is responsible to achieve amplification of the electromagnetic wave. To achieve the non-equilibrium condition having population inversion, there are many methods that have been investigated and proposed.

Basically, there are two schemes / systems with virtue of which laser operation / population inversion can be achieved. These are termed as three-level laser system and four-level laser system. Out of the two, the first system that achieved laser operation was the three-level laser system; however, more widespread is the four-level laser system because of its improved suitability for practical applications. The basic difference between the two laser systems or schemes is the energy level of lower laser. For the three-level laser system, the lower level of laser is the ground state of the system: whereas, for the four-level laser system, it is an excited state of the system. It is supposed that this excited state instantly decays back to the ground state. To establish population inversion in a three-level laser system, the requirement is that at least a half number of atoms of the ground state are excited out of it. This makes use of a considerable amount of pump energy. On the contrary, for a four-level laser system, only a few atoms are required to be excited out of the ground state to achieve population inversion.

2.6.2 Fiber Laser Amplifier

Light amplification can be achieved in a fiber whose core is doped with the atoms that can be laser activated. It is possible provided the wavelength of the optical signal lies within the gain spectrum. This is established by optical pumping to achieve population inversion of the doped atoms. In this scenario, as the fiber guides the light, the

amplification keeps increasing with the fiber length, until a point of saturation is reached. In contrary, in a bulk amplifier, the interaction length is limited owing to the Gaussian type beam propagation, and hence its major limiting factor. So, the level of amplification that is achieved in such fiber lasers is quite high and limited basically by two factors. One is the amount of pump power that is available; second is the initiation of laser oscillations once the amount of amplification becomes equal to optical feedback. This optical feedback occurs because of stimulated Brillouin scattering, Rayleigh scattering, reflections from connections between fibers, and from the ends of the fiber. The gain potential of these fibers is high, and it enables them to achieve laser operation even at lower values of optical feedback. This eases up the actualization of fiber lasers.

The common rare earth elements that are utilized as active dopants in optical fibers include thulium, ytterbium, erbium, or neodymium. Such elements are also termed as lanthanides. When these atoms get ionized in a silica or glass, they make a trivalent state (Er^{3+}). In this scenario, two electrons of 6s shell and one electron of the 4f shell gets discharged, while the outer 5s and 5p shells remain as they are. As a result, the perturbations from external field do not fully influence the remaining 4f electrons, and they remain partially screened out. In contrast, the ions of the transition elements behave differently, in that; their electronic shielding is not at par to that of the rare earth ions. Thus, for rare earth ions, the wavelengths of fluorescence and absorption bear little dependence on the external fields.

2.6.3 Erbium-Doped Fiber

Researchers and scientists showed extraordinary interest in the erbium-doped fiber amplifiers (EDFAs) around the late 1980s, the fruit of which resulted in ubiquitous availability of associated components and related parts and equipment. This further incited preliminary research in various erbium-doped fiber lasers (EDFLs), which had

potential for telecommunication applications. The research on the EDFLs included Q-switched lasers, mode-locked lasers, and multiple-wavelength lasers. This was the period of early 1990s. The energy state diagram for trivalent erbium Er^{3+} in silicate glass is shown in Figure 2.4. In EDFA, the primary transition is ${}^4I_{13/2} \rightarrow {}^4I_{15/2}$, and it provides gain for the spectral region of 1.55 μm . This is because, for the common oxide glasses, ${}^4I_{13/2}$ is the sole metastable state at room temperature, and for these materials, the gain is only available at ${}^4I_{13/2} \rightarrow {}^4I_{15/2}$ emission band of 1.55 μm (Ngo, 2018). 1530 nm is the region around which lie the wavelengths of peak absorption and emission. Thus, the in-band choice of wavelength of operation should be such that the cross section of emission is considerably larger than the cross section of absorption. This is around 1.55 μm region. With the latest technology, the laser diode is used to pump the EDFA around 810, 980, and 1480 nm wavelengths. However, the common practice is to use pump wavelengths of 980 and 1480 nm. The wavelength of 810 nm is avoided as it suffers from intense excited state absorption (ESA), which is wasteful for the pump photons. The most common pumping practice is to use the wavelength of 980 nm (typically in InGaAs/GaAs based lasers) which energizes Er^{3+} ions to ${}^4I_{13/2}$ level. Particularly, for small signal amplifiers, this offers the superiority to achieve greater efficiency in gain and higher signal to noise ratio (SNR) (Piovella & Volpe, 2021). Additionally, for power amplifiers, this also offers superior noise figures (NFs) and enhanced quantum conversion efficiencies.

Erbium-doped fiber (EDF) is beneficial for ultra-short pulse fiber lasers as it possesses wider range of spectrum and has an irregular dispersion at 1.5 μm . The soliton pulse regime of mode-locked fiber laser is supported by the irregular dispersion. In the research presented in this thesis, EDF has been used, obtained as a commercial component from

FiberCore™. The single mode InGaAs laser diode has been used to achieve pumping at 980 nm wavelength. The lasing achieved has been in ~1530-1600 nm wavelength region.

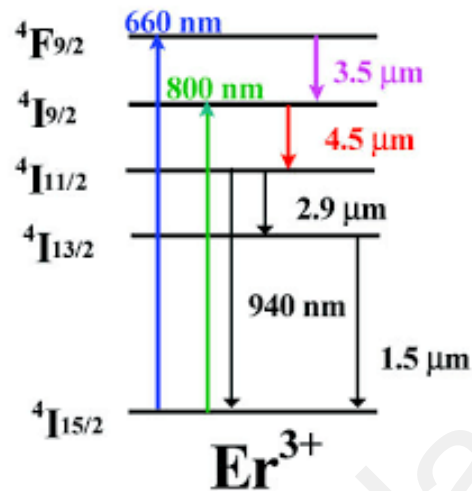


Figure 2.4. Energy level diagram for Er³⁺. Pump transitions are shown in blue, and the specific laser transitions are shown in red.

2.6.4 Ytterbium-Doped Fiber

Fiber laser was discovered first in 1961 (Koester & Snitzer, 1964), and since then, it has emerged as the primary and preferred laser configuration and has grasped the attention of many researchers. After the maiden laser demonstration by Maiman (Maiman, 2010), its role in the progress of the development of photonics technology has been pivotal in its demeanour. The light produced in lasers is based on the quantum impact of excited emission. Lasers are composed of following constituents: an active medium that gives gain, a pumping source that generates the optical energy, and an optical cavity for strengthening and controlling the optical field (Agrawal & Dutta, 1986). The efficiency of Ytterbium-doped fiber laser (YDFL) is the highest among the fiber lasers and finds a variety of utilizations in varying application areas.

Ytterbium (Yb) is an element of the periodic table and lies among the rare earth metals. It can produce laser in the region of 1 micron when its trivalent ion Yb^{3+} is employed as a laser active dopant. The energy diagram of Yb^{3+} depicting sub-level Stark splitting is

illustrated in Figure 2.5. The concentration and location of Yb^{3+} glass dictates the sub-level splitting (Barua, Sekiya, Saito, & Ikushima, 2008; Qiao et al., 2008). Yb^{3+} possesses only one excited state manifold (${}^2F_{5/2}$) that lies inside the reach of the ground-state manifold (${}^2F_{7/2}$).

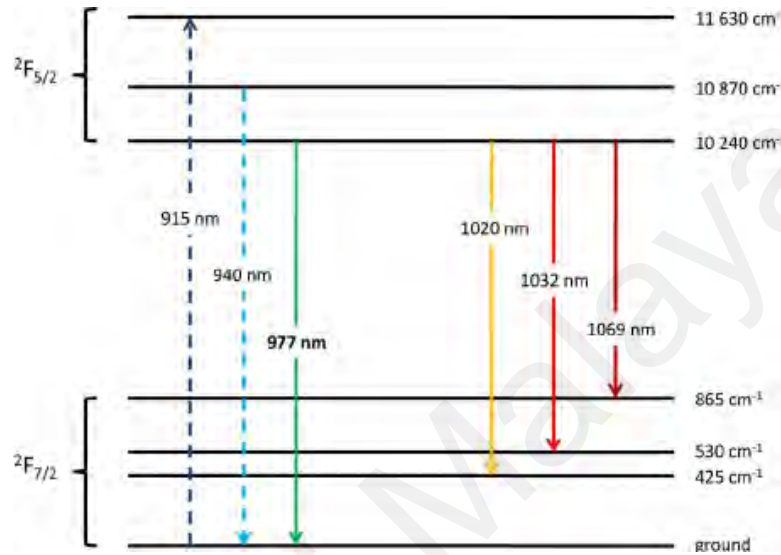


Figure 2.5. Energy diagram of Yb^{3+} ions exhibiting sub-level Stark splitting.

The emission and absorption cross section of ytterbium-doped fiber (YDF) is displayed in Figure 2.6 (Qiao et al., 2008). A wideband absorption spectrum is exhibited by Ytterbium, and which becomes a multi-wavelength pumping process, and later transforms into a high-power operation. Furthermore, this broad spectrum of absorption allows the application of pumps that are low cost and unstable. This aids in reducing the design complexities as well as costs to greater extents and helps in having the fiber lasers that are high powered and remain stable over longer terms. Additionally, thanks to the simplified electronic structure, excited state absorption and other various damaging quenching processes are successfully exterminated. The lifetimes of upper state generally lie in the range of 10 to xx fs, and that is particularly advantageous for mode-locked and Q-switched pulses. Within the wavelength range of 950 to 1100 nm, Yb^{3+} ion has a number of emission transitions. Additionally, a contiguously wide emission spectrum also exists in the 1 μm band. This is by virtue of homogeneous / inhomogeneous widening of

the transitions that occur inside a glass host. It is displayed in Figure 2.6. The host medium determines the lifespan of absorption and emission spectrum (Weber, Lynch, Blackburn, & Cronin, 1983). The wide emission and absorption transitions which constitute the spectrum above appear between the sublevels of ground and the Yb's first excited state. It is necessary to mention that the degeneracy of Yb gets lifted because of the Stark effect. $[Xe] 4f^{13}$ is the electronic configuration of Yb^{3+} .

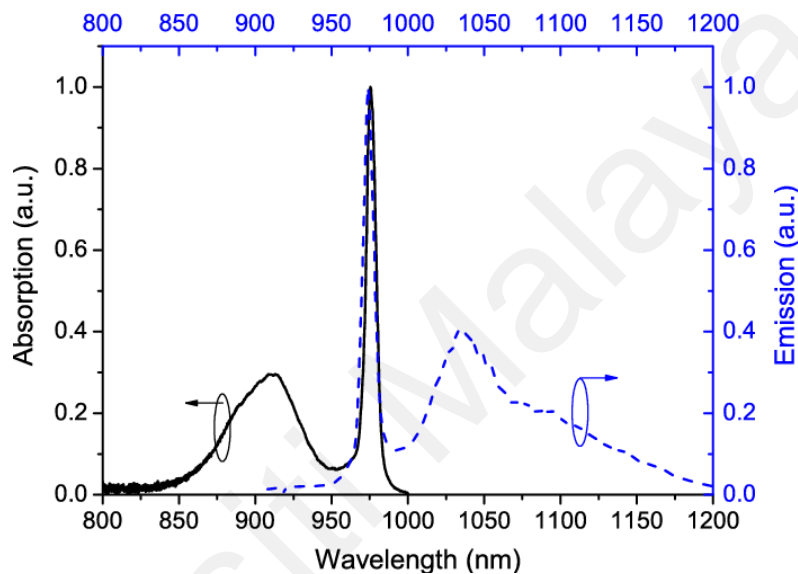


Figure 2.6. Typical absorption and emission spectra of YDF. (Weber et al., 1983)

2.7 Pulse Formation in Fiber Laser Cavity

There has been a growth of tremendous interest recently in short and ultrafast pulsed fiber lasers. These find useful applications in telecommunications, diagnostics and medicine, and micromachining. Furthermore, these are compact in size, can be easily set up, and are of low costs (Grelu & Akhmediev, 2012). These lasers can be produced either passively or actively, depending on the employed technique, and are categorized into two configurations: Q-switched fiber lasers, and mode-locked fiber lasers. The active technique for laser generation is implemented by incorporating an acoustic-optic modulator, which is an external controller device that actively modulates the intra-cavity light (Haikun Zhang, Xia, Song, Wang, & Li, 2018). On the other hand, in the passive technique, the adoption of saturable absorption of optical material to vary the light of

intra-cavity produces the laser pulse (Al-Masoodi, Ahmad, Ahmed, Arof, & Harun, 2017; Alani et al., 2019). In this section, details of the operation principle of Q-switched laser and mode-locked laser are presented, along with a review of the previous literature on these lasers.

Q-switched and mode-locked lasers can be produced by either active or passive techniques. Q-switched laser generated by the passive technique relies on saturable absorber (SA) and gain medium. The saturable absorber acts as a Q-switcher. The lasing starts when flux of the photon begins to show gain and fixed saturable loss (in saturable absorber) after several round trips. The maiden saturable absorber that produced pulse in Nd glass laser was presented in the year 1966 (Stetser & DeMaria, 1966). In the case of passive mode-locking, a saturable absorber is used to generate a significantly shorter pulse width in a range from nano to femtoseconds. This technique is based on the realization of a fixed-phase relationship that exists between those modes of the resonant cavity that are longitudinal in nature. The rate of repetition is the free spectral range, with units of MHz, that is defined for a cavity which has a length of a few meters (Soboh, Al-Masoodi, Erman, Al-Masoodi, Yasin, et al., 2021; Uehara et al., 2019). The primary aim to generate laser with mode-locking approach is to achieve higher rate of repetition. Owing to its simplicity, the passive technique is preferred over the active one for generating Q-switched and mode-locked fiber lasers. These lasers have been thoroughly investigated in recent years, where many different SAs have been proposed (B. Zhang et al., 2020). This thesis aims to present and practically demonstrate the use of new saturable absorbers (SA) to generate Q-switched and mode-locked fiber lasers, operating in the 1- and 1.5-micron region.

2.7.1 Q-Switching

Q-switching is in fact a technique to produce optical pulses. It is realized by modulating the quality (Q) factor of the laser cavity, and the pulses generated are of extremely short duration, ranging about microseconds to nanoseconds. It is important to highlight Q factor here. It is the ratio of stored cavity energy to the energy lost in each cycle of oscillation. The Q factor modulation is realized by incorporating the cavity with an optical loss modulator. The following equivalent equation is used to express the Q factor of the cavity resonator:

$$Q = \nu_o T_{rt} \frac{2\pi}{I} \quad (2.27)$$

where ν_o is the optical frequency, I is the fractional power loss per round trip and T_{rt} is the round-trip time (Su et al., 2018). The initial settings of the modulator give higher losses (and low Q factor), because of which the laser action is avoided. Once the laser is pumped into the cavity, population inversion is enhanced owing to the accumulation of energy in the gain medium.

Once the cavity loss is reduced (realizing high Q factor), output power undergoes an exponential increase as the gain is considerably higher than the loss. This causes the gain medium to saturate, thereby decaying the power to form a pulse. A series of short pulses is generated by cycling the loss modulation, as is shown in Figure 2.7. Electronic shutter, which is a device with an active control, can function as the loss modulator. On the other hand, loss modulation can be realized by a SA. SA is a passive element that yields absorption based on the intensity levels of incident pulse energy. Passive Q-switching technique is beneficial in that the modulator does not require complex electronic system. However, the duration of laser pulse and the rate of repetition rely on the power. The

typical pulse repetition rate of Q-switched fiber lasers is in kHz. The pulse duration is of the order of micro to nanoseconds.

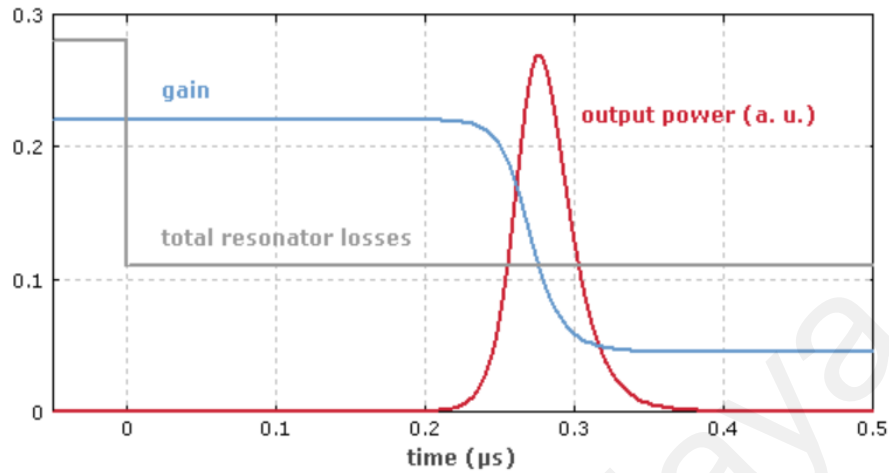


Figure 2.7. Process of the formation of Q-switched pulse, depicting cavity gain and loss modulation.

2.7.2 Mode-Locking

Mode-locking is another technique that produces laser of ultrashort pulses and can be implemented passively by SA. The SA modulates the loss once per cavity roundtrip. A constant phase relationship exists among longitudinal modes. Therefore, the oscillating laser in a mode-locked configuration generates a series of ultrashort pulses. The duration of these pulses is of the order of nanoseconds to femtoseconds, and their rate of repetition is in MHz. The pulse train corresponds to the cavity's free spectral range or to the number of pulses achieved in one second (Chowdhury, Manna, Chatterjee, Sen, & Pal, 2019). In the passive mode-locking, the rate of pulse repetition (f) is expressed as:

$$\text{Repetition Rate, } f(\text{ring cavity}) = \frac{c}{nL} \quad (2.28)$$

where, c is the speed of light ($3 \times 10^8 \text{ms}^{-1}$), n is the medium's refractive index ($n = 1.46$ for silica fiber), and L represents cavity length. From the equation, it can be obtained that the total length of the cavity determines the rate of repetition, and thus, for a short length of the cavity, an increased repetition rate of pulse is achieved.

Full width at half maximum (FWHM) represents the width of the optical pulse. The width is taken at half of the maximum value of power of the laser pulse. Mode-locked laser can generate extremely short widths of the pulse. The greater the number of longitudinal modes characterized by constant phase relationship, the shorter the pulse width. The short pulse duration of the mode-locking mode is process. The relationship between pulse width and bandwidth of the optic fiber pulses useful for many applications including fast optical data transmission and time resolving. Time-resolving is referred to the time-bandwidth product (TBP). As per the Heisenberg principle, there is a limit of TBL below which it is unlikely for the TBP to drop. TBL is given as:

$$TBL \leq \Delta t \times \Delta \nu \quad (2.29)$$

where, Δt represents temporal width of the pulse (in seconds), and $\Delta \nu$ represents the spectral width of pulse (in hertz) measured at FWHM. TBP or TBL limit depends on the shape of the pulse, as elaborated in Table 2.2. The laser's output spectrum (operating wavelength and bandwidth) determines the pulse bandwidth. Its equation is given as:

$$Pulse\ width\ (PW) = \frac{T_{BL}}{BW} \quad (2.30)$$

It is observed from the equation that the width of the pulse can also be approximated from the given optical bandwidth. An auto-correlator is typically utilized to measure the width of the mode-locked pulse. This measurement is based on the estimated pulse shape. The shape of the pulse can be of Gaussian type or secant hyperbolic type, and depends on total cavity depression, output spectrum, and mode-locked operation characteristics. When the depression of the cavity is either zero or approximately zero, the achieved pulse shape is of Gaussian type, and is like a laser with a stretched pulse.

2.8 Saturable Absorber (SA)

Passive Q-switching and mode-locking requires a saturable absorber (SA) device to provide an intensity dependent loss or gain in the laser cavity. SAs are intracavity elements that introduce lower loss for higher intensities. This can be used to discriminate between high intensity pulses and low intensity CW radiation. SAs can be classified as either slow or fast depending on their response time relative to the pulse duration. A slow SA recovers its absorption on a time scale longer than the pulse duration, and its transmission scales with the pulse fluence. A fast SA responds instantaneously to changes in the pulse intensity, and therefore its transmission scales with the pulse intensity. In general, both types of SAs help to form a net gain window that determines the pulse duration and stabilizes the pulse against perturbations. SA is also categorized into two types: real SA, and artificial SA. A real saturable absorber is a material that demonstrates a nonlinear reduction in its intrinsic absorption with increasing intensity of light. On the other hand, an artificial saturable absorber copies the real saturable absorber and induces a transmission that is intensity dependent, but by exploiting the nonlinear effects.

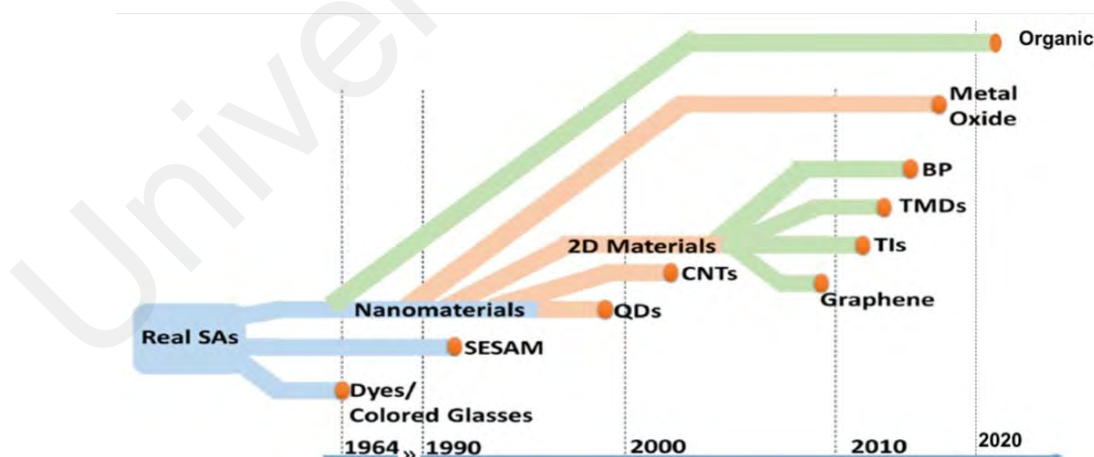


Figure 2.8. The technological evolution of saturable absorber for fiber lasers.

To realize mode-locked and Q-switched lasers, so far, a plethora of saturable absorbers having varying parameters have been studied and explored. In 1965, the maiden SA was tested and demonstrated (Mocker & Collins, 1965). It was made using rhodamine based

organic dye and aided in generating a mode-locked pulse with a width of 10 ns. The history of SA and its technological development is summarized in Figure 2.8 (R. I. Woodward & Kelleher, 2015). After preliminary development of the lasers produced through dye based mode-locked techniques, the further technological progress got slowed until early 1990s, when semiconductor saturable absorber mirror (SESAM) was presented (Keller et al., 1996). Owing to a number of its lucrative features, SESAM quickly turned out to be a successful technological development for generating mode-locked fiber lasers (Okhotnikov, Grudin, & Pessa, 2004). However, it also had some shortcomings such as narrow operating bandwidth, costly manufacturing, diminished damage threshold, lengthened recovery times, and requirement of expensive clean room instruments and equipment. These shortcomings paved the way to research of new SA materials suitable for photonics and laser applications. This included using artificial techniques to manufacture artificial SAs for fiber lasers. The techniques were nonlinear-optical loop mirror (NOLM) (Doran & Wood, 1988), nonlinear-amplifying loop mirror (NALM) (Nakazawa, Yoshida, & Kimura, 1991) and nonlinear polarization rotation (NPR) (Ippen, 1994).

The research and development in nanomaterial SA technology pulled in a large interest of scientists and engineers in the late 1990s. This included the research on one dimensional (1D) carbon nanotubes (CNTs). Since the research demonstrating the nonlinear optical properties of single walled carbon nanotubes (SWCNTs) had been published (Kataura et al., 1999; Margulis & Sizikova, 1998), the interest of researchers had increased manifolds to develop CNTs for various applications. Maiden SWCNT based mode-locked fiber laser was demonstrated in 2004 (Set, Yaguchi, Tanaka, & Jablonski, 2004). Afterwards, SAs based on CNTs have been considered a viable choice for their ease of manufacturing and low cost. It is to note that the wavelength of the CNT based SA relies on the diameter of the nanotube (Zhou, Wei, Dong, & Liu, 2009). Laser

scientists have always been highly ambitious in finding and developing newer and cheaper SAs (example being graphene) to achieve improved broadband performances.

After initial successful demonstration of fiber lasers based on graphene (Bao et al., 2009; Markom et al., 2020; Yusoff et al., 2019), graphene based SAs are considered extremely suitable for mode-locked and Q-switched fiber lasers, and their performance has been significantly ameliorated with time (Popa et al., 2011; Sun et al., 2010). The successful utility of graphene nanomaterial has lured the scientists and researchers to delve deeper into finding other similar two dimensional (2D) nanomaterials to be used in photonics applications (Ahmed, Al-Masoodi, Latiff, Arof, & Harun, 2017; Bonaccorso & Sun, 2014). Lately, SA based on topological insulators (TIs) having an indirect band-gap energy of 0.35 eV and gapless surface states was explored, that turned out to be much efficient for producing pulse in fiber lasers (Y. Chen et al., 2013; Luo et al., 2013). However, its utilization has been unsuitable for photonics applications because of its complex manufacturing process, which consists of preparing a compound of two dissimilar elements.

Recently, the use of black phosphorous (BP), (Y. Chen et al., 2015; D. Li et al., 2016; Sotor, Sobon, Macherzynski, Paletko, & Abramski, 2015; Xia, Wang, & Jia, 2014) and transition-metal dichalcogenides (TMD) such as WSe₂, WS₂, MoSe₂, and MoS₂ (B. Chen et al., 2015; H. Li et al., 2014; Mao et al., 2016; K. Wang et al., 2013; R. Woodward et al., 2014; Han Zhang et al., 2014) have been investigated in SAs for achieving fiber lasing. Graphene is a semi-metal that has zero band-gap energy.

In contrast to this, the band-gap energy of MoS₂ is determined by its thickness. For bulk layers, its indirect band-gap energy is 1.29 eV; and for monolayer, direct band-gap energy is 1.9 eV (S. Wang et al., 2014). Furthermore, the direct band-gap energy of BP varies with the number of layers. For monolayer, it is ~1.5 eV, which tunes down to ~0.3

eV for black phosphorus in bulk (Tran, Soklaski, Liang, & Yang, 2014). This fills up the gap between semi-metallic graphene and wide bandgap TMDs.

Recently, the organic materials have also demonstrated as new SA candidate for generating short optical pulse train due to their fast recovery time, friendly with environment, high optical damage threshold, and large optical nonlinearity. These organic materials are hybrid organic – inorganic perovskites (Huang et al., 2017), tris-(8-hydroxyquinoline)aluminium (Alq₃) (Salam, Harun, et al., 2019) and Bis[2-(4,6-difluorophenyl) pyridinato-C₂,N] (picolinato) iridium(III) (FIrpic) (Salam, Al-Masoodi, et al., 2019). This thesis is aimed to explore the use of two new organic materials: zinc phthalocyanine (ZnPc) and lawsone dye as SA in generating both Q-switching and mode-locking applications.

2.9 Organic Material

2.9.1 Zinc Phthalocyanine

It is widely known and documented that the electrical conductance of phthalocyanines has a strong dependence on the oxygen that gets absorbed in the solid (Ouedraogo, Meunier-Prest, Kumar, Bayo-Bangoura, & Bouvet, 2020). This is because it is supposed that within the lattice, oxygen accepts electrons, leading to the creation of an extrinsic semiconductor of p-type. The chemical and thermal stability of Phthalocyanines (Pcs) is high. They are semiconductors of p-type and yield interesting properties that make them highly desired for technologically advanced applications. They demonstrate photo and dark semiconductivity, as well as photophysical properties. They are particularly coveted for following applications: nonlinear optics (Gounden, Nombona, & van Zyl, 2020), optical recording (M. Yang, Wang, Liu, & Feng, 2018), photodynamic therapy (X. Li et al., 2018), light emitting diodes (LEDs) (Q. Chen et al., 2020), gas sensors (Şahin et al., 2021), and serve as footing for optical sensing (Acikbas et al., 2021). Basing on the

research efforts that aim to find new organic semiconductor materials, a tremendous effort is being put to design and develop cost effective and highly efficient photovoltaic energy converters. The Pcs were employed as a thin film in these devices. The knowledge about microscopic characteristics of these materials is obtained based on optical constants of the thin films. This knowledge serves as the basis of the way these films are going to be utilized in the design of these devices. The effect on the absorption spectrum of phthalocyanine films because of its central metal atom has been explored and measured by Davidson (Davidson, 1982). The spectra of near ultraviolet and visible regions have been observed for thin films made of the following: FePc, MgPc, CoPc, H₂Pc, and ZnPc. The measurements of the spectra of absorption index and refractive index were not done. These measurements are based on the film's optical properties, such as reflectivity and transitivity.

Zinc phthalocyanine (ZnPc) is also a promising organic semiconductor for optical applications. The crystal structures of the ZnPc polymorphs are shown in Figure 2.9. Zinc phthalocyanine (ZnPc) yields strong absorption cross section with a span of 650-900 nm, and serves as an efficacious photosensitizer, ensuring utmost tissue penetration. The ZnPc molecules in the LB thin film on a solid substrate demonstrate three aggregates. These are: H, J and monomer. The variation in the aggregation or arrangement of ZnPc molecules takes place once annealing is achieved on the surface of the substrate. This is confirmed by observing modification of the absorption spectrum in Q-band. The annealing takes place once the temperature is above 55 °C. ZnPC thin film, after annealing, comprises of different proportions of monomer and H aggregates.

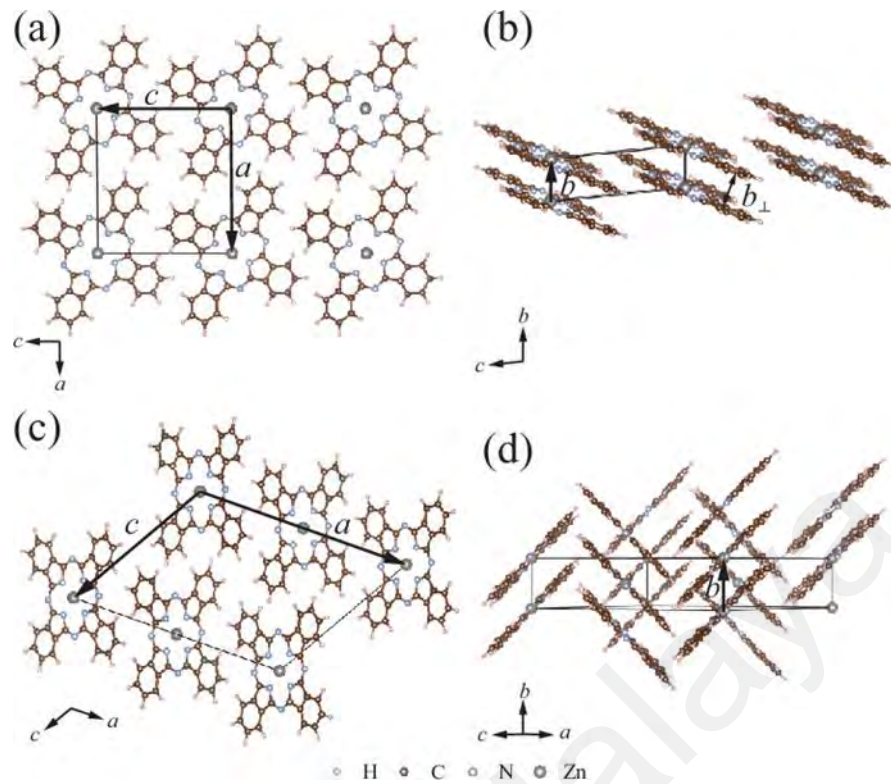


Figure 2.9. Crystal structures of the ZnPc polymorphs. For α -ZnPc, projection is shown on (a) [010] plane and (b) [100] plane. For β -ZnPc, the projection is illustrated on (c) [010] plane and (d) [110] plane.

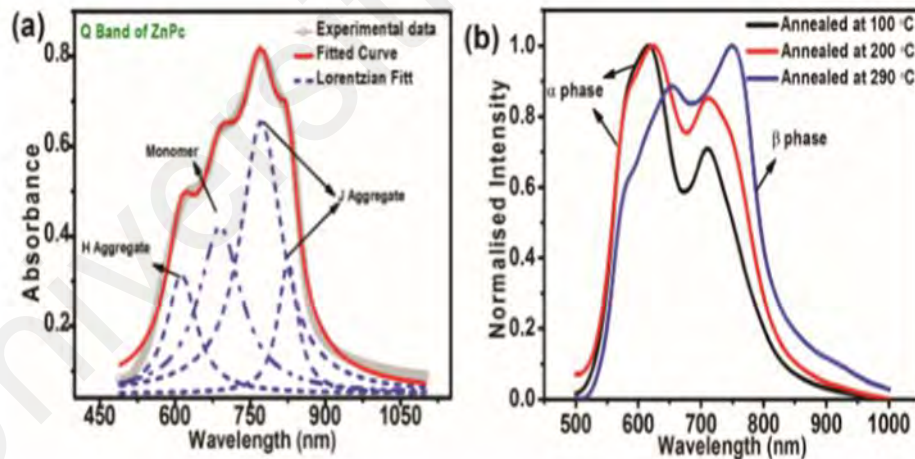


Figure 2.10. Q-band absorbance spectra of ZnPc thin film in (a) as-deposited state, and (b) at different annealing temperatures.

The J aggregates are not found. Up until the annealing temperature of 200 °C, the absorption spectra of the thin film remain unchanged. This is termed as the α -phase of ZnPc(Kozlik, Paulke, Gruenewald, Forker, & Fritz, 2012; Roy, Das, Shakti, & Gupta, 2014). The α -phase is identified by the intensity of low energy absorbance peak observed in the Q-band. If it remains less than the intensity of the high energy absorbance peak,

ZnPc is in the α -phase. On further increase of annealing temperature, i.e. above 200 °C, the configuration of absorbance spectra of Q-band gets reverted. This corresponds to the phase transformation of the ZnPc LB thin film. The α -phase gets translated to the β -phase, and the transformation finishes around 290 °C. This process is illustrated in Figure 2.10 (Kozlik et al., 2012; Roy et al., 2014).

2.9.2 Lawsone Dye

The use of natural materials for dyeing wool was hypothesized as far back as 415 BC (Singh, Jain, Panwar, Gupta, & Khare, 2005). The first synthetic dye -Mauve- was discovered in 1856. However, due to the toxic effect of synthetic dyes on the environment, the use of eco-friendly natural dyes became the subject of immense importance (Samanta, Awwad, & Algarni, 2020). Over the past decades, the natural dyes have been increasingly used as an alternative of synthetic dyes, particularly because of their influence on biological systems (Chomean, Nantabut, Kongtia, Saenguthai, & Kaset, 2019). Lawsone (2-hydroxyl- 1,4- naphthoquinone) is a prominent natural dye. It is the major coloring element present in the dried leaves of henna plant, with a concentration of about 1-1.5%. Lawsone reacts chemically with the protein keratin in the skin and hair, via Michael addition, and makes a permanent stain. The lawsone is used as a classified electrochemical and colorimetric sensor for anions, such as cyanide (Chaudhary, Goyal, & Poonia, 2010; Jain, Shah, Sonani, Dhakara, & Patel, 2010; Muhammad & Muhammad, 2005). Presently, different approach is being used for the synthesis of non-biodegradable chemical compounds. Such compounds cause health and environmental concerns. Based on the properties of the natural dye, its use in the pharmaceutical industry has been witnessed since long; however, the exact structure of the natural dye has been known just recently. Most of the plant extracts of the dye are classified for medicinal uses and have been recently proved to have antimicrobial agents- owing to the presence of many tannins. The properties of Henna correlate to the existence of this natural compound. It is

practically insoluble in water; whereas, it is soluble in methanol, dichloromethane, acetone, chloroform, ethyl acetate, isopropyl alcohol, diethyl ether, dimethylformamide (DMF), and dimethyl sulfoxide (DMSO) (Borade, Kale, & Shete, 2011). UV absorption and corrosion inhibition is attributed to the presence of lawsone (Dananjaya, Edussuriya, & Dissanayake, 2012). The solubility of these dyes is limited, and this problem is resolved by virtue of dye polymers. The dyes can either integrate into the polymer backbones, or get enclosed as side chains (Mahkam, Kafshboran, & Nabati, 2014).

Based on their structures, they are categorized as graft and block types. Either to be of graft or block type, polymeric dyes offer the advantage of allowing a range of physical properties, such as tunable absorption, viscosity, solubility, and migration. The range of colors and the polymeric chemistry is endless (Armenta-Villegas, Perez-Martinez, Navarro, & Ogawa, 2009). Presently, they are being applied in hair dyes (García et al., 2012), fibers (Mahkam, Nabati, Latifpour, & Aboudi, 2014), jet-printing (Feldman, 2008; Koseva, Novakov, Rydz, Kurcok, & Kowalczyk, 2010), and solid-state polymeric dye lasers (Beristain, Nakamura, Nagai, & Ogaw, 2009; Pillai, 2010).

CHAPTER 3: PREPARATION AND CHARACTERIZATION OF ORGANIC MATERIAL BASED SATURABLE ABSORBERS

3.1 Introduction

Recently, several new SAs based on organic material have also been proposed for pulse generation owing to their large optical nonlinearity, fast recovery time, high optical damage threshold and friendly with environment. These organic materials are Bis[2-(4,6-difluorophenyl)pyridinato-C2,N](picolinato) iridium(III) (FIrpic) (Salam, Al-Masoodi, et al., 2019), tris-(8-hydroxyquinoline) aluminium (Alq_3) (Salam, Harun, et al., 2019) and hybrid organic–inorganic perovskites (J. Wang, Wang, Chen, Yang, & Lv, 2019).

In this thesis, the use of two types of organic materials: zinc phthalocyanine (ZnPc) and lawsone dye as SA device are explored for pulse generation. In this chapter, the preparation and characterization of these SAs are thoroughly described.

3.2 The Preparation and Characterization of Zinc Phthalocyanine Thin Film Based SA

Phthalocyanine (Pc) is a well-known organic semiconductor which optical, electronic and photoelectronic properties are being extensively investigated and it is suitable for use in photovoltaic devices since its physical and chemical durability is very high (W. Li, Yu, Higgins, Llanos, & Chen, 2010; Martinez-Diaz, de la Torre, & Torres, 2010). Many kinds of phthalocyanines, such as metal-free phthalocyanines and phthalocyanines with various metals have been synthesized and are now utilized in a wide variety of fields like solar cells, clinical photodynamic therapy and electrocatalytic oxidation (Matsuo, Ogumi, Jeon, Wang, & Nakagawa, 2020; Valli, Vior, Roguin, & Marino, 2020; A. Wang et al., 2019). Among these materials, zinc phthalocyanine (ZnPc) is a promising organic semiconductor for optical applications. For instance, ZnPc can absorb the incident light in the visible region to effectively contribute in photocarrier generation in the

photovoltaic application (Louazri, Amine, Bouzzine, Hamidi, & Bouachrine, 2016). Moreover, ZnPc was also used in the characterization of the excited states of the Pc ring (McKearney et al., 2018). Furthermore, the Zn gives phthalocyanines valuable fluorescence and singlet oxygen production properties, which allow their use in the detection and treatment of tumors, has been the interest in the spectroscopic properties of ZnPc and its peripherally substituted derivatives (Kruchinin, Klyamer, Spesivtsev, Rykhlitskii, & Basova, 2018).

On the other hand, the ZnPc has a high absorbance in red-visible region with high extinction coefficient, good optical stability, and high emission ability in the near infrared region. Their thermal stability is good which has possibility of processing in the form of thin films. However, it has low solubility in most organic solvents that restricts of their application (Borovkov, Odintsova, Petrenko, & Kolker, 2019). Three methods were performed in the study which showed the liquid phase exfoliation is the most effective approach. It leaves the agglomeration particles with not uniform distribution and spin-coated removes the large undissolved particles leading to reduction in the absorbance intensity. Liquid phase exfoliation spreads the undissolved particles within the polymer in most uniform along the thin films and produces higher absorbance in near infrared region. This is due to the existence of large amount of undissolved ZnPc particles (Hussein & Kadhim, 2019).

In this section, the fabrication and characterization of ZnPc based SAs are described. The SAs were prepared in three different methods, which are referred to embedding ZnPc:PVA, casting ZnPc/PVA, and spin-coating ZnPc/PVA thin film.

3.2.1 Preparation of the SA Films.

Organic dye material, Zinc phthalocyanine (ZnPc) and polyvinyl alcohol (PVA) powders were used for fabricating the composite thin film, and they were purchased from Sigma Aldrich. The molecule structures of ZnPc and PVA are shown in Figures 3.1 (a) and (b), respectively. Pure PVA solution was prepared by adding 1 g of the PVA powder into 100 ml of distilled-water and then sonicating the solution for one hour at room temperature using ultrasonic bath sonicator. On the other hand, ZnPc solution was produced by adding 10 mg of ZnPc powder into 0.5 ml of acetone before it was stirred using magnetic stirrer for about 30 minutes at 45°C temperature to produce homogenous solution. Composite material of the organic dye material was integrated with polymer thin film by three methods. The first method was based on a liquid phase exfoliation which involves stirring and casting processes of the mixing solution contained 5ml of PVA and 0.5 ml of ZnPc solution. The stirring process was carried out for about 3 hours at room temperature. In the casting process, the mixing solution was poured onto a borosilicate glass petri dish was a diameter of 60 mm and then annealed at 45°C temperature for about 3 hours. This method produced homogenous thin film of organic material with polymer mixture, which is then referred to embedding ZnPc:PVA thin film. The thickness of the film was about 50 μm . Figure 3.2 summarizes the fabrication process of the embedding ZnPc:PVA thin film.

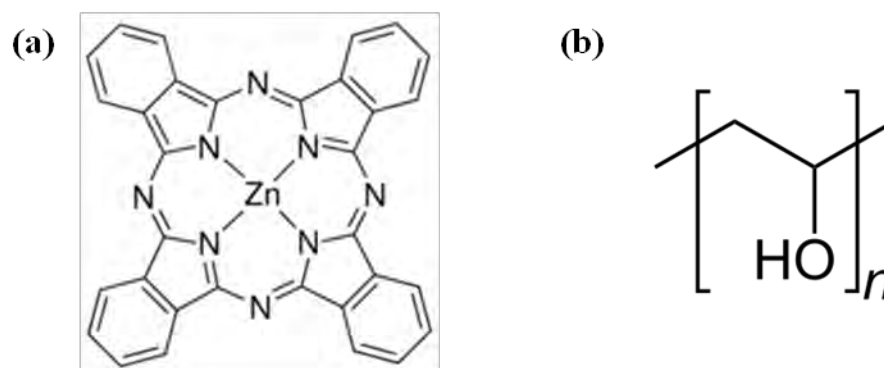


Figure 3.1. Molecular structures of (a) ZnPc and (b) PVA.

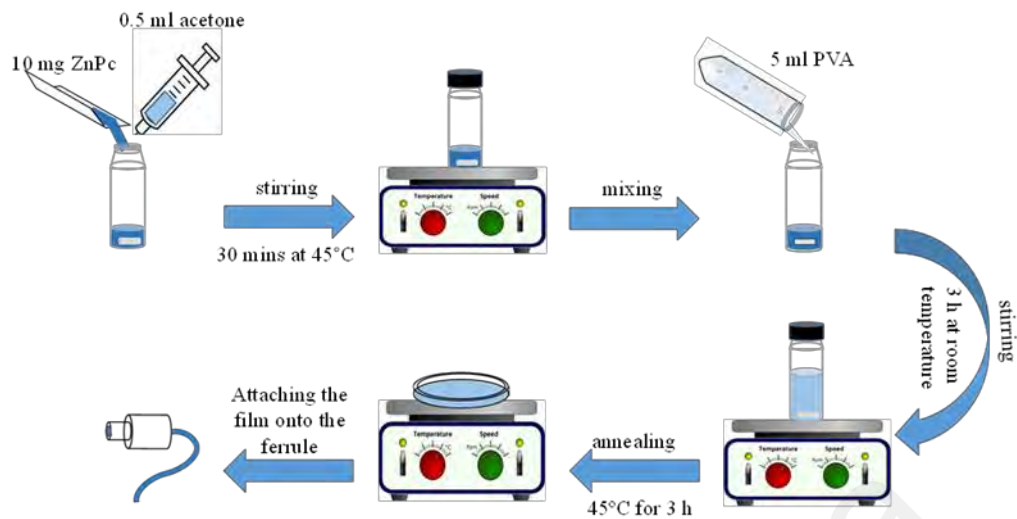


Figure 3.2. Step by step process on fabricating ZnPc:PVA thin film based on embedding technique.

The second film was obtained by a casting method. The organic material solution was poured onto a PVA thin film and it was dried at 45°C temperature for about 30 minutes to produce a casting ZnPc/PVA thin film. The PVA thin film was prepared by pouring 5ml of PVA solution into the glass petri dish and drying at room temperature for 3 days. The third film was prepared based on spin-coating method, where the organic material solution that was spin-coated onto the PVA thin film. Previously, the thin PVA was prepared onto a glass substrate. After the spin-coating, the ZnPc coated onto the PVA film was annealed at 45°C temperature for 30 minutes to produce spin-coating ZnPc/PVA thin film. The thickness of organic thin film on the polymer was in nanometer scale, so the whole thickness of the prepared thin films was about the same thickness to the prepared polymer thin film which is about 50 μm . Finally, small piece of the thin film was inserted between two clean fiber ferrules to form a SA device for Q-switching and mode-locking applications.

3.2.2 Characterization of the SA films.

Chemical groups in the composite materials were investigated using Perkin Elmer Spectrum 400 Fourier Transform Infrared Spectroscopy (FTIR) Spectrometer. ZnPc:PVA thin film was analyzed by FTIR using transmission mode. Scanning electron

microscopy (SEM) images were also obtained at 1 kV of electron accelerating voltage and 3.1 mm for the working distance. UV-VIS-NIR spectrophotometer (Perkin Elmer, Lambda 750) is used to measure the absorbance of the prepared composite material thin films prepared in different methods in the wavelength range of 250-2000 nm.

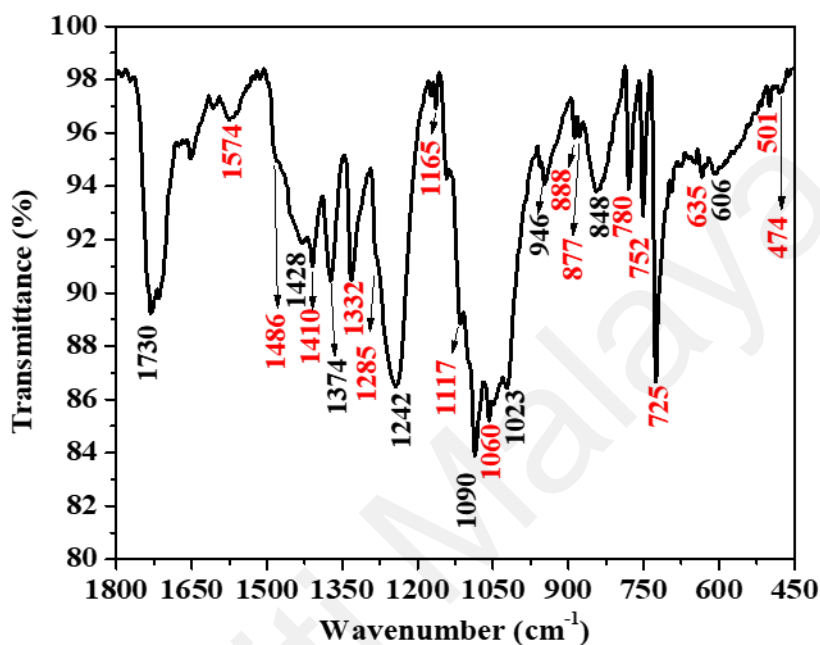


Figure 3.3. FTIR of ZnPc:PVA thin film; the black and red numbers are the vibration peaks of PVA and ZnPc, respectively.

The FTIR spectrum of ZnPc:PVA thin film, which was obtained through embedding approach is plotted and shown in Figure 3.3. It was obtained within the wavenumber range from 1800 to 450 cm^{-1} and a resolution of 2 cm^{-1} . As shown in the figure, the spectrum peaks at 1428, 1374, 1242, 946 and 606 cm^{-1} , which corresponds to CH₂ bending, (CH+OH) bending, CH wagging and CH₂ rocking and (OH) wagging vibration peaks, respectively. Other peaks were also obtained at 1730, 1090, 1023 and 848 cm^{-1} , which are belonged to C=O stretching, C-O-C, C-O and C-C stretching vibration peaks of the pristine PVA, respectively (Alhazime, Barakat, Benthami, & Nouh, 2021). The ZnPc is a complex molecule leading to appearance of stretching and bending vibrations in the spectra. The ZnPc stretching vibration peaks are shown at 1574, 1410 and 888 cm^{-1} which are related to C=C, isoindole and Zn-N, respectively. The in-plane bending

vibration peaks of ZnPc are located for C-H bend at 1285, 1165, 117, 1060 and 752 cm^{-1} , Zn-N at 877 and 501 cm^{-1} , C-N-C at 1486 cm^{-1} , pyrrole at 1332 cm^{-1} , and isoindole at 635 and 474 cm^{-1} (Socol, Preda, Stanculescu, Stanculescu, & Socol, 2017). Moreover, out-plane C-H deformation peak is shown at 725 cm^{-1} , and benzene breathing vibration peaks are at 888 and 780 cm^{-1} . It is worthy to note that two other films show the similar spectrum.

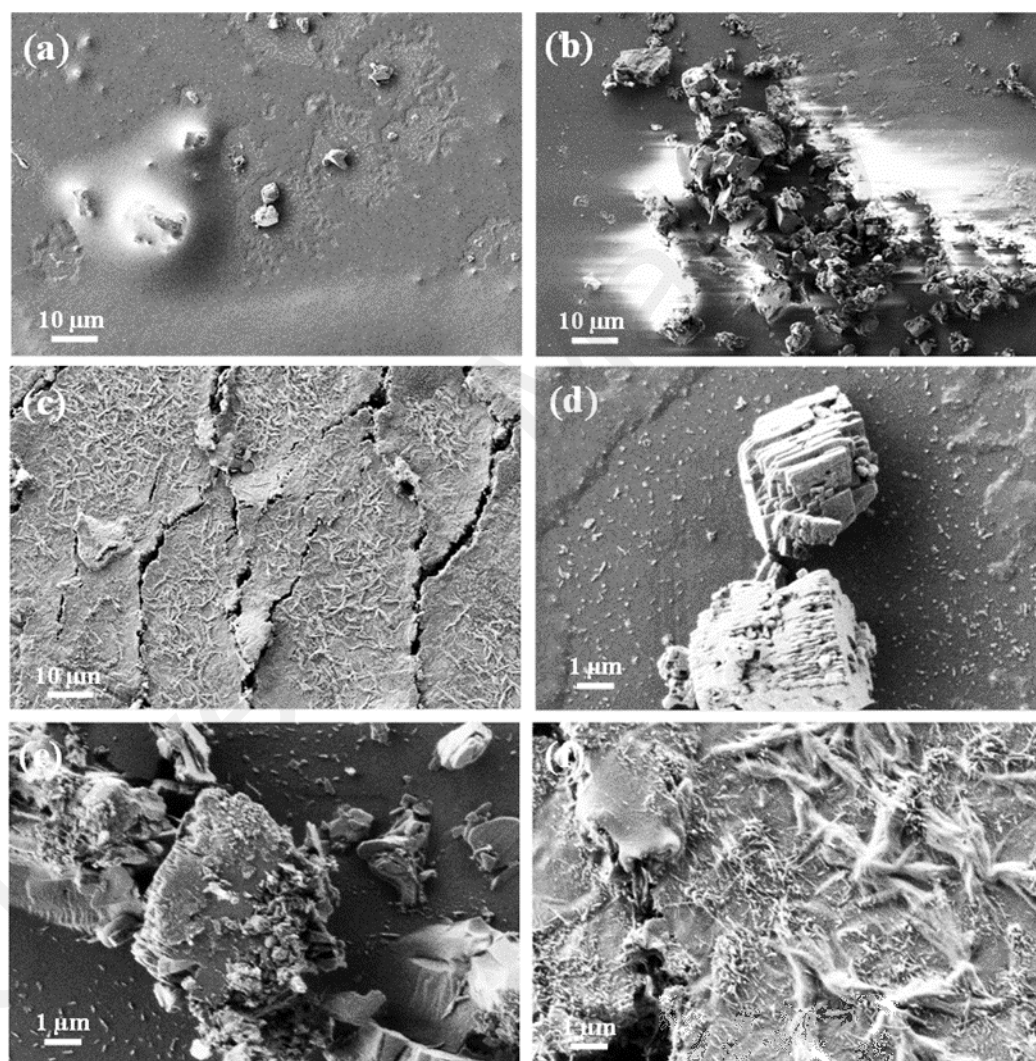


Figure 3.4. (a–c) SEM images for different methods of spin-coating ZnPc/PVA, casting Znpc/PVA, and embedding ZnPc:PVA thin films, respectively. (d–f) High magnification SEM of the respective methods.

SEM images of the prepared thin films at different methods are shown in Figure 3.4 (a – c). The surface morphology of the spin-coating ZnPc/PVA and casting ZnPc/PVA thin films reveals the formation of flat surface with some particles coming from undissolved

particles (Figures 3.3(a & b)). However, the particles at casting method showed more size and higher agglomeration than at spin-coating method due to the spin process that removes the large particles and prevent the particles agglomeration as can be seen in Figures 3.4 (d & e). Figure 3.4 (c) illustrates the embedding ZnPc:PVA thin film in wrinkled surface due to the undissolved particles in the mixed solution. The annealing temperature increases the mobility of the undissolved particles along the polymer molecule leading to increase the surface area by wrinkles, as clearly shown in the high magnification SEM image of Figure 3.4 (f).

Optical absorbance spectra of pure PVA and different methods for ZnPc thin films in wavelength range from 250nm to 2000 nm formation are shown in Figure 3.5 (a). The PVA peak is at around 317 nm which is assigned to $\pi \rightarrow \pi^*$ transition of PVA material (Aziz, Rasheed, Saeed, & Abdullah, 2017; Elashmawi, Hakeem, & Selim, 2009). The ZnPc organic material produced two types of energy bands; B-band and Q-band, as can be seen by two broad peaks in Figure 3.5 (a). The B-band is centered at 346 nm while the Q-band is at 618-630 nm with shoulder at 677 nm. The Q-band energy was related to the first $\pi \rightarrow \pi^*$ transition on the phthalocyanine macrocycle and the shoulder was assigned to an exciton state (Hamam & Alomari, 2017; Hussein & Kadhim, 2019; Novotný et al., 2016). The change in the Q-band energy with different methods belongs to the different aggregation of the ZnPc particles along the thin film and showed red-shift with increasing in the absorbance intensity due to increase in the aggregation of ZnPc particles. Moreover, the wider Q-band energy was at ZnPc:PVA thin film that is due to a whole stacking of organic molecules along the PVA molecules. The absorption coefficient (α) is to be measured by Beer-Lambert's law follows: $(\alpha) = 2.303 \times Abs(\lambda)/d$, where d is the thin film thickness which is equal to 50 μm . The optical band gap, E_g , can be measured from the absorption coefficient in equation $(\alpha hv)^n = B(hv - E_g)$ by extrapolating hv to $\alpha = 0$, where B is a constant relative to the material, hv is the

photon energy and n equals to 2 for direct transition. The energy band gaps of bulk ZnPc are 2.97 and 1.53 eV belongs to B-band and Q-band energy, respectively (Hamam & Alomari, 2017). There are three observed band gaps of the composite thin films which are at 4.2, 3-2.7, and 1.75-1.2 eV corresponding to modified PVA, and B-band and Q-band for ZnPc, respectively. The increasing and decreasing of the band gap in the composite thin film prepared at different methods compared to the bulk ZnPc are due to different dispersion of the ZnPc particles along the thin film. It is also worthy to note that the zinc-phthalocyanines has a high nonlinear absorption coefficient in polymeric matrix (Mgidlana, 2019). The nonlinear optical coefficient, β , was calculated to be within 29 to 43 cm/GW at 500 nm.

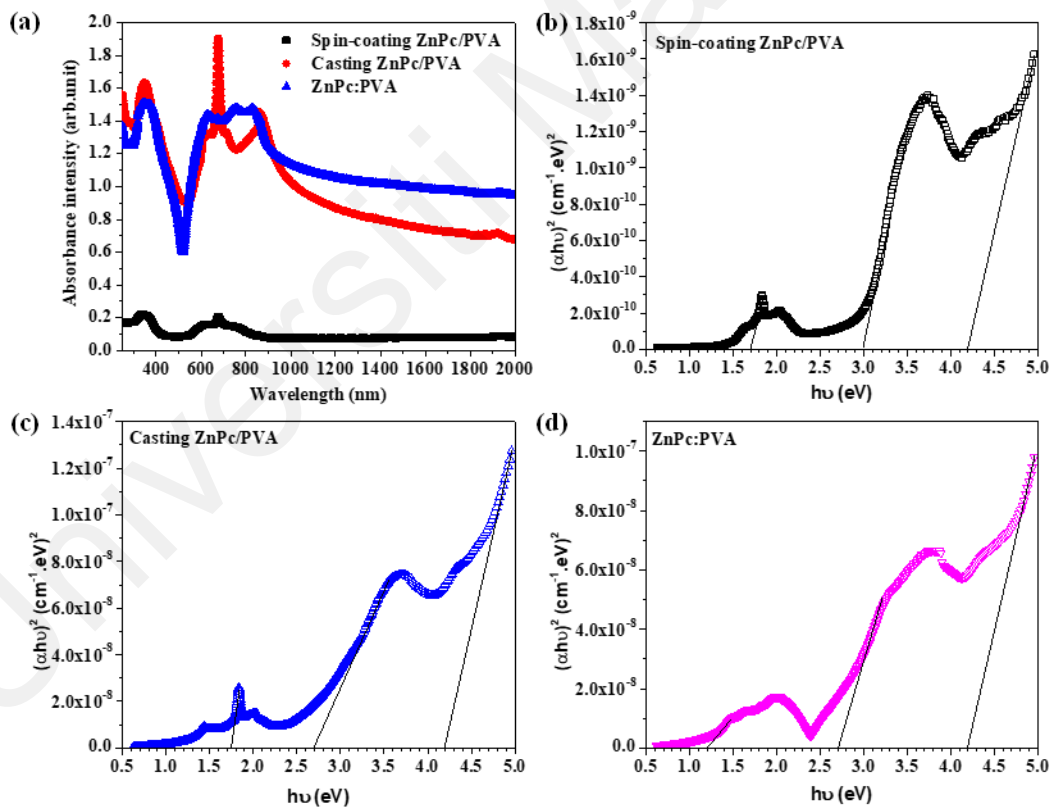


Figure 3.5. (a) Optical absorption spectrum of pure PVA and ZnPc thin films prepared at different methods. (b-d) Tauc's plot for the composite materials of ZnPc and PVA thin films prepared at different methods.

The nonlinear absorption property of the prepared ZnPc:PVA thin film is characterized utilizing a standard balance twin-detector measurement scheme at the operation

wavelength of 1566 nm. A mode-locked laser, which is amplified by the EDFA medium is used as a light source while attenuator is used to control the laser output power so that the nonlinear optical transmission curve can be obtained. Figure 3.6 shows the nonlinear curve for the embedding ZnPc:PVA thin film. As seen, the modulation depth and saturation intensity of the ZnPc:PVA SA are estimated to be approximately 10% and 6 MW/cm² respectively, by calculating the readings from the power meters with fitting the readings data based on the formula shown below (Q. Li et al., 2019):

$$T(I) = 1 - \Delta T \times \exp\left(-\frac{I}{I_{sat}}\right) - T_{ns} \quad (3.1)$$

where T , ΔT , and T_{ns} are the transmission ratio, modulation depth and non-saturable absorption while I , I_{sat} are the incident laser intensity and saturation intensity on the sample, respectively. The nonlinear property of other thin films was also measured using the similar approach. The modulation depth of the casting and spin-coated ZnPc:PVA thin films are 7.8% and 7.2 %, respectively.

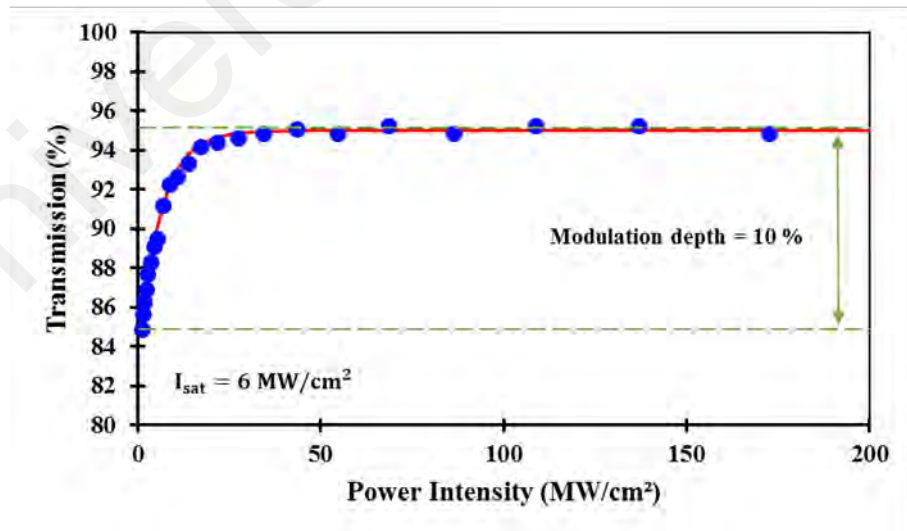


Figure 3.6. Nonlinear optical transmission curve of the embedding ZnPc:PVA thin film SA.

3.3 The Preparation and Characterization of Lawsone Dye Material-Based SA

Natural dyes are dyes or colorants acquired from plants, minerals, and/or invertebrates. They are widely utilized in the dyeing of cosmetic industries, textile materials, and traditional medicine because they have a non-carcinogenic, non-toxic, and biodegradable nature (Makhija et al., 2011; Soboh, Al-Masoodi, Erman, Al-Masoodi, Nizamani, et al., 2021). Henna (*Lawsonia inermis*) is one of the dye materials, which is the plant's leaf, traditionally practiced in obtaining the colored scheme on the woman's hands. The plant's leaf is dried, smashed, and then boiled with water to remove the dye from the leaf. The mordanted fabric produces color from brown to dark yellow color. For instance, *Lawsonia* colors silk and wool by providing a brighter brown color. Besides, Henna is generally known as lawsone. The main component of henna sheets is hennotannic acid, which is a red-orange color. From a chemical perspective, hennotannic acid is a 2-hydroxy-1,4-naphthoquinone, and its color molecules have powerful stability for protein fiber. Furthermore, lawsone dye does not afford degeneration against UV – irradiation, electrochemical perturbation, and sonication. Consequently, the natural dye can stay longer on the skin or fabric without any harmful effects. (Chandrakalavathi, Sudha, Sindhuja, Harinipriya, & Jeyalakshmi, 2018). Lately, lawsone dye was derived from henna and applied as photosensitizers in the dye-sensitized solar cell's preparation and fabrication process (Saadaoui et al., 2017; Safie et al., 2015). Lawsone presented large nonlinear optical properties at low input power and it has advantages over other materials for its stability and viability in nature (Bhuiyan, Islam, Ali, & Islam, 2017). In this thesis, the potential of lawsone based SA, which was fabricated using liquid-phase exfoliation technique is investigated for generating Q-switched and mode-locked pulses, for the first time. This section describes the fabrication and characterization of the SA.

The composite lawsone: PVA thin film was obtained based on the liquid-phase exfoliation technique. The lawsone and PVA molecular structures are shown in Figure

3.7. PVA solution was made by adding a commercial PVA powder (1 g) into distilled water (100 ml) followed by sonicating them using the ultrasonic machine for one hour, to obtain a homogenous liquid solution. The PVA was preferred as a polymer host due to its high chemical resistance and robustness (Wu, Zhang, Wang, Li, & Chen, 2015). The mixture solution of lawsone and PVA was obtained by adding 15 mg of lawsone powder into 5 ml of previously prepared PVA liquid solution. It was then stirred at temperature of 50°C for about an hour. After that, the small portion of the mixed solution was dropped into a petri-dish, which was then dried in an oven. The oven was set at the drying temperature and time of 60°C and 24 hours, respectively, to compose a thin solid film of lawsone: PVA. The thin film was cut into a tiny piece and then attached to the tip of the fiber ferrule so that it can be mated to another ferrule to prepare a fiber compatible SA device. The thin film thickness was measured to be about 45 μm using a stylus surface profiler (KLA Tencor P-6).

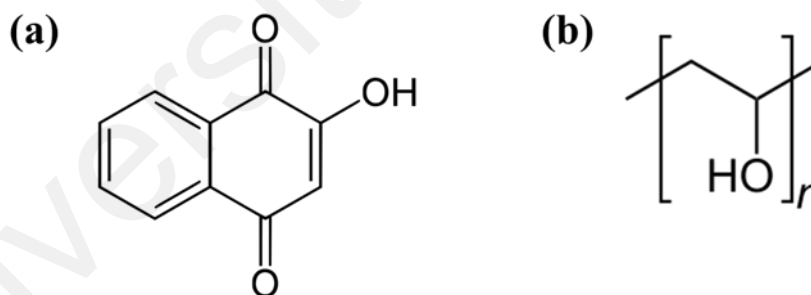


Figure 3.7. Molecular structures of (a) lawsone and (b) PVA.

Fourier Transform Infrared (FTIR) Spectrometer (Perkin Elmer Spectrum 400) was deployed to observe the chemical groups of the lawsone powder and lawsone:PVA thin film. The FTIR spectra of the lawsone powder and lawsone:PVA were achieved and analyzed based on transmittance mode. Figure 3.8 presents the FTIR results within a wavenumber range from 4000 to 600 cm^{-1} at 2 cm^{-1} resolution. The broad bands centered at 3300 and 3274 cm^{-1} were obtained due to the stretching vibration of hydroxyl-group from the intermolecular and intramolecular hydrogen bonds of both lawsone and PVA

molecules and the free hydroxyl-group of phenol of lawsone powder, respectively(Chandrakalavathi et al., 2018; Salam, Harun, et al., 2019). Small sharp bands at 2930 and 2849 cm^{-1} attributed to the C–H stretch from alkyl groups in the PVA and aliphatic and aromatic C–H group in the lawsone molecules. The vibration of carbonyl bond (C=O) was observed at bands of 1727 and 1621 cm^{-1} from the saponification reaction of polyvinyl acetate in PVA and the aromatic ring in the lawsone molecular (Alhosseini et al., 2012; Safie et al., 2015). The small band at 1514 cm^{-1} which appeared in the FTIR of the lawsone powder is attributed to aromatic C=C stretching of lawsone molecules (Chandrakalavathi et al., 2018). The peaks 1446, 1380 and 1314 cm^{-1} are attributed to C=C aromatics of the lawsone molecules (Saadaoui et al., 2017). The peak at 1236 cm^{-1} is attributed to C-H vibration that increases at thin film due to the mixture with PVA (Salam, Harun, et al., 2019). The peaks at 1095 and 1009 cm^{-1} were assigned to the C-O stretch vibration mode in the PVA and lawsone molecules. The peak bands at 835 and 764 cm^{-1} are corresponding to the C-H wagging group in the molecules.

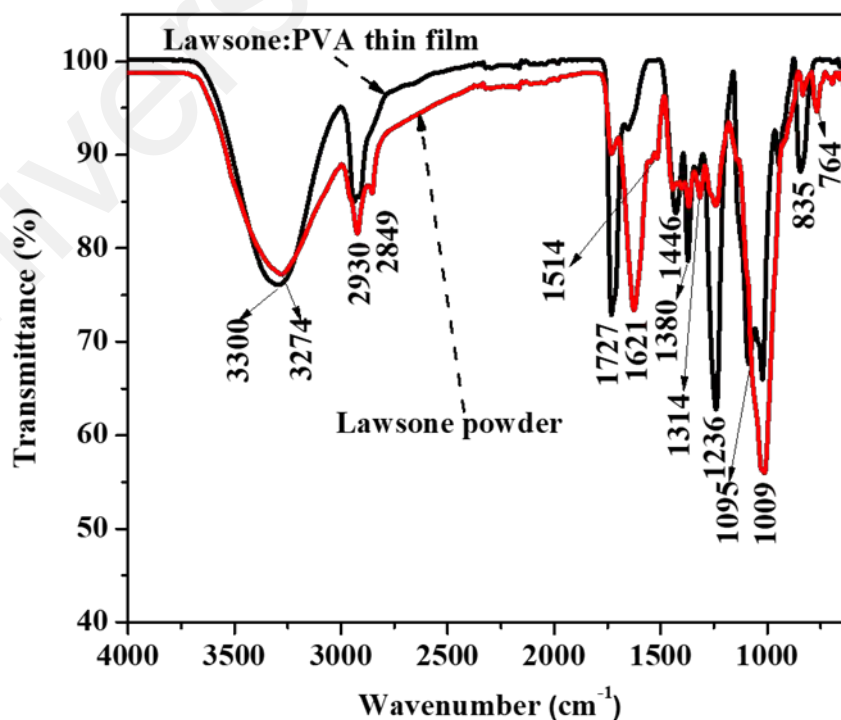


Figure 3.8. FTIR spectra of lawsone powder and lawsone: PVA thin film.

The optical absorbance spectra of the lawsone: PVA and pure PVA thin films are illustrated in Figure 3.9. A peak spotted at 669 nm belongs to the absorption band of the lawsone molecule. Absorbance band in the range of 250-300 nm corresponds to the $\pi \rightarrow \pi^*$ transition of PVA material (Aziz et al., 2017; Soboh et al., 2020). The lawsone:PVA thin film's optical band gap, E_g can be determined from the equation of $(\alpha h\nu)^n = B(h\nu - E_g)$, where B is a constant relative to the material, $n=2$ for direct transition, and $h\nu$ is the photon energy. The absorption coefficient (α) was calculated from the Beer-Lambert's law: $(\alpha) = 2.303 \times Abs(\lambda)/d$, where d is the thin film's thickness. The horizontal axis of the linear region of $(\alpha h\nu)^2$ was extrapolated against $h\nu$ to calculate the optical bandgap. As displayed in the inset of Figure 3.9, the bandgap was estimated at approximately 1.9 and 2.7 eV. These band gaps correspond to the lawsone and doped PVA by lawsone material, whereas pure PVA's original band gap is 6.28 eV (Abdullah, Aziz, Omer, & Salih, 2015; Safie et al., 2015).

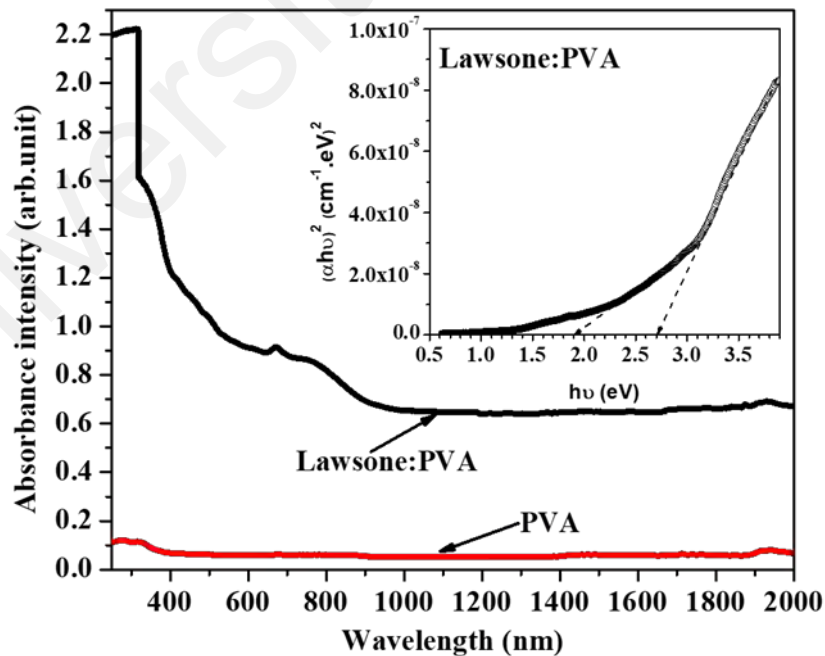


Figure 3.9. Absorbance spectrum of lawsone: PVA and PVA thin films. An inset figure is the calculated optical band gap of lawsone: PVA thin films obtained by extrapolation to $\alpha = 0$.

The surface structure of the fabricated Lawsone: PVA film was investigated by scanning Electron Microscope (SEM) image, as illustrated in Figure 3.10, at a low electron-accelerating voltage of 1 kV and working distance of 4.8 mm. The SEM image appeared uniform several islands in size range between 0.5 to 7.5 μm on the thin film surface coming from the dispersion of lawsone pigment dye along with the polymer (Figure 3.10 (a)). The SEM at higher magnification shows the random shapes of the lawsone dye segments due to the expansion of the polymer during the drying process, as observed in Figure 3.10 (b).

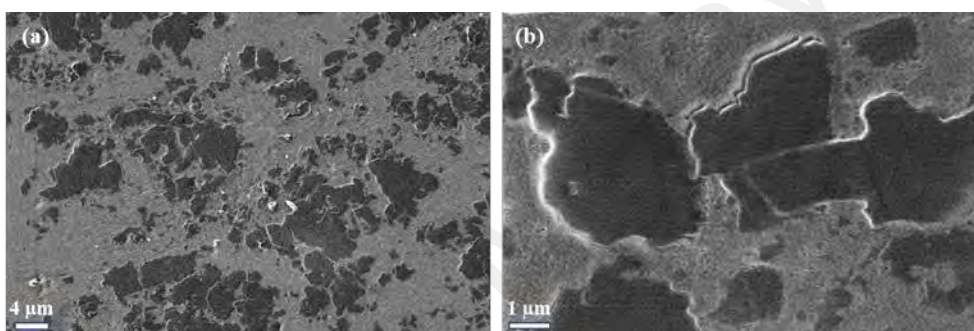


Figure 3.10. The lawsone: PVA thin film SEM image in magnification of (a) 2 K X, and (b) 10 K X.

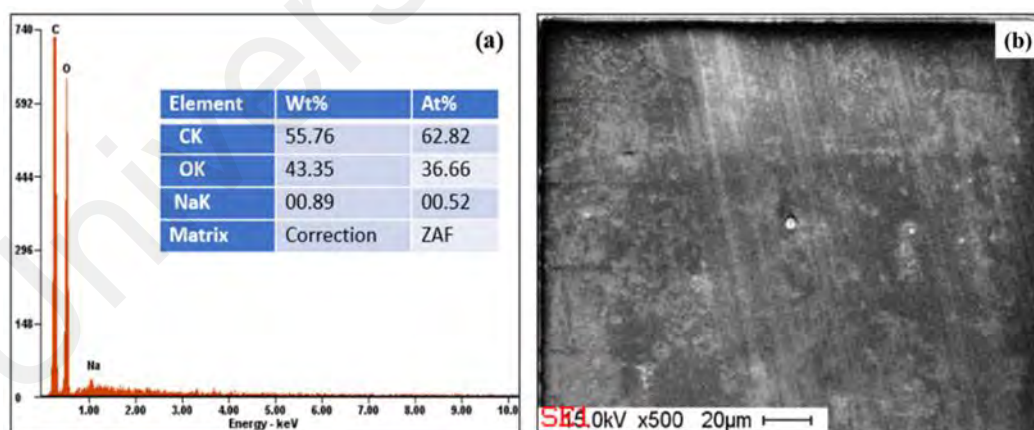


Figure 3.11. (a) The EDX measurement of lawsone: PVA thin film. (b) The used SEM image for EDX measurement.

The composition and elements on the surface of lawsone: PVA thin film have obtained using energy-dispersive X-ray (EDX) spectroscopy. The EDX (Figure 3.11 (a)) shows high percentage of carbon (C) and oxygen (O) elements which are the main constituents

of the lawsone and PVA molecules. The small percentage of sodium (Na) appeared in the EDX that comes from the lawsone plants. Figure 3.11 (b) shows the SEM image that was used for EDX measurement.

The nonlinear absorption property of the fabricated lawsone: PVA thin film has characterized using a standard balance twin-detector measurement scheme at the operation wavelength of 1566 nm. The mode-locked laser used as a source, which the mode-locked signal was amplified using EDFA and then linked to an attenuator to record the output power of the laser. Subsequently, a 3 dB coupler was inserted after the output for the need of simultaneously measure the output power through the SA and directly without SA to determine the SA absorption. Finally, As shown in Figure 3.12, the modulation depth and saturation intensity of the casting ZnPc SA are estimated to be approximately 12% and 3.5 MW/cm^2 , respectively, by calculating the readings from the power meters with fitting the readings data based on equation 3.1.

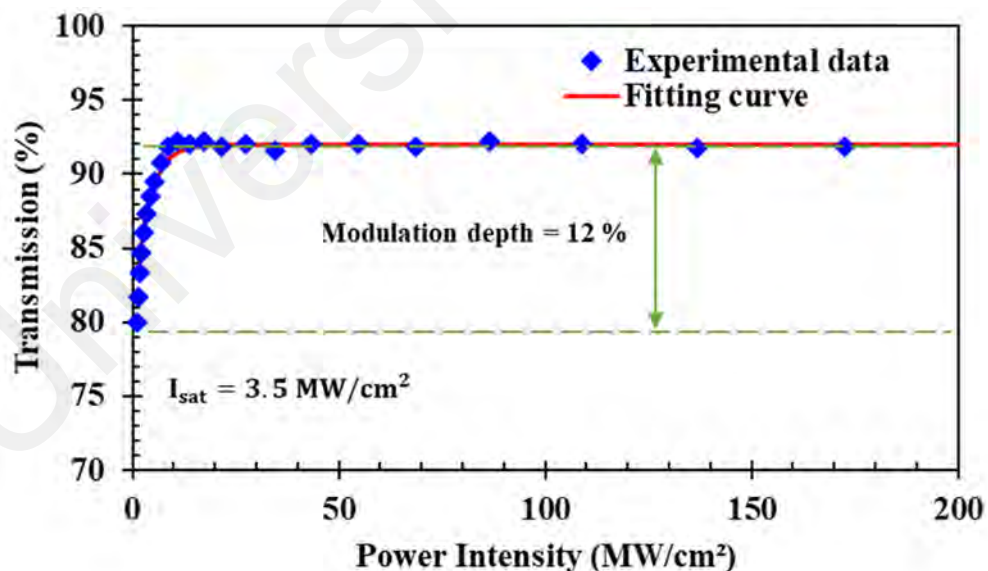


Figure 3.12. Nonlinear optical transmission properties of the lawsone:PVA thin film SA.

3.4 Summary

Two types of organic thin films were successfully developed based on liquid exfoliation technique. ZnPc and Lawsone materials were selected as a base material and PVA was used as a host polymer. The ZnPc based thin film was prepared in three different methods; ZnPc was embedded into, casted onto and spin-coated onto the polyvinyl alcohol (PVA) film and the samples are referred to embedding ZnPc:PVA, casting ZnPc/PVA, and spin-coating ZnPc/PVA, respectively. The lawsone based film was prepared by embedding lawsone material into the PVA film. These thin films were successfully characterized in terms of linear absorption, bandgap, FTIR spectra, SEM image, and nonlinear transmission. The embedding ZnPc:PVA and lawsone film have a modulation depth of 10% and 12%, respectively and thus suitable for Q-switching and mode-locking applications.

CHAPTER 4: ZINC PHTHALOCYANINE THIN FILM AS SATURABLE ABSORBER TO GENERATE Q-SWITCHED AND MODE-LOCKED PULSES IN ERBIUM DOPED FIBER LASER CAVITY

4.1 Introduction

Recently, the optical pulse train generation has gained notable attentions whereas it possesses significant potentials for the utilization in various implementations, such as industry, biomedical and remote sensing (J. Ding, Liu, Wei, & Xu, 2017; P. Ding et al., 2014; Malinauskas et al., 2016). The most effective approach is the SA method which could be utilized in different gain media. Thulium-, Erbium-, and ytterbium-doped fibers were utilized extensively as the gain medium for optical pulse generation in the wavelength operation region of 2-, 1.5-, and 1- μm , respectively (Luo et al., 2014). However, Erbium gain medium has received more interests especially for sensing and optical communication applications (Bogachkov & Gorlov, 2016; Osellame, Cerullo, & Ramponi, 2012).

Phthalocyanine (Pc) is a well-known organic semiconductor and the optical, electronic and photoelectronic properties of Pc are extensively investigated. Pc is suitable to be used in photovoltaic devices since its physical and chemical durability is very high (Guo et al., 2018; Salam, Al-Masoodi, et al., 2019; Song et al., 2017). Many kinds of phthalocyanines, such as metal-free phthalocyanines and phthalocyanines with various metals have been synthesized and are now utilized in a variety of fields like solar cells, clinical photodynamic therapy and electrocatalytic oxidation (Huang et al., 2017; Kuzyniak et al., 2017). Among these materials, zinc phthalocyanine (ZnPc) is a promising organic semiconductor for optical applications. For instance, ZnPc can absorb the incident light in the visible region to effectively contribute in photocarrier generation in the photovoltaic application (Islam et al., 2020). Moreover, ZnPc was also used in the characterization of the excited states of the Pc ring (McKearney et al., 2018).

Furthermore, the Zn gives phthalocyanines valuable fluorescence and singlet oxygen production properties, which allow their use in the detection and treatment of tumors.

The main approaches to generate optical pulsed lasers are passive Q-switching and passive mode-locking, which can be realized by several methods including the usage of saturable absorber (SA) device. In this chapter, we investigate the potential of ZnPc based SAs, for Q-switched and mode-locked pulse laser generation at 1.5 μm region for the first time. The preparation of the SA was described in the previous chapter. The SA is inserted between two optical fiber ferrules in the Erbium-doped fiber laser (EDFL) cavity to act as a Q-switcher and mode-locker, for microsecond and picosecond pulse generation, respectively.

4.2 ZnPc Thin Film as Saturable Absorber for Q-switched Pulse Generation

This section demonstrates the use of ZnPc thin films as SA to generate Q-switched pulse trains in EDFL cavity. The films were prepared by three methods which were referred as embedded ZnPc:PVA, casted ZnPc/PVA and spin coated ZnPc/PVA. The insertion of SAs was done between two optical fiber ferrules in the laser cavity for pulse generation.

4.2.1 Q-switched EDFL Setup

The experimental setup of the Q-switched EDFL based on ZnPc SA is shown in Figure 4.1. The pump laser of the EDFL was a laser diode (LD) with 980 nm wavelength, which was launched into the gain medium via a 980/1550 wavelength division multiplexer (WDM). The gain medium of the laser was Erbium-doped fiber (EDF) with cladding and core diameters of 125 μm and 4 μm , respectively. The EDF had erbium ion absorption of 23 dB/m at 980 nm and a numerical aperture (NA) of 0.16. The unidirectional propagation of light inside the optical resonator was assured by employing a polarization insensitive isolator after the gain medium. Then, the SA device obtained by inserting the SA film

between two clean fiber ferrules, was integrated between the isolator and a 50/50 optical coupler. 3 dB output coupler was used to feedback 50% of the oscillating light to the cavity through the 1550 nm port of the WDM for the purpose of amplification. The output of the laser was tapped out from the second port of the 3 dB coupler. Finally, another 3dB coupler was used to split the output laser so that the optical spectrum and the time domain of the generated pulses can be observed simultaneously. The cavity length of the proposed laser was approximately 6 m.

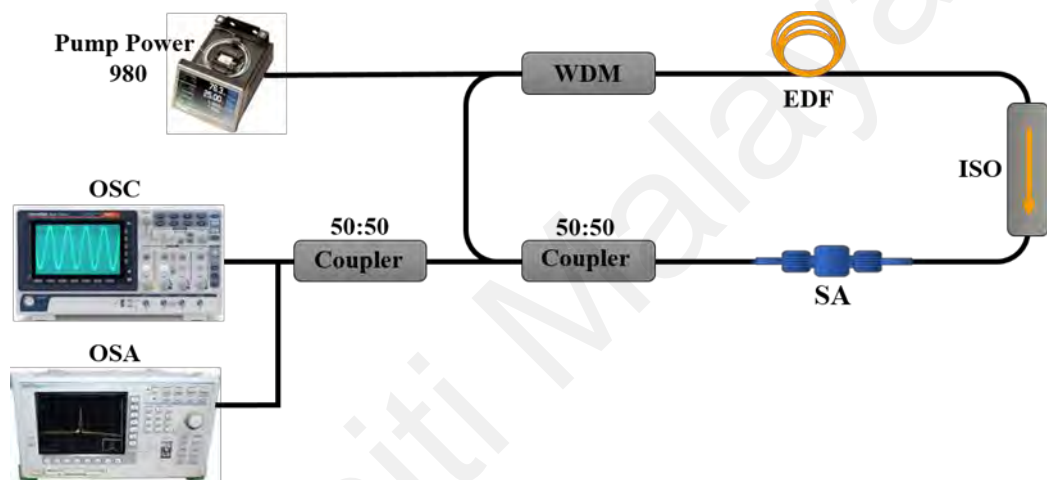


Figure 4.1. Experimental setup of the passively Q-switched EDFL with insertion of ZnPc film SA.

4.2.1.1 Results and Discussion

The operation of EDFL cavity was realized by modifying the 980 nm pump power. At the beginning, when ZnPc film was not inserted into the ring cavity, the continuous wave (CW) laser was obtained and no pulse was observed with increasing the pump power. Moreover, by integrating the Zinc phthalocyanine (ZnPc) film SA between the two fiber ferrules in the laser cavity, a stable and self-starting Q-switched performance has been successfully initialized at pump power of 115.8, 119, and 109.6, mW for embedding ZnPc:PVA, casting ZnPc/PVA, and spin coating ZnPc/PVA respectively. The Q-switched pulse generation turned into more stable operation by raising the pump power. The pulse width became narrower while the repetition rate increased with the increase in pump power. Where, pulse repetition rate is the number of emitted pulses per second or

the inverse temporal pulse spacing, while the optical pulse duration (also called pulse width) is defined as the full width at half maximum (FWHM) of the optical power versus time.

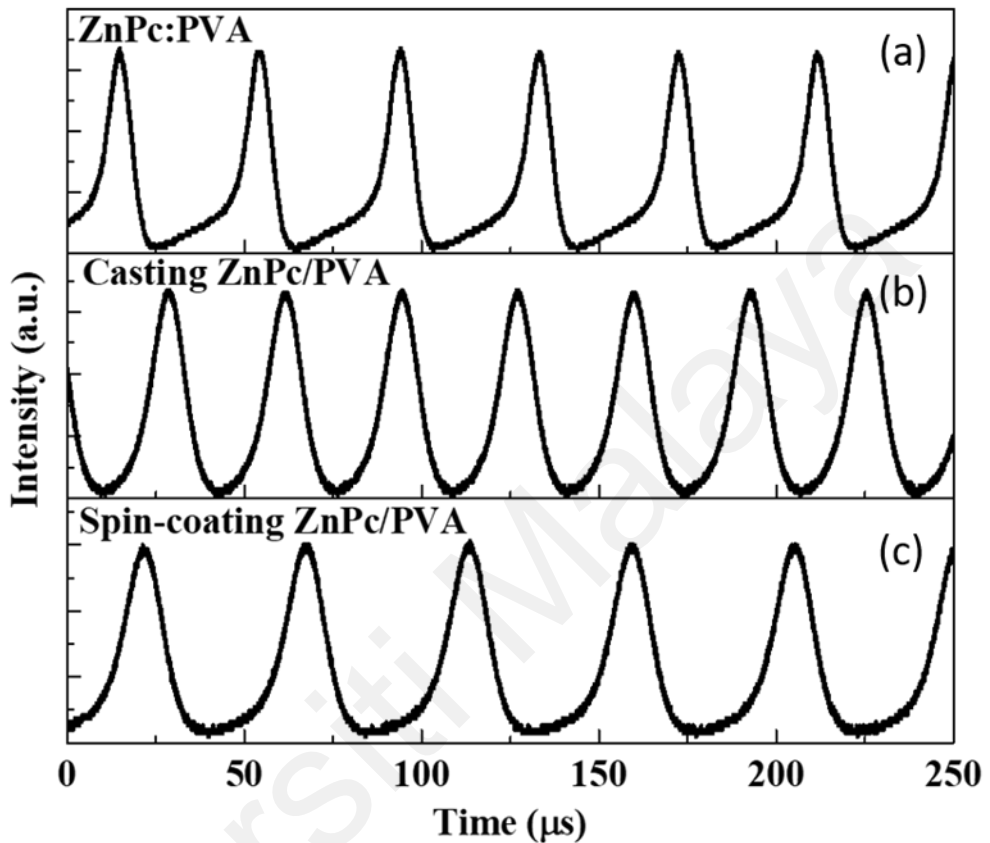


Figure 4.2. Pulse trains recorded at the threshold pump power of (a) 115.8 mW (embedding ZnPc:PVA), (b) 119 mW (Casting ZnPc/PVA), and (c) 109.6 mW (Spin-coating ZnPc/PVA).

Figure 4.2 shows the typical pulse trains by a 1.2 GHz photodetector connected to oscilloscope (GDS-3352) using three fabrication methods of ZnPc based SA (embedding ZnPc:PVA, casting ZnPc/PVA and ZnPc/PVA) at the threshold of 115.8, 119, and 109.6 mW pump power. Figure 4.2 (a) illustrates the oscilloscope trace of the laser configured with embedding ZnPc:PVA SA at threshold pump power of 115.8 mW, which display a repetition rate and pulse width of 25.19 kHz and 8.28 μ s, respectively with an average output power of 0.92 mW. Figure 4.2 (b) shows the pulse trains of casting ZnPc/PVA SA with repetition rate of 30.3 kHz and pulse width of 10.8 μ s at the threshold pump power of 119 mW. For spin coating ZnPc/PVA SA, the pulse repetition rate of 21.5 kHz operated

at the lowest threshold pump power of 109.6 mW. This is attributed to the spin coating effect, which distributes the ZnPc particles homogeneously onto the film and reduces the insertion loss. The pulse width and pulse energy are 12.34 μ s and 23.26 nJ, respectively. From the oscilloscope trace, it can be seen that the pulse train is clean without noise or fluctuations at least 48 hours without any noticeable degradation of performance, which confirm the stability of the Q-switched operation. Moreover, it is worthwhile to note that the experiment is repeated several times and the SA devices were able to reproduce the stable Q-switched pulses. We have increased the pump power up to its maximum of 300 mW. As the pump power was decreased back to the value below 148 mW, the Q-switched pulse was re-generated. Thus, we confirm the damage threshold is more than 300 mW.

The typical pulse performances of the Q-switched EDFL with embedding ZnPc:PVA, casting ZnPc/PVA, and spin-coating ZnPc/PVA based SA recorded at maximum pump power of 148, 141, and 135 mW respectively are summarized in Figure 4.3. As indicated in Figure 4.3 (a), the output spectrum was measured by an optical spectrum analyzer (MS9710C) with 0.2 nm resolution. As shown, the spectrum of embedding ZnPc:PVA, casting ZnPc/PVA, and spin-coating ZnPc/PVA -based Q-switched EDFLs oscillated at a central wavelength of 1561.4, 1560.4 and 1559.5 nm with 3dB bandwidth of 0.4, 0.12 and 0.12 nm, respectively. Figure 4.3 (b) shows the Q-switching pulse train with repetition rate of 48, 43 and 32.2 kHz and the pulse interval of 20.6, 23.14, and 31 μ s for the SA fabrication methods of ZnPc:PVA, casting ZnPc/PVA, and spin-coating ZnPc/PVA at the pump power of 148, 141, and 135 mW, respectively. The corresponding single pulse profiles with pulse width of 3.6, 4.9, and 6 μ s respectively are shown in Figure 4.3 (c). To prove the stability of the Q-switched performance, we measured the Radio Frequency (RF) spectrum using a RF spectrum analyzer with a 1.2 GHz photodetector. The Q-switched pulses configured with embedding ZnPc:PVA SA, casting ZnPc/PVA SA, and spin-coating ZnPc/PVA SA show signal-to-noise ratios (SNRs) of

65, 60, and 56 dB at the fundamental frequencies of 48, 42 and 32.2 kHz, respectively, as shown in Figure 4.3 (d). The high SNR values indicate good stabilities of Q-switched operations. The obtained SNR is comparable to other works at 1.5 μm such as Molybdenum disulfide (MoS_2) SA and Zinc oxide (ZnO) which had SNRs of about 42.5 dB and 56 dB respectively (H. Ahmad et al., 2016; H. Li et al., 2014). The SNR can be improved by reducing cavity loss as well as the non-saturable loss of the SA.

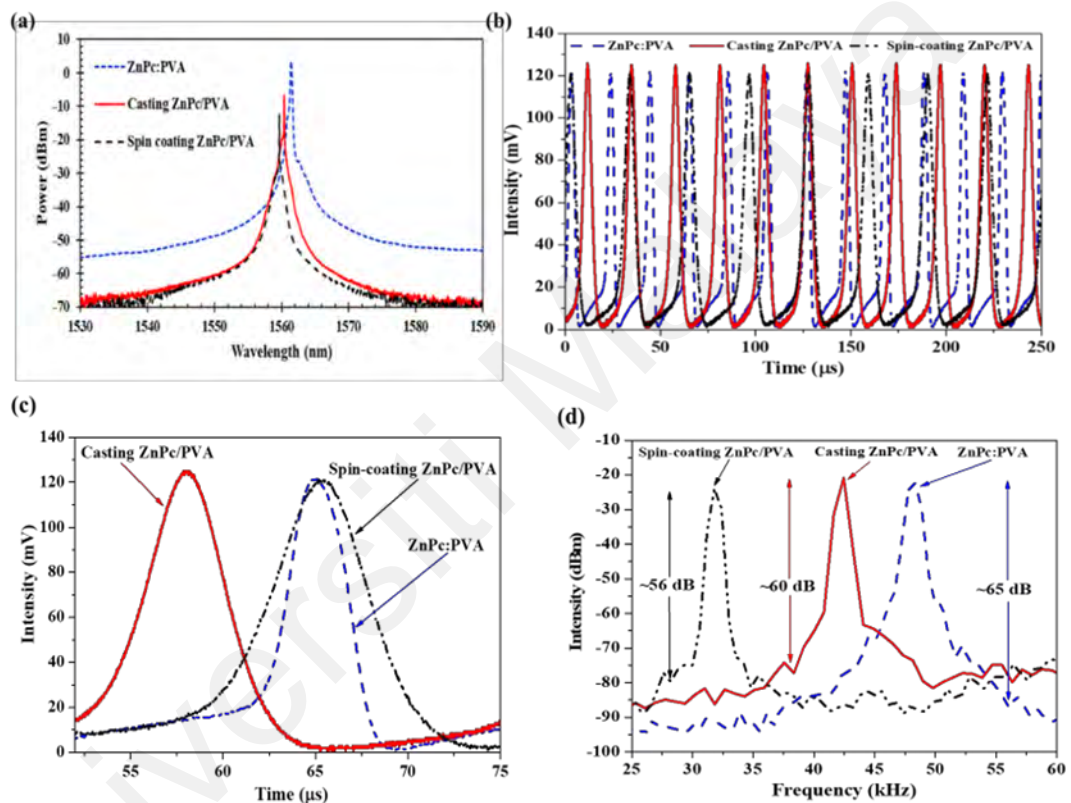


Figure 4.3. The typical pulse performance of the Q-switched EDFL with embedding ZnPc:PVA, casting ZnPc/PVA, and spin-coating ZnPc/PVA based SA recorded at maximum pump power of 148, 141, and 135 mW (a) Optical spectrum, (b) Pulse train, (c) Single envelope pulse profile, and (d) the RF spectrum.

The measurement of pulse repetition rate and pulse width with increasing pump power for three fabrication processes of ZnPc based SA for Q-switched laser is shown in Figure 4.4 (a). The repetition rate linearly increases, while the pulse width decreases with the rise of the pump power. This is due to the higher pump power generates a larger population inversion, which in turn increase the amplification or gain in the EDFL. The increasing and falling times of the passive Q-switching pulse obtain narrower

concurrently as SA saturation turn into a faster with higher intensity in the laser configuration. This corresponds with the Q-switching theory for SA based laser. The pulse repetition rate increases from 25.19 to 48 kHz, 30.3 to 43 kHz, and 21.5 to 32.2 kHz as the pump power rises from 115.8 to 148 mW, 119 to 141 mW, and 109.6 to 135 mW for the SA fabrication methods of embedding ZnPc:PVA, casting ZnPc/PVA, and spin-coating ZnPc/PVA, respectively. However, the pulse width decreases from 8.28 to 3.6 μ s for embedding ZnPc:PVA, 10.8 to 4.9 μ s for casting ZnPc/PVA, and 12.3 to 6 μ s for spin-coating ZnPc/PVA. The highest repetition rate and shortest pulse duration are obtained at 48 kHz and 3.6 μ s respectively.

On the other hand, the variation of average output power and pulse energy at the same range of pump powers and SA methods is shown in Figure 4.4(b). Both output power and pulse energy are increased with increasing pump powers where the maximum output powers are obtained at 3.5 mW, 1.4 mW and 1.6 mW, while the maximum pulse energies are calculated to be 71, 32 and 50 nJ for the three SA fabrication methods of embedding ZnPc:PVA, casting ZnPc/PVA, and spin-coating ZnPc/PVA. These results indicate that the embedding ZnPc:PVA is the best SA where the maximum pulse energy is achieved at 71 nJ. It is worthy to note that the mode-locking operation could not obtained by the current cavity. The mode-locked pulses could be achieved by the modification of the cavity to balance the dispersion and self-phase modulation effects inside the cavity.

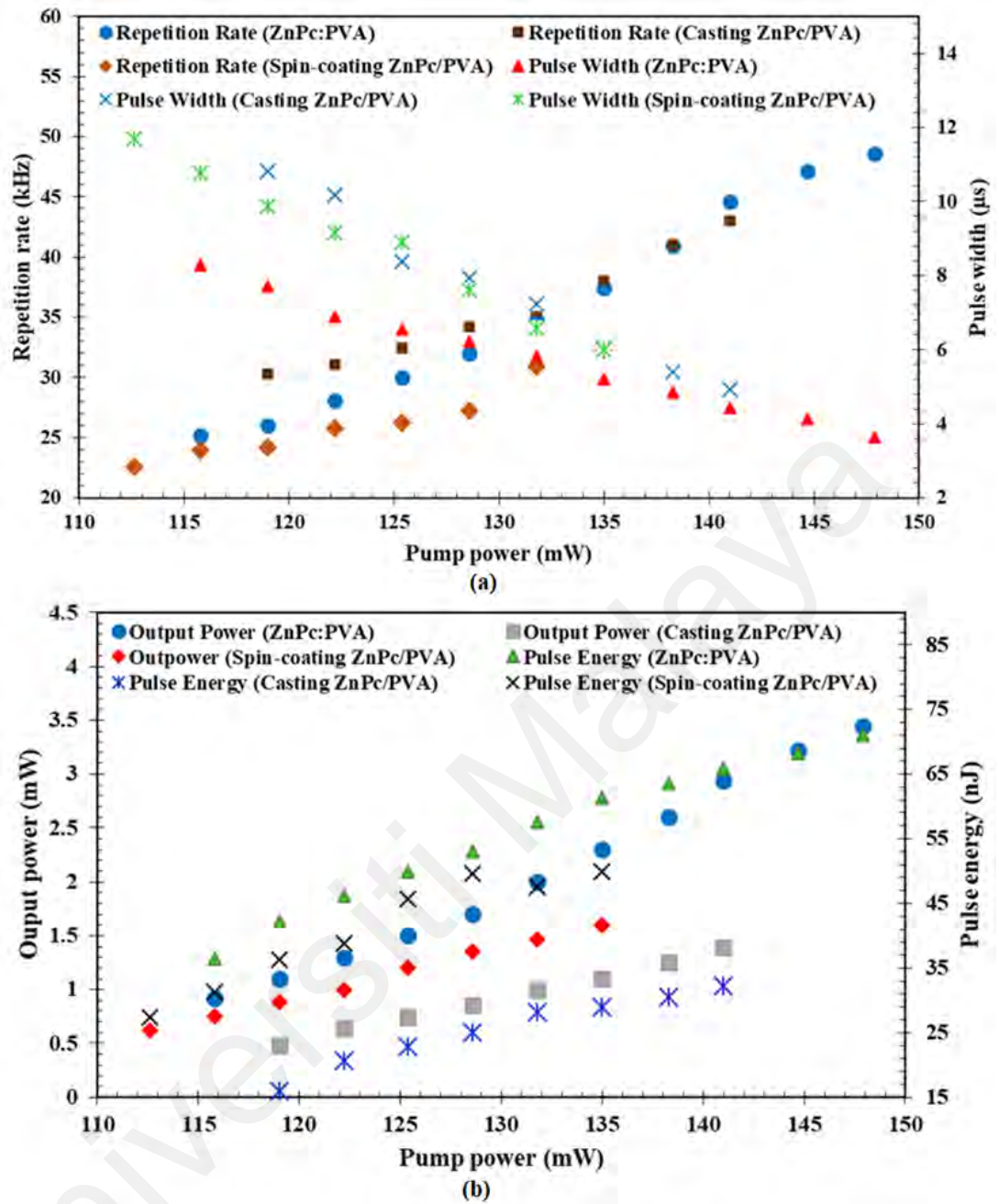


Figure 4.4. Pulse repetition rate and pulse width variation with pump power. (b) Average output power and pulse energy versus pump power.

4.3 ZnPc Thin Film as Saturable Absorber for Picosecond Soliton Pulse Generation

In this section, ZnPc, which was embedded into PVA thin film is used in an EDFL cavity to generate mode-locked ultrashort pulses. The SA was prepared by using phase exfoliation technique as described in the previous chapter. It was referred as the embedding of ZnPc PVA thin film which has excellent optical properties and a broadband

absorption. During fabrication, a homogeneous solution of ZnPc was prepared and then mixed with diluted PVA polymer solution. After the mixture was dried to form a thin film, a small piece was cut from it and fitted in between two fiber ferrules to form an SA.

The prepared ZnPc:PVA film-based SA is inserted into EDFL cavity as shown in Figure 4.5, for generating a mode-locked pulse train. The laser diode operating at 980 nm is utilized for pumping the cavity. The pump light is launched through a wavelength division multiplexer (WDM) into a 2.4 m long Erbium-doped fiber (EDF) gain medium to generate an amplified spontaneous emission, which oscillates in the cavity to produce laser in the 1550 nm region. An optical isolator is inserted into the cavity to prevent the back-reflection that could damage the laser diode, and to ensure a unidirectional light propagation. The EDF used has a core and cladding diameters of 4 and 125 μm with a numerical aperture of 0.23. The Erbium ion absorption is 23 dB/m at 980 nm. A 90/10 coupler is utilized to keep 90% of the light to oscillate in the gain medium and 10% as an output. The constructed ZnPc:PVA film SA is inserted into the laser cavity between isolator and 90/10 coupler.

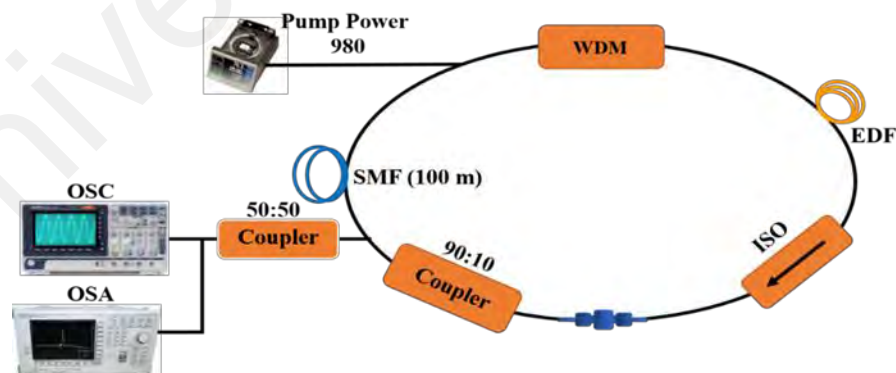


Figure 4.5. The proposed cavity setup for the soliton mode locked EDFL.

The dispersion and the sufficient intracavity non-linearity are ensured by appending 100 m commercial single-mode fiber (SMF) before SA. Also, the use of SMF has improved the pulse energy and decreased the pulse repetition. The output pulse train was characterized in the frequency and time domain by using a radio frequency spectrum

analyzer (RFSA) with a pre-connected photodetector and digital oscilloscope (OSC), respectively. The optical spectrum analyzer (OSA) was utilized to record the output laser spectrum whereas the output power is measured by the utilization of optical power meter.

The EDFL with ZnPc film SA achieved a continuous wave (CW) state at the pump power of 70 mW, whereas a stable soliton mode-locked performance was attained at threshold pump power of 102.9 mW. The mode-locking operation was maintained with the increase of pump power up to 335.7 mW. As the pump power further increased up to the maximum pump power of 345 mW, the mode-locked pulses train disappeared, and the CW state reappeared with a soliton sharp transferred into a peak wavelength of 1560 nm. When the pump power decreased back to 335.7 mW, the soliton mode-locked operation was observed again, which proves that the PVA film SA was not damaged. When we removed the ZnPc:PVA SA from the fiber laser cavity no laser pulses were obtained despite changing the input pump power over a wide range. When the ZnPc:PVA SA was added back into the optical laser cavity, we obtained the mode-locked pulses again. Thus, the mode-locked pulse operation was maintained within the input power range of 102.9 mW and 335.7 mW.

Figure 4.6(a) shows the output optical spectrum of a soliton mode locked EDFL with ZnPc:PVA film SA. In the same figure, a symmetrical Kelly sidebands centered at 1560 nm wavelength can be seen with a typical soliton-like shape with a 3dB spectral bandwidth of 5.2nm. The EDFL mode-locked repetition rate is 1.826 MHz recorded from a stable pulse period of 546 ns as shown in Figure 4.6(b). This result agrees with the cavity length and pulse repetition rate.

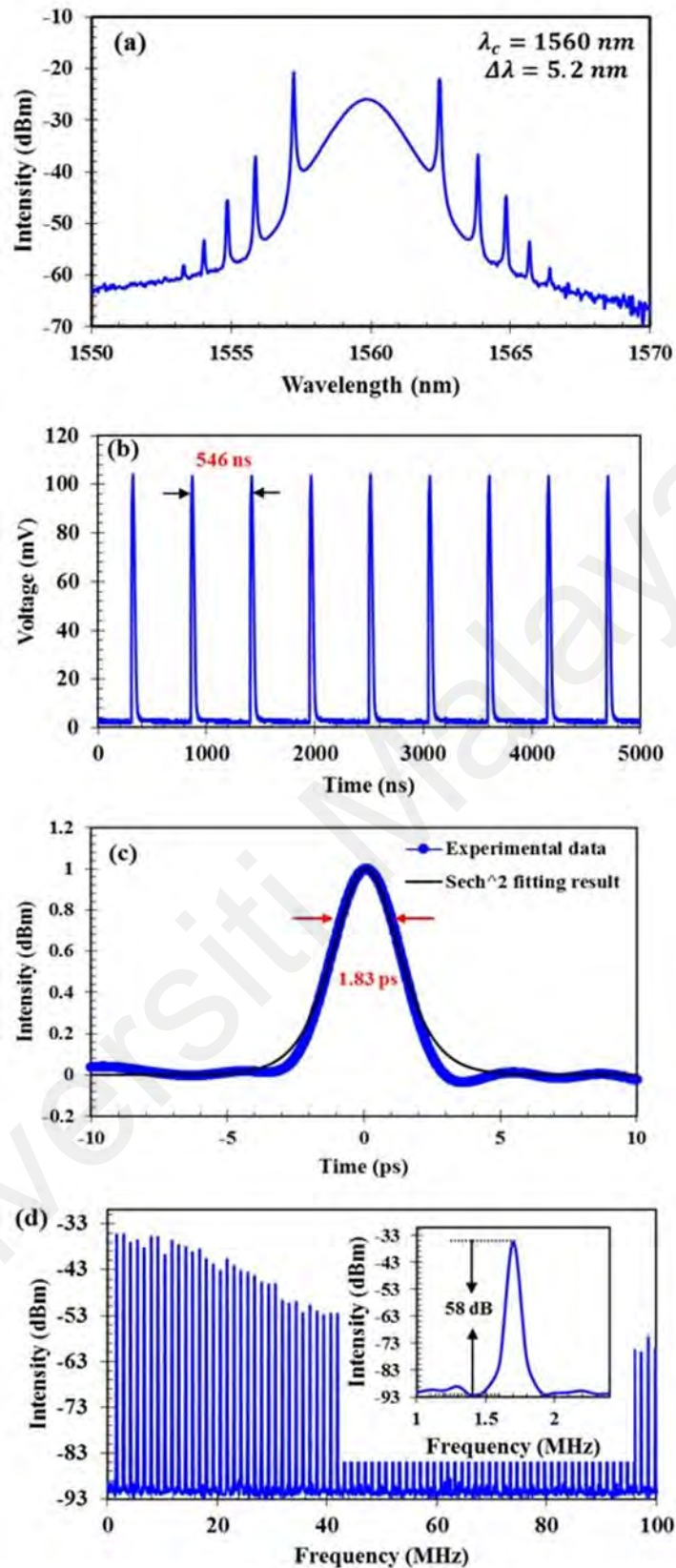
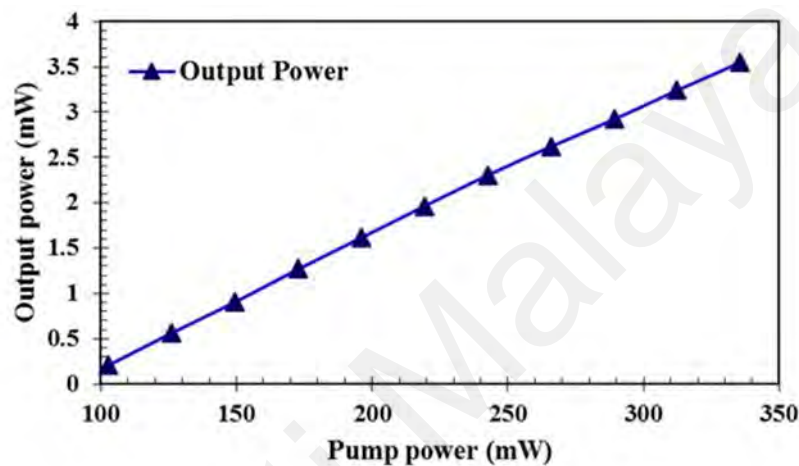


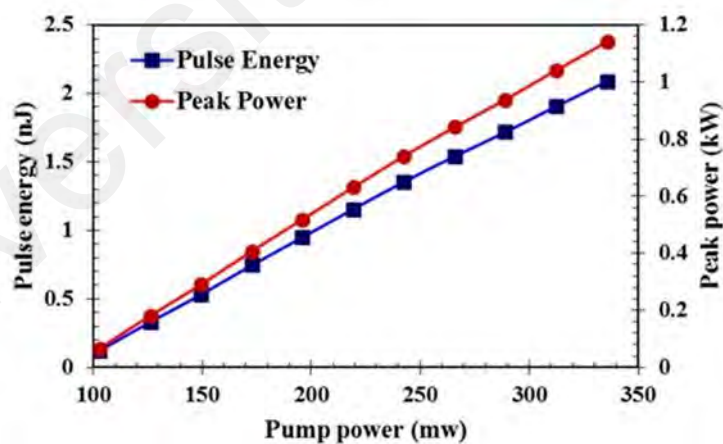
Figure 4.6. Properties of the mode-locked EDFL. (a) Optical spectrum. (b) Wavelength of the pulse train. (c) Autocorrelation trace. (d) RF spectrum.

Figure 4.6(c) displays the autocorrelation trace of the mode-locked operation using ZnPc thin film SA, where the measurement of the pulse width with a sech2 fitting is

approximately 1.83 ps. The recorded radio frequency (RF) spectrum using a RF spectrum analyzer with a 1.2 GHz photodetector is utilized to evaluate the stability of mode-locked operation. The fundamental frequency was obtained at 1.826 MHz with a signal to noise ratio (SNR) of 58 dB as shown in Figure 4.6(d). The spectrum also shows a high number of cavity harmonics in a span of 100 MHz with pure spectral with no significant spectra modulation.



(a)



(b)

Figure 4.7. (a) Measured output power as a function of pump power. (b) Pulse energy and peak power against the pump power.

Figure 4.7 (a) shows the relation between the pump power and the output power of the pulsed laser. The increment of pump power from 102.9 mW to 335.7 mW causes the output power to rise from 0.2 mW to 3.55 mW. Figure 4.7 (b) shows the result of changing

the pump power on the pulse energy. It is observed that the pulse energy increases from 0.12 nJ to 2.1 nJ as a result of the increment in the pump power from 102.9 mW to 335.7 mW. The peak power changes from 0.07 kW to 1.15 kW for the same variation in pump power.

4.4 Summary

The Q-switching and mode-locking performances of the ZnPc thin film in EDFL cavity have been successfully investigated. At first, Q-switching pulse generation was demonstrated based on three SA fabrication methods of embedding ZnPc:PVA, casting ZnPc/PVA, and spin-coating ZnPc/PVA operating in the 1.5- μ m region. Stable and self-starting Q-switched pulse trains centered at 1561.4, 1560.4 and 1559.5 nm were obtained for embedding ZnPc:PVA SA, casting ZnPc/PVA SA, and spin-coating ZnPc/PVA SA respectively. The shortest pulse width and maximum pulse energy were achieved at 3.6 μ s and 71 nJ for embedding ZnPc:PVA SA. All the SAs show good performance of Q-switching pulse trains in the 1.5- μ m wavelength region. The soliton mode-locked pulse operation was also successfully realized in another EDFL cavity, which was configured with an additional 100 long SMF in the cavity utilizing a ZnPc SA. A stable mode-locked operation with 1.83ps pulse width is obtained at the pump power of 102.9 mW by integrating the fabricated ZnPc:PVA film as SA inside the ring cavity. The fundamental repetition rate and center wavelength are at 1.826 MHz and 1560 nm, respectively. At the pump power of 335.6 mW, the pulse energy is 2.1 nJ while the maximum peak power is 1.15 KW. These results show that the ZnPc film has an excellent application as SA for generating both microsecond Q-switched and picosecond mode locked pulses.

**CHAPTER 5: ZINC PHTHALOCYANINE THIN FILM AS SATURABLE
ABSORBER TO GENERATE Q-SWITCHED AND MODE-LOCKED PULSES
IN YTTERBIUM DOPED FIBER LASER CAVITY**

5.1 Introduction

The Ytterbium-doped fiber laser (YDFL) exhibits reliable and robust performances in 1.0 μm operation region. It has many outstanding characteristics in terms of compactness, high power capability, high efficiency, and broad gain bandwidth (Soboh, Al-Masoodi, Erman, Al-Masoodi, Yasin, et al., 2021) whereas it can be utilized in diverse applications including telecommunications, sensing, manufacturing, and medicine (H. B. Ahmad, Ismail, Aidit, Bayang, & Yusoff, 2020; Salim et al., 2018; Ye et al., 2021). A SA device can be integrated into the YDFL cavity by placing a film in middle of the two clean fiber ferrules to function as a passive Q-switcher (Soboh et al., 2020). In this chapter, an organic material, Zinc phthalocyanine (ZnPc) embedded into a polyvinyl alcohol (PVA) is proposed and demonstrated as a SA in an YDFL cavity. The SA film was prepared by a straightforward process based on drop casting technique as described in Chapter 3.

5.2 Passively Q-switched YDFL Using ZnPc Thin Film as Saturable Absorber

This section presents a ZnPc:PVA film as SA for Q-switched pulse generation at 1-micron region. The SA film was obtained by embedding the ZnPc into polyvinyl alcohol (PVA). It was inserted into an YDFL cavity to act as a Q-switcher. The schematic setup of the proposed Q-switched fiber laser operating at 1-micron region is illustrated in Figure 5.1. A 980-nm laser diode (LD) was used to pump the gain medium via 980/1064 wavelength division multiplexer (WDM), which was positioned between the LD and isolator in the ring cavity. The gain medium was a 2m long of Ytterbium-doped fiber (YDF) with Ytterbium ion concentration of 1500 ppm, numerical aperture of 0.20 and 280 dB/m peak absorption at 980 nm. In this work, a small piece of the prepared ZnPc:PVA thin film was attached onto the ferrule by applying a tiny amount of index

matching gel to hold the film. The ferrule was then matched with another clean ferrule to form as SA device. The SA was placed between output 3dB coupler and isolator inside the YDFL cavity to generate Q-switched pulse. In the cavity, the unidirectional light propagation is maintained by the utilization of optical isolator at the output of the ZnPc SA. A 3 dB output coupler was placed after the YDF, which allows half of light to propagate in the cavity, and another half to output from the laser. The output Q-switched pulse was measured by an optical spectrum analyzer (AQ6370C, YOKOGAWA), an oscilloscope (INSTEK GDS-3352), and a radio frequency (RF) spectrum analyzer (MS2724C, Anritsu) for analysis. The total cavity length was about 10 m.

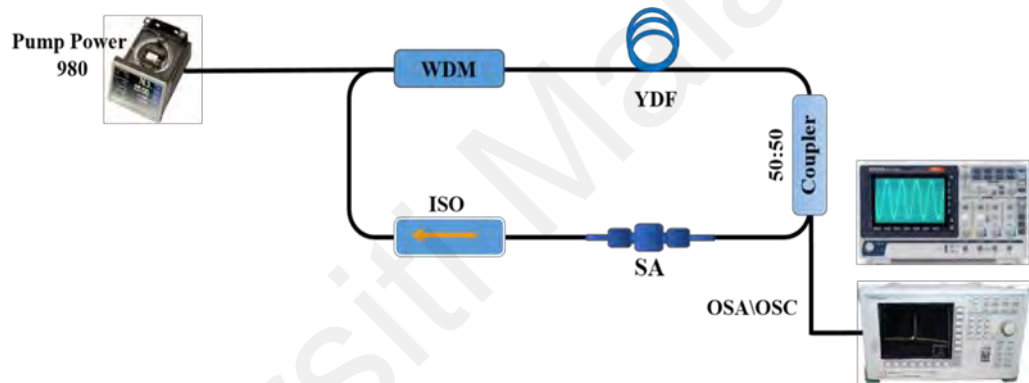


Figure 5.1. Experimental setup of Q-Switched YDFL.

The stable continuous wave YDFL was achieved when the pump power was increased above 200 mW. As we further increased the pump power, the Q-switched pulse train was observed at the threshold of pump power of 246.3 mW. The stable operation of Q-switched laser was maintained in the ring cavity as the pump power was increased further up to 276.8 mW. As the pump power increased beyond 276.8 mW, the Q-switched state became unstable. In addition, no Q-switched pulse had been obtained when ZnPc:PVA SA was removed from the cavity, which confirmed that the ZnPc:PVA SA is necessary for the entire Q-switched procedure.

A typical Q-switched spectrum obtained by the proposed YDFL is shown in Figure 5.2 as the ZnPc SA was incorporated inside the laser cavity. It was measured by an OSA

with 0.2 nm resolution. The laser operated at center wavelength of 1036 nm with a 3 dB spectral bandwidth of 0.9 nm at pump power of 276.8 mW. The performance of Q-switched YDFL was summarized in Figure 5.2. Figure 5.3 (a) shows the typical pulse train measured by the oscilloscope at a threshold pump power of 246.3 mW. The pulse operated at a repetition rate of 54.7 kHz with pulse width of 2.5 μ s, pulse energy of 87.38 nJ and output power of 4.78 mW. Figure 5.3 (b) shows the Q-switched pulse train at the highest pump power of 276.8 mW. It operated at repetition rate of 63 kHz. Figure 5.3 (c) shows the corresponding single pulse envelop, which indicates the lowest attainable pulse width of 2.2 μ s. To prove the stability of the Q-switching performance in the YDFL cavity, we measured the Radio Frequency (RF) spectrum using a RF spectrum analyzer with a 1.2 GHz photodetector. Figure 5.3 (d) shows the measured spectrum at 276.8 mW pump power, which indicates the fundamental frequency at 63 kHz with many other harmonic frequencies. The fundamental frequency has a single-to-noise ratio (SNR) of 49 dB, which further verified the good stability of the Q-switched pulses.

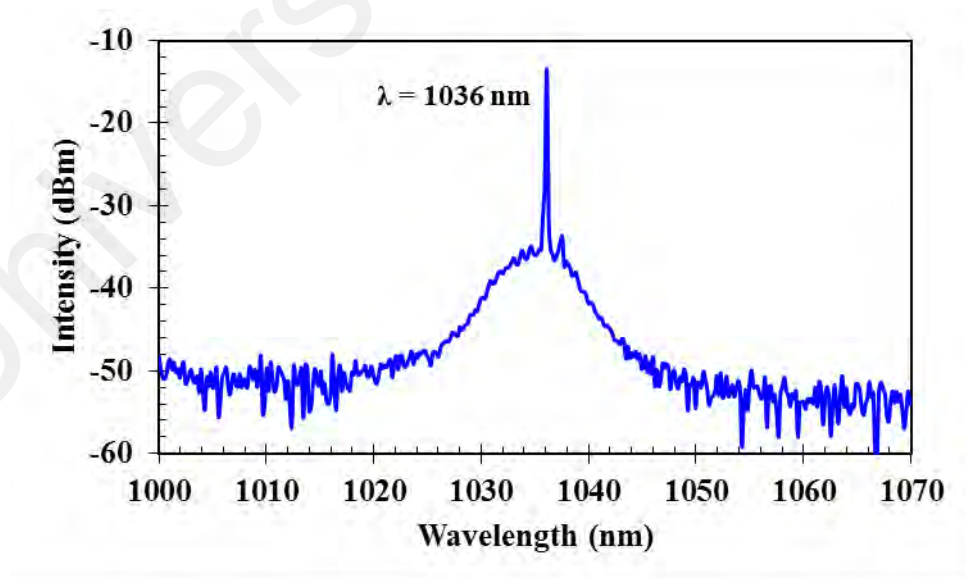
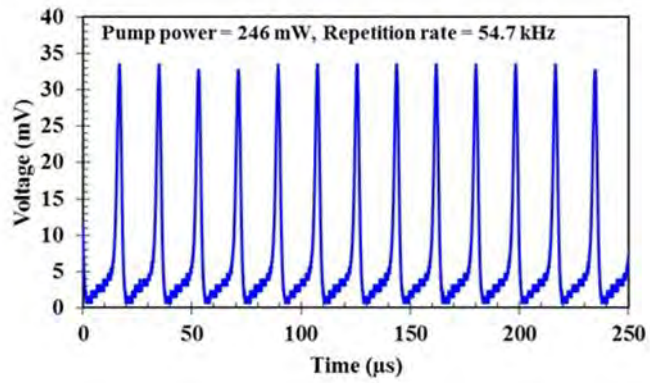
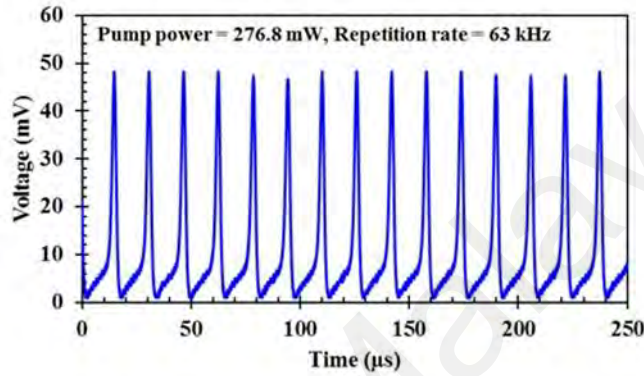


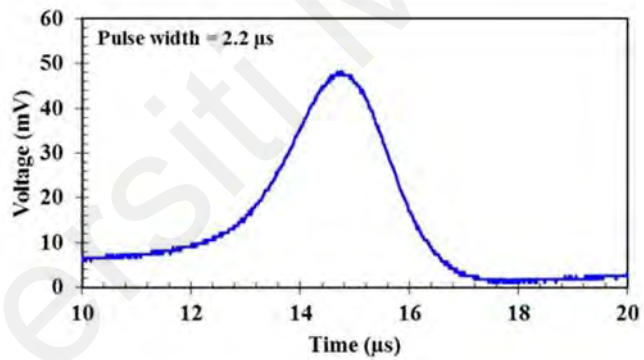
Figure 5.2. Optical spectrum of Q-switched YDFL with ZnPc:PVA SA at 276.8 mW pump power.



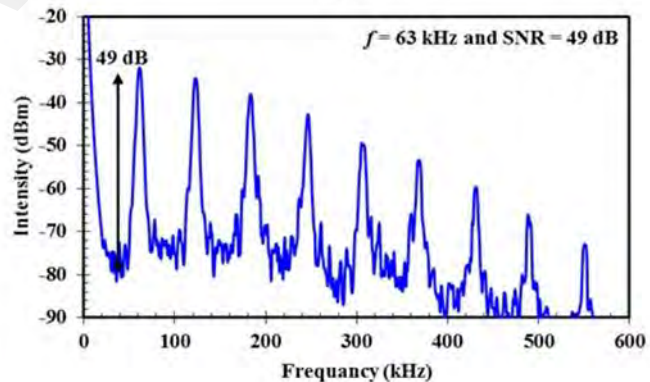
(a)



(b)



(c)



(d)

Figure 5.3. The typical pulse performance of Q-switched YDFL with embedding ZnPc:PVA based SA. (a) Pulse train at threshold pump power of 246 mW. (b-c) Pulse and single envelope pulse at maximum pump power of 276.8 mW. (d) RF spectrum at the maximum pump power of 276.8 mW.

The performance of pulse repetition rate and pulse width of the proposed ZnPc based Q-switched laser were measured as shown in Figure 5.4 (a). The repetition rate increased while the pulse width decreased with increasing in the pump power. This is expected due to the higher input pump power produced a greater population inversion and thus increased the attainable gain in the proposed YDFL cavity. The higher gain, in turn, increases the laser intensity. Subsequently, the increasing and falling times of the passive Q-switching pulses become narrower due to the SA saturation. At the maximum pump power of 276.8 mW, the repetition rate and pulse duration were 63 kHz and 2.2 μ s, respectively. Figure 5.4 (b) shows the variation of output power and pulse energy with the pump power. Both output power and pulse energy are increased with increasing pump powers, where the maximum output power of 5.7 mW and pulse energy of 91 nJ were obtained.

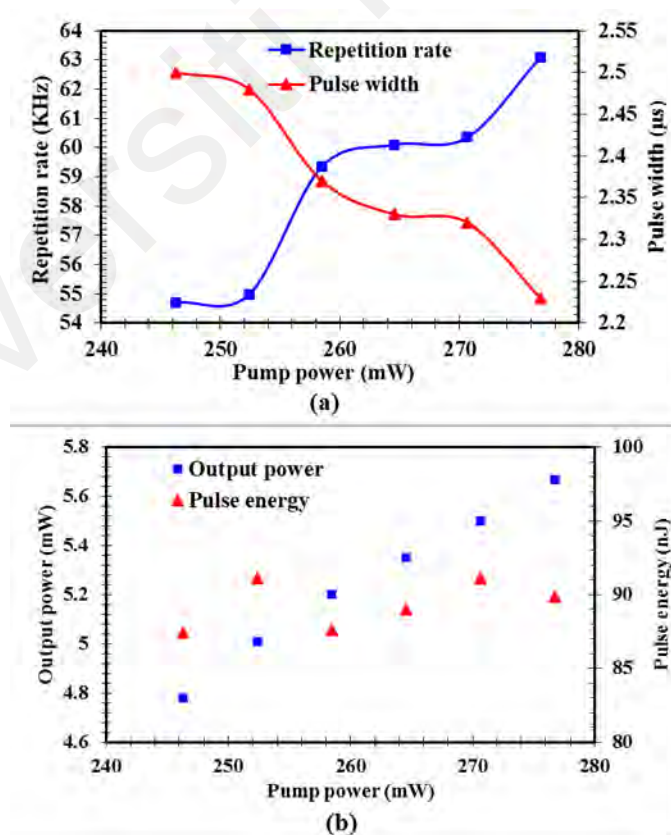


Figure 5.4. Q-switched laser performance against pump power utilizing a newly developed ZnPc:PVA based SA. (a) Repetition rate and pulse width. (b) Average output power and pulse energy.

5.3 Passively Mode-Locked YDFL Using ZnPc Thin Film as Saturable Absorber

In this section, the ZnPc based SA has been utilized for the generation of YDFL mode-locked pulses operating at 1 μm region for the first time. The SA thin film was fabricated by embedding ZnPc material into polyvinyl alcohol (PVA) film. A small piece from the ZnPc thin film was attached onto the fiber ferrule and applying into the ring YDFL cavity to generate a stable mode-locked pulses. The undissolved particles within polymer have spread along the thin film in most uniform shape due to the liquid phase exfoliation, where the high existence of these undissolved ZnPc particles makes the absorbance higher in near infrared region (Novotny et al., 2014).

Figure 5.5 shows the experimental arrangement for generating mode-locked pulses train in YDFL cavity using the prepared ZnPc SA as a mode-locker. It uses a commercial Ytterbium-doped fiber (YDF) as the gain medium and 980 nm laser diode (LD) as the pump source. The YDF received the pumped laser via a wavelength division multiplexer (WDM). The YDF used has core diameter, cladding diameter, and numerical aperture of 4 μm , 125 μm , 0.20, respectively. After the gain medium, a polarization-insensitive isolator ensures the unidirectional propagation of light inside the optical resonator. The SA thin film was inserted between two clean ferrules as a SA device, which was positioned after the isolator and before the optical coupler (90:10). The output coupler functions to allow 90% of the photon to oscillate in the YDFL cavity. Other 10% was tapped out from the coupler to another 3 dB coupler which gives the ability of observing the time domain and the optical spectrum simultaneously. The ring cavity consists of 1.5 m long YDF and 58.5 m long single mode fiber (SMF) with group velocity dispersion (GVD) of 24.22 ps^2/km and 21.91 ps^2/km , respectively. The total length of the ring cavity is about 60 m with the calculated normal net cavity dispersion of approximately 1.3 ps^2 .

The output laser characteristic of the YDFL with and without SA was investigated by varying the 980 nm pump power. It is worth noting that we obtained a continuous wave (CW) laser operation at pump power of 150 mW and no pulse was generated by raising the pump power to maximum value, before the integration of ZnPc thin film into the ring cavity. Then, after integrating the ZnPc film SA between the optical fiber ferrules in the YDFL cavity, a self-started and stable mode-locked optical pulse train was generated at threshold pump power of 246.3 mW reaching up to the maximum pump power of 277 mW. The repetition rate of the mode-locked pulses were unchanged with an increment in pump power. The optical spectrum of mode-locked fiber laser is shown in Figure 5.6 (a) at pump power of 277 mW. As seen, the center wavelength was obtained at 1034.5 nm with 3dB spectral bandwidth of 0.6 nm without Kelly sideband, which shows the pulse operation is in normal dispersion.

The optical pulse train of the ZnPc SA based mode locked YDFL is shown in Figure 5.6 (b) at 277 mW pump power. The pulse train is observed at oscilloscope (GDS-3352), which is connected via 1.2 GHz photodetector. It is observed that the repetition rate is 3.3 MHz and peak to peak spacing of the pulse train is approximately 276 ns, which corresponds to the frequency for the ring cavity, having the length of 60 meters. As it is seen over the oscilloscope, the pulse width is around 123 ns, which is much wider than the actual pulse width. This is because our oscilloscope resolution is limited. To calculate the actual pulse width, we use mathematical model for the time bandwidth product (TBP), which TBP is equal to 0.441 for Gaussian pulse profile (A. H. H. Al-Masoodi et al., 2017) and the estimated shortest possible pulse width is calculated to be around 2.6 ps. The stability of mode locked YDFL performance is proven from the radio frequency (RF) spectrum, which was obtained by utilizing RF spectrum analyzer in conjunction with a 1.2 GHz photodetector as shown in Figure 5.6 (c). The spectrum indicates the signal-to-noise-ratio (SNR) of 55.7 dB, at the fundamental frequency of 3.3 MHz, which indicates

the excellent stability of mode-locked operation. The SNR value could be further boosted by decreasing the non-saturable loss of the SA and the cavity loss.

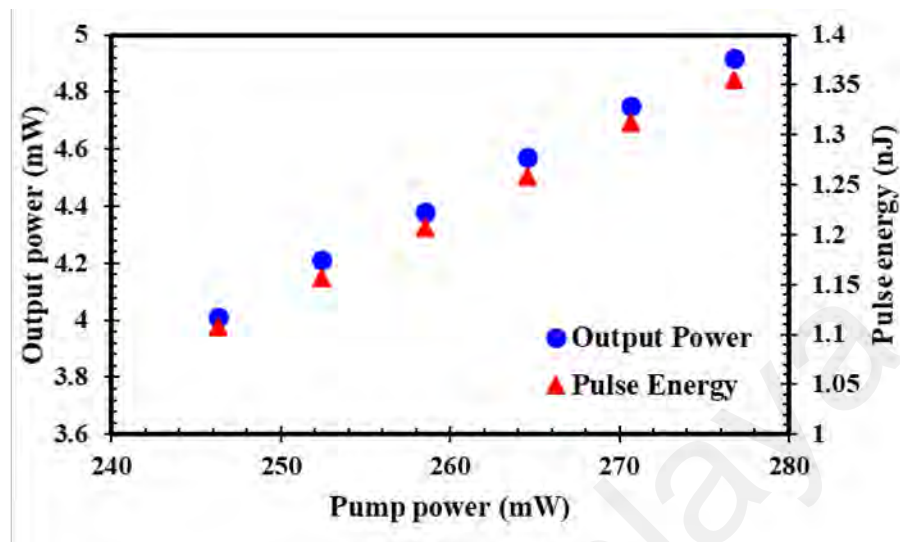


Figure 5.7. Average power and pulse energy at various pumping power.

On the other hand, the relationship between the average power and pulse energy of the mode locked YDFL output at the same range of pump powers is shown in Figure 5.7. It is observed that as the pump power was raised, both pulse energy and output power also are incremented. This is attributed to the larger population inversion induced by the higher pump power, which in turn raise the gain/amplification in the YDFL gain medium. The maximum average power and pulse energy are 4.92 mW and 1.36 nJ, respectively.

5.4 Summary

Q-switched and mode-locked EDFLs have been successfully demonstrated using an organic SA based on ZnPc:PVA thin film, which was obtained by embedding the ZnPc into PVA. At first, the ZnPc:PVA was inserted into an YDFL cavity to act as a Q-switcher. The Q-switching operation was realized at the center of wavelength of 1036 nm with the minimum pulse width of 2.2 μ s. The highest repetition rate and the maximum pulse energy were obtained at 63 kHz and 91 nJ, respectively. A signal to noise ratio (SNR) as high as 49 dB was observed, which indicates a stable operation of Q-switching in the YDFL cavity. The generation of mode-locked pulses was also successfully

demonstrated in YDFL cavity using the ZnPc/PVA thin film-based SA as a mode-locker. A stable and self-starting mode-locked optical pulse train located at 1034.5 nm wavelength was achieved within the pump power range from 246 to 277 mW. It performs at a fixed repetition rate of 3.3 MHz with picosecond pulse width. The highest energy of pulse obtained was 1.36 nJ, at pump power of 277 mW. The results indicate that the ZnPc thin film has a great potential as alternative SA material in 1- μ m operation region. The better experimental results could be obtained through the using of ZnPc thin film with improved quality. This is the first demonstration of the use of ZnPc as SA in 1-micron wavelength region.

Universiti Malaysia

CHAPTER 6: LAWSONE THIN FILM AS SATURABLE ABSORBER FOR Q-SWITCHING AND MODE-LOCKING APPLICATION

6.1 Introduction

Previously, chapters 4 and 5 demonstrated the use of Zinc phthalocyanine (ZnPc) thin film as SA to generate Q-switched and mode-locked pulse train in erbium-doped fiber laser (EDFL) and Ytterbium-doped fiber laser (YDFL) cavity, respectively. In this chapter, the potential of lawsone based SA is investigated for generating Q-switched and mode-locked pulses in EDFL cavity, for the first time.

6.2 Lawsone Dye Material as Potential SA for Q-Switched EDFL

In this section, lawsone (2-hydroxy-1,4-naphthoquinone), a natural dye material is proposed and demonstrated as a SA for passive Q-switching operation in EDFL cavity. The lawsone-based SA was fabricated using a liquid-phase exfoliation technique as described in Chapter 3. A tiny piece of the lawsone film was then cut and slot-in between two fiber ferrules so that it can easily be incorporated into a laser cavity as a Q-switcher. An optical ring configuration of the Q-switched EDFL using lawsone thin film as SA is shown in Figure 6.1. The erbium-doped fiber (EDF) is pumped by a 980 nm single mode semiconductor laser (LD), through a 980/1550 nm wavelength division multiplexer (WDM). To output the signal a 50:50 fiber-merged coupler is used. The EDF has a numerical aperture of 0.23, core and cladding diameter of 4 μm and 125 μm respectively, and the absorption coefficient of about 25 dB/m at 980 nm. To ensure that the propagation of light is unidirectional inside the cavity, isolator is inserted in between WDM and the SA device. The frequency of signal was observed with radio frequency spectrum analyzer (RFSA) and the time domain analyses were reported by Oscilloscope (GDS-3352). Both the RFSA and Oscilloscope were connected via a 1.2 GHz photodetector. We got the output optical spectrum by OSA, having the resolution of 0.07 nm. Besides that, optical power meter was used to measure the output power in milliwatt (mW).

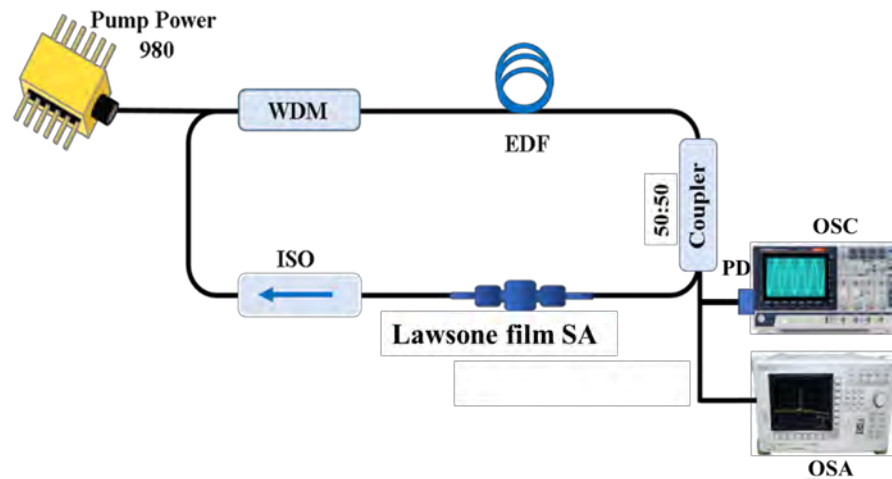


Figure 6.1. Experimental configurations of Q-switched EDFL with lawsone film SA.

In this study, the power of the input pump was increased steadily and the output of the EDFL was analyzed using an oscilloscope and a spectrum analyzer. In the beginning, only a continuous wave laser was produced when no lawsone SA was used in the laser configuration. The CW laser persisted throughout the range of power available to the input pump. However, when a lawsone film SA was positioned between the coupler and isolator in the cavity, a stable and self-started Q-switched pulses replaced the CW laser starting from the threshold pump power of 26 mW until 43.3 mW. Figure 6.2 shows the pulse trains and single pulse plots of the Q-switched laser at pump power of 26, 33.6, and 43.3 mW respectively. They were captured via a 1.2 GHz photodetector connected to an oscilloscope.

The pulse train shown in Figure 6.2 (a) is produced at the pump power of 26 mW. It has a repetition rate of 70 kHz and a pulse width of 2.25 μ s. At the pump power to 33.6 mW, the repetition rate of the pulse train increases to 75.4 kHz while its pulse width drops to 1.8 μ s, as shown in Figure 6.2 (b). At the maximum pump power of 43.3 mW, the pulse repetition rate and pulse width are 80 kHz and 1.7 μ s. They are shown in Figure 6.2 (c). It was observed that the pulse train remained smooth with little noise or fluctuation for more than 48 hours continuously. This observation proves the stability of the Q-switched laser. The experiment was repeated several times, and each time the lawsone SA was able

to produce the same Q-switched laser output without a noticeable difference in quality. However, when the pump power went past 45 mW up to the maximum value of 300 mW, the Q-switched pulses became unstable. After reducing the pump power back to 43.3 mW, the stable Q-switched pulse trains re-emerged. This shows that the SA was not damaged and its damage threshold is more than 300 mW.

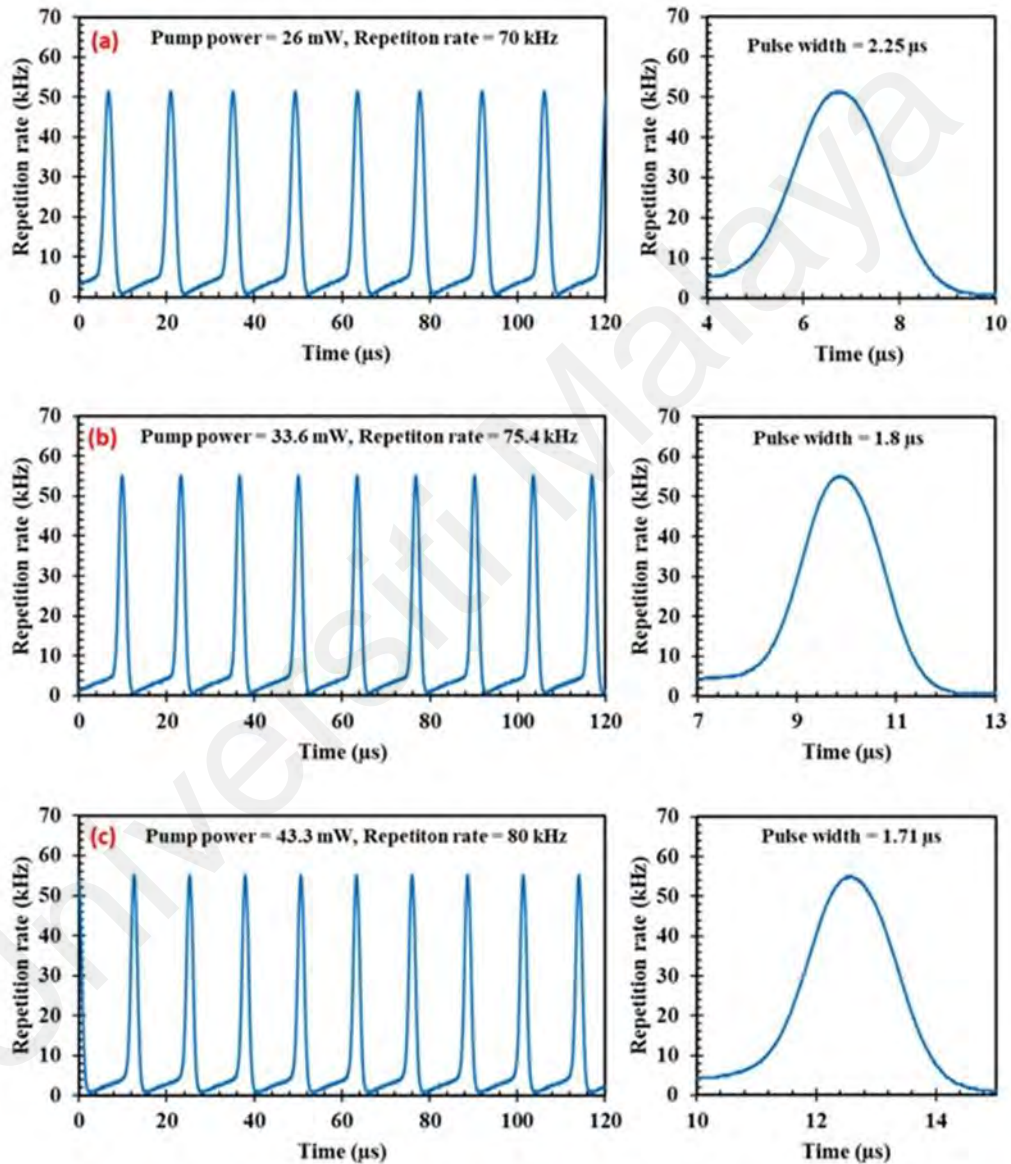


Figure 6.2. Typical oscilloscope traces and single pulse profile of the Q-switched pulse trains with pump powers of (a) 26 mW, (b) 33.6 mW, and (c) 43.3 mW.

The output spectrum of the EDFL pulses using lawsone:PVA SA in Figure 6.3 (a) shows a 3 dB spectral bandwidth of ~ 1.6 nm and central wavelength of 1564 nm. The analysis was done by an optical spectrum analyser (MS9710C) with a 0.2 nm resolution

at the input pump power of 43.3 mW. Figure 6.3 (b) shows the linear relation between the input pump power and the output power, in the range of 26 to 43.3 mW for the input and 3 to 4.3 mW for the output.

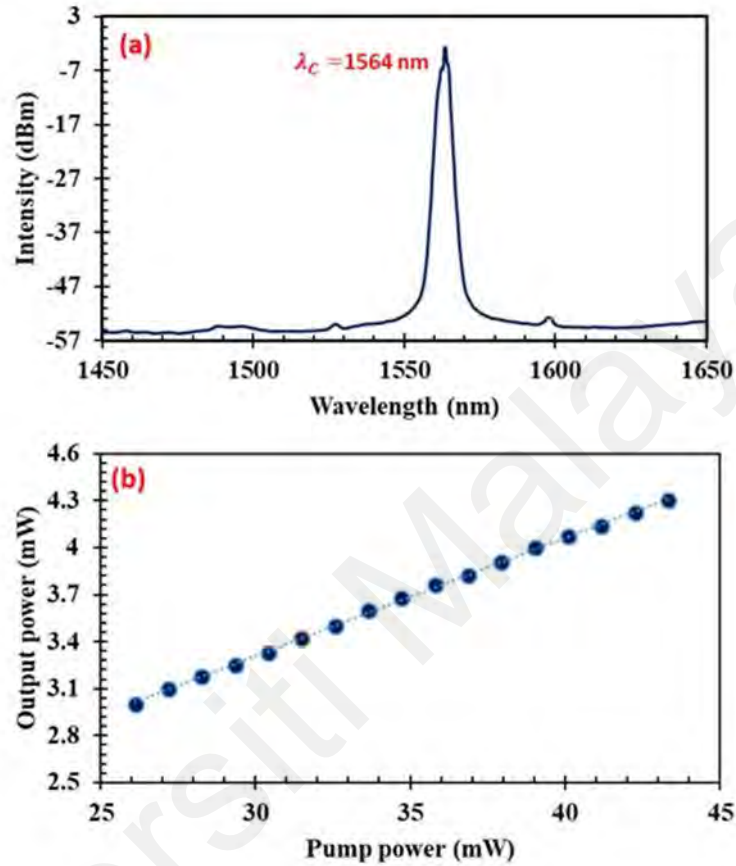


Figure 6.3. (a) Optical spectrum of EDFL at pump power of 43.3 mW. (b) The relationships between output power and pump power.

Figure 6.4(a) displays the direct relation between the repetition rate and the pump power, and the inverse relation between the pulse width and the pump power, in one graph. It should be noted that the relations are directly and inversely proportional but not exactly linear. Logically, a higher pump power generates a higher population inversion, and thus a higher gain in the EDFL. Consequently, the rise and fall times of the Q-switched pulse become smaller as the SA saturation time becomes shorter with a higher intensity. This usual behaviour of the Q-switched laser (Al-Masoodi et al., 2020; Nizamani, Jafry, et al., 2020; B. Zhang et al., 2020) corroborates the Q-switching theory of an all fiber laser utilizing a SA. The pulse repetition rate rises from 70 to 80 kHz while

the pulse width declines from 2.25 to 1.7 μs , as the pump power increases from 26 to 43.3 mW. The resulting pulse energy and peak power are shown in Figure 6.4 (b). Both of them increase together with the pump power. The maximum pulse energy and peak power are 53.7 nJ and 31.4 mW, respectively.

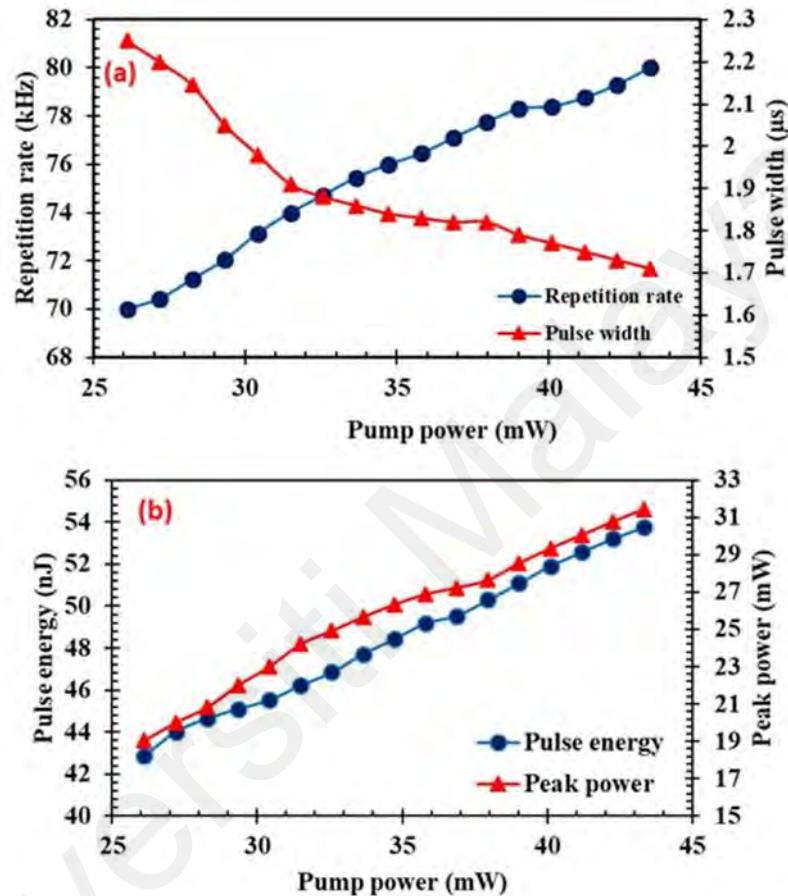


Figure 6.4. (a) Pulse repetition rate and pulse width as function of pump power. (b) Pulse energy and peak power as functions of pump power.

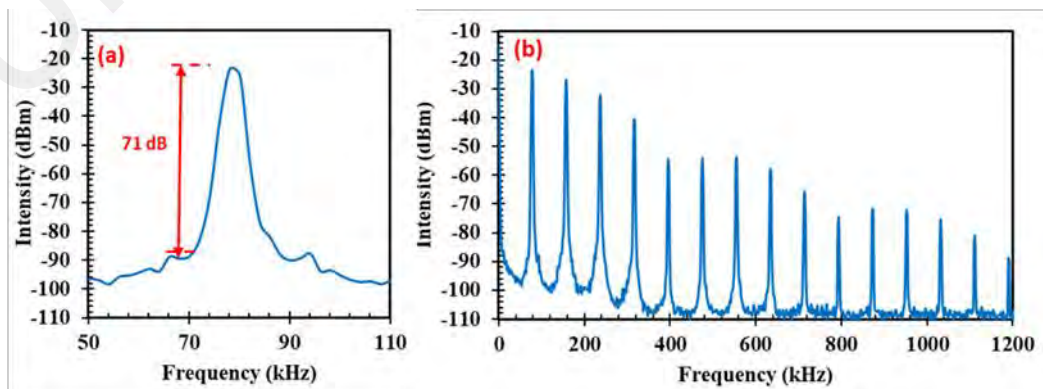


Figure 6.5. (a) Radio frequency spectrum of the Q-switched fiber laser at pump power of 43.3 mW. (b) The broadband RF output spectrum.

The radio frequency (RF) spectrum of the laser at the pump power of 43.3 mW in Figure 6.5 verifies the stability of the Q-switched operation with the lawsone film SA. It registers a good SNR of 71 dB at 80 kHz repetition rate as shown in Figure 6.5 (a). Within a wide frequency span of 1.2 MHz as illustrated in Figure 6.5 (b), there was no additional frequency between the harmonics, which proves its high stability.

6.3 Lawsone Dye Material for Mode-Locking

Beside soliton pulses, stretched pulses mode-locked states is also interesting and important. Dispersion plays a critical role when ultrafast pulses propagate within optical fibers for realizing stretched-pulse fiber lasers. By alternating normal and anomalous group velocity dispersion (GVD) in the cavity, pulses periodically experience stretching and compression. Compared with mode-locked soliton pulses, wider spectrum bandwidths and thus shorter pulse durations can be realized. These stretched-pulse fiber lasers with high output pulse energy have a wide range of applications in the areas of optical amplification, optical frequency doubling and spectroscopy. Previously, Sotor et. al. reported the generation of stretched pulse operating at 1565 nm using a topological insulator as a SA (Sotor, Sobon, & Abramski, 2014). In another work, they also demonstrated sub-90 fs stretched-pulse from a mode-locked EDFL by deploying a graphene SA (Sotor, Pasternak, Krajewska, Strupinski, & Sobon, 2015). In this section, a stretched-pulse fiber laser by using a lawsone SA for the first time.

In this experiment, a tiny piece of lawsone PVA film was sandwiched between two fiber ferrules and incorporate into the fiber laser cavity as depicted in Figure 6.6. A 2.4 m long piece of EDF (with erbium ions concentration of 1500 ppm, numerical aperture of 0.20 and core diameter of 4 μ m) was used as an active fiber. The fiber was forward pumped by a 980 nm laser diode via a fused 980/1550 nm WDM. The optical isolator was used to force unidirectional light propagation inside the ring cavity while the output

laser was coupled out using a 50:50 output coupler. The laser cavity was designed in the near-zero dispersion regime. The laser cavity consisted of two types of normal dispersion fibers: 2.4 m EDF with group velocity dispersion (GVD) of $48.5 \text{ ps}^2/\text{km}$ and 1.5 m WDM fiber with GVD of $27.6 \text{ ps}^2/\text{km}$. The rest of the cavity was a single mode fiber with anomalous dispersion of $-21.7 \text{ ps}^2/\text{km}$. The total bet group delay dispersion is approximately -0.971 ps^2 . It is worthy to note that all components used in the resonator were polarization insensitive. Hence, the mode-locking mechanism based only on saturable absorption of lawsone material. The performance of the mode-locked laser was monitored by using an OSA, digital oscilloscope coupled with 2GHz photodetector, 7.8 GHz RF spectrum and optical autocorrelator.

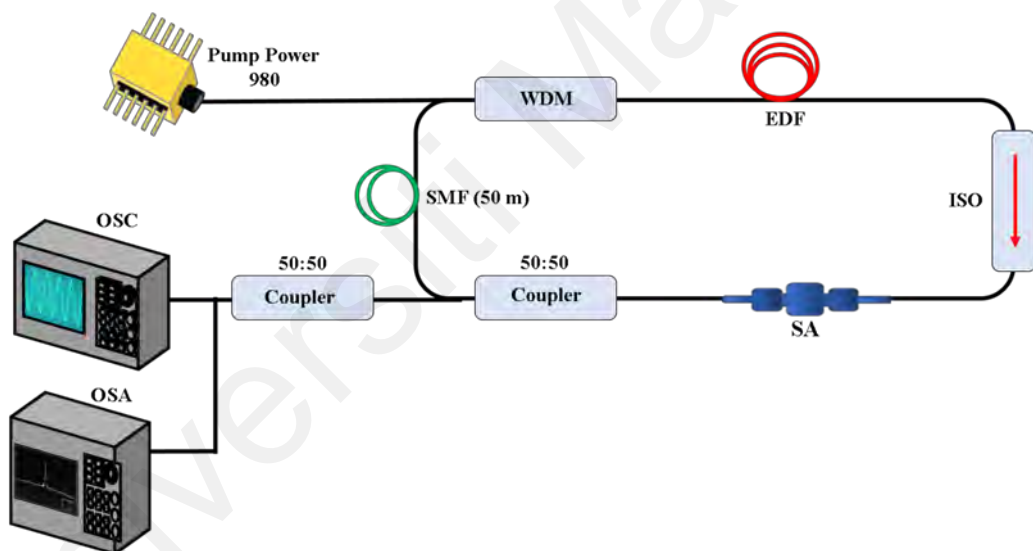


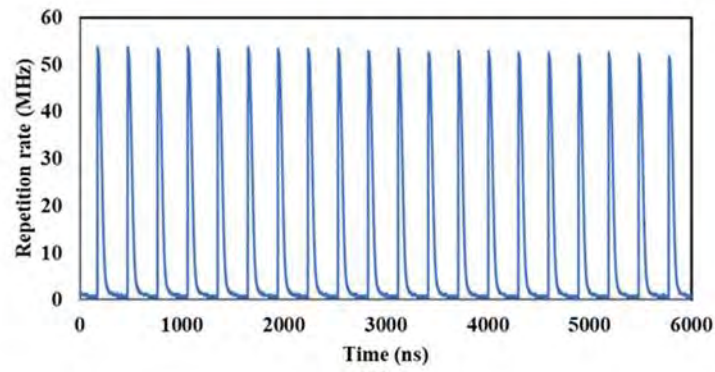
Figure 6.6. Experimental configuration of mode-locked EDFL with lawsone film SA.

The mode-locking performance was investigated by varying the input pump power. In the beginning, a continuous wave (CW) was produced when the input power of LD is 20.0 mW. To obtain the mode-locked operation the resonator was pumped above the threshold. The pulse operation in mode-locked regime was observed when the pump power reached the 33.6 mW threshold. Stable mode-locked operation with a fixed repetition rate of 3.4 MHz is was observed for the pumping powers ranging from 33.6 mW to 43.3 mW. Figure 6.7 (a) shows a stable and uniform pulse train with an interval

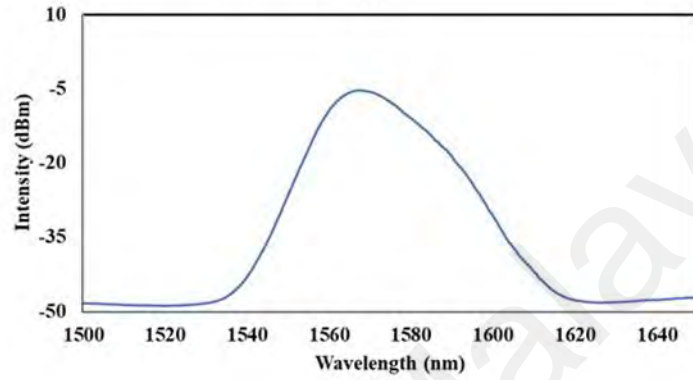
of 294.1 ns, which corresponded to repetition rate of 3.4 MHz. The optical spectrum of the generated pulses measured with the 0.1 nm resolution at the 43.3 mW pump power is depicted in Figure 6.7 (b). The pulses were centered at 1567.5 nm with the full-width half maximum (FWHM) of 16 nm. The broad spectral bandwidth can be attributed to high net dispersion of the cavity along with minimal nonlinearity (Sathiyar, Velmurugan, Senthilnathan, Babu, & Sivabalan, 2016).

Figure 6.7 (c) presents the measured autocorrelation trace which indicates the stretched-pulse width of 1.47 ps. Therefore, the time-bandwidth product is 2.87, implying that the output pulse is chirped. To attain pulses with theoretically limited TBP, a compressor needs to be used in the cavity because the higher order dispersion components need to be managed. Figure 6.7 (d) shows the wide span RF spectrum at pump power of 43.3 mW. The SNR of the fundamental frequency is measured to be more than 70 dB, indicating stable stretched-pulse mode locking operation. By further slightly increasing the pump power above 43.3 mW, we observe that the mode locking state becomes unstable and the fluctuation waveform of single-pulse train is obvious. This kind of multi-pulsing instability attributes to excessive non-linear phase induced by SA in the mode-locked laser cavity.

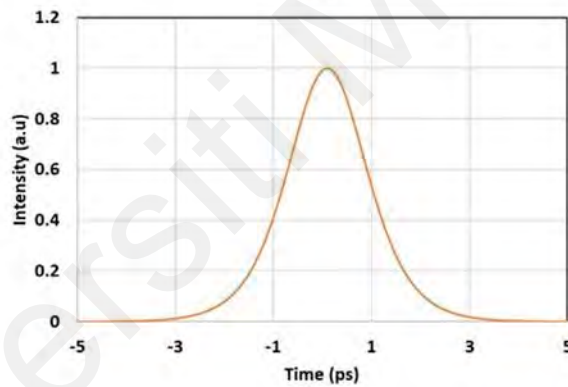
Figure 6.8 displays the variation of average output power and pulse energy from the 50% output port with the injected pump power. Obviously, both output power and pulse energy are almost linear function as the incident power. The largest output average power of 5.21 mW and pulse energy of 1.54 nJ are obtained the maximum pump power of 43.3 mW. If the experimental conditions are kept unaltered, the stretched-pulse fiber laser can work stably for several days continuously.



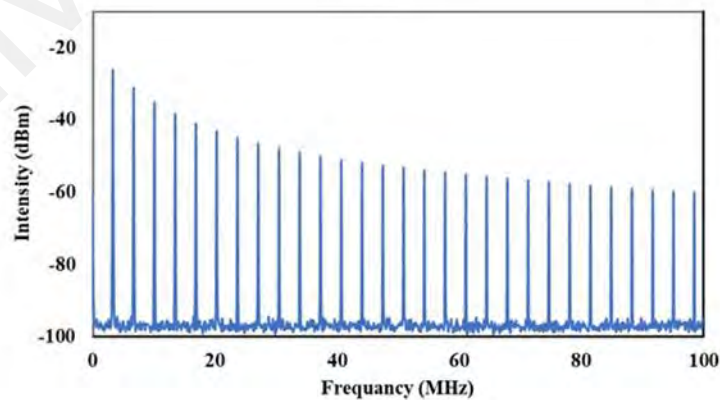
(a)



(b)



(c)



(d)

Figure 6.7. Stretched-pulse operation characteristics at 43.3 mW pump power. (a) Measured oscilloscope trace with a repetition rate of 3.4 MHz. (b) Output spectrum centered at 1567.5 nm. (c) Autocorrelation trace obtained by 50% output ratio. (d) Measured RF spectrum profile.

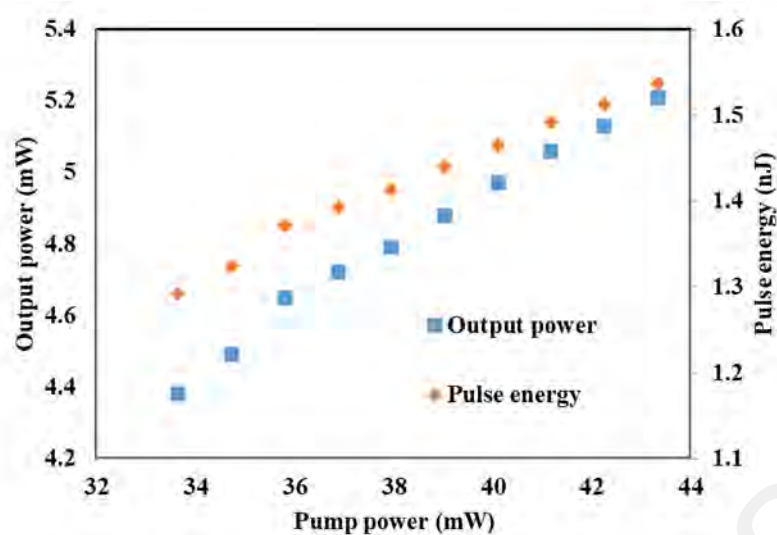


Figure 6.8. The linear variation of average output power and pulse energy versus injected pump power.

6.4 Summary

In Q-switched and mode-locked EDFLs have been successfully demonstrated using an organic SA based on lawsone PVA thin film, which was obtained by embedding the lawsone material into PVA. At first, the prepared lawsone film was incorporated into an EDFL cavity for generating a passively Q-switched EDFL. The stable range of Q-switched operation is observed from 26 to 43.3 mW pump power, at the center wavelength of 1564 nm and the repetition rate of 70-80 kHz. The highest pulse energy and shortest pulse width are obtained to be 53.7 nJ and 1.7 μ s, respectively. By adding 50 m long SMF into the EDFL cavity, a stretched-pulse mode-locked laser was also realized. The mode-locked laser operated at wavelength of 1567.5 nm within a pump power range from 33.6 mW to 43.3 mW. It produced a stable pulse train with a fixed repetition rate of 3.4 MHz and pulse width of 1.47 ps. At 43.3 mW pump power, the laser generated average output power of 5.21 mW and pulse energy of 1.54 nJ. These results experimentally indicate that lawsone SA is feasible to form microsecond Q-switched and picosecond mode-locked pulses in EDFL cavity operating at 1.5-micron region.

CHAPTER 7: CONCLUSION AND FUTURE WORK

7.1 Conclusion

Fiber laser technology is attracting a great deal of interest due to its applications in various fields including telecommunications, micromachining, biology or medical sciences and its potential as a substitute for solid-state lasers. Fiber lasers have the advantages of compactness, cost-effective, alignment-free, reliability and maintenance-free. Pulsed lasers have been thoroughly investigated and extensively used for various applications. They can be produced by either active or passive techniques, but passive approach based on saturable absorbers (SAs) are preferable due to their simplicity of design, low cost, compactness, and flexibility. The SAs act as an optical switch that provides an intensity-dependent transmission without the implementation of expensive and complicated external modulators. Up to date, various types of saturated absorbing materials have been used and they include semiconductor saturable absorber mirrors (SESAMs), nanomaterials such as carbon nanotubes (CNTs), graphene, topological insulators (TIs), transition metal dichalcogenides (TMDs), black phosphorus, metal oxide and MXene. These materials, however, have many limitations and thus finding a new material to be used as a high-performance SA is of great interest in recent years. It is worth mentioning that very little efforts have been made to investigate the potential of organic materials as SAs. Therefore, this research work aimed to develop new SAs based on organic dye material and demonstrate Q-switched and mode-locked fiber lasers using these SAs. In this thesis, two new organic materials: zinc phthalocyanine (ZnPc) and lawsone dye were successfully employed to fabricate practical SAs. Various passively Q-switched and mode-locked fiber lasers operating in both 1.5 and 1.0 μm regions were also successfully demonstrated by using these newly developed SAs.

Four objectives have been outlined in this research. The first one is to fabricate and characterize new passive SAs based on new organic materials based on ZnPc and lawsone dye. In this work, ZnPc and lawsone dye thin films were successfully developed based on liquid exfoliation technique as described in Chapter 3. The ZnPc based thin film was prepared in three different methods; ZnPc was embedded into, casted onto and spin-coated onto the polyvinyl alcohol (PVA) film and the samples are referred to embedding ZnPc:PVA, casting ZnPc/PVA, and spin-coating ZnPc/PVA, respectively. The lawsone based film was prepared by embedding lawsone material into the PVA film. These thin films were successfully characterized in terms of linear absorption, bandgap, FTIR spectra, SEM image, and nonlinear transmission. It is found that the embedding ZnPc:PVA and lawsone film have a modulation depth of 10% and 12%, respectively and thus suitable for Q-switching and mode-locking applications.

The second objective is to design and optimize Erbium-doped fiber laser (EDFL) cavity to generate Q-switched and mode-locked pulse train in 1.5 μm region using the newly developed ZnPc SA. In chapter 4, Q-switching pulse generation was demonstrated based on three SA fabrication methods of embedding ZnPc:PVA, casting ZnPc/PVA, and spin-coating ZnPc/PVA operating in the 1.5- μm region. Stable and self-starting Q-switched pulse trains centered at 1561.4, 1560.4 and 1559.5 nm were obtained for embedding ZnPc:PVA SA, casting ZnPc/PVA SA, and spin-coating ZnPc/PVA SA respectively. The shortest pulse width and maximum pulse energy were achieved at 3.6 μs and 71 nJ for embedding ZnPc:PVA SA. All the SAs show good Q-switching performance in the 1.5- μm wavelength region. The mode-locking performance of the ZnPc based SA was also successfully investigated in Chapter 4. The soliton mode-locked pulse operation was also successfully realized in another EDFL cavity, which was configured with an additional 100 long SMF in the cavity utilizing a ZnPc SA. A stable mode-locked operation with 1.83ps pulse width is obtained at the pump power of 102.9

mW by integrating the fabricated ZnPc:PVA film as SA inside the ring cavity. The fundamental repetition rate and center wavelength are at 1.826 MHz and 1560 nm, respectively. At the pump power of 335.6 mW, the pulse energy is 2.1 nJ while the maximum peak power is 1.15 kW. These results verified that the second objective was fulfilled.

The third objective is to design and optimize Ytterbium-doped fiber laser (YDFL) cavity to generate Q-switched and mode-locked pulse train in 1.0 μm region using the newly developed ZnPc SA. The Q-switched and mode-locked YDFLs have been successfully demonstrated in Chapter 5. At first, the thin film obtained by embedding the ZnPc into PVA, was inserted into an YDFL cavity to act as a Q-switcher. The Q-switching operation was realized at the center of wavelength of 1036 nm with the minimum pulse width of 2.2 μs , highest repetition rate of 63 kHz and the maximum pulse energy of 91 nJ, respectively. A mode-locked YDFL was also successfully demonstrated using the ZnPc/PVA thin film-based SA. A stable optical pulse train operating at 1034.5 nm wavelength with a 3.3 MHz repetition rate, was achieved within the pump power range from 246 to 277 mW. The highest energy of pulse obtained was 1.36 nJ, at pump power of 277 mW.

The final objective of this research is to demonstrate Q-switched and mode-locked fiber lasers based on the newly developed lawsone dye SA. In Chapter 6, Q-switched and mode-locked EDFLs have been successfully demonstrated using the lawsone PVA thin film as SA. The stable range of Q-switched operation is observed from 26 to 43.3 mW pump power, at the center wavelength of 1564 nm and the repetition rate of 70-80 kHz. The highest pulse energy and shortest pulse width are obtained to be 53.7 nJ and 1.7 μs , respectively. By adding 50 m long SMF into the EDFL cavity, a stretched-pulse mode-locked laser was also realized. The mode-locked laser operated at wavelength of 1567.5

nm within a pump power range from 33.6 mW to 43.3 mW. It produced a stable pulse train with a fixed repetition rate of 3.4 MHz and pulse width of 1.47 ps. At 43.3 mW pump power, the laser generated average output power of 5.21 mW and pulse energy of 1.54 nJ. These results indicate that lawsone SA is feasible to form microsecond Q-switched and picosecond mode-locked pulses in EDFL cavity operating at 1.5-micron region.

The performances of the Q-switched and mode-locked lasers explored in this thesis are summarized in Table 7.1. In summary, the organic ZnPc and Lawsone based SAs were successfully fabricated and characterized. Q-switched fiber lasers were successfully produced with these SAs in both 1.5 and 1.0 μm region. The highest pulse energy of 53.7 nJ was obtained by the employment of Lawsone SA. Mode-locked pulses were also produced with these SAs by a slight modification on the cavity. The Lawsone based mode-locked laser produced the shortest pulse width of 1.47 ps and the highest repetition rate of 3.4 MHz. The results indicate that both ZnPc and Lawsone thin film has a great potential as alternative SA material.

Table 7.1. Comparison of Q-switching and Mode-locking performances

Laser Operation	SA	Wavelength (nm)	Pulse Width	Repetition Rate	SNR (dB)	Pulse Energy (nJ)
Q-Switch	ZnPc	1561.4	3.6 μs	48 kHz	65	71
Mode-lock	ZnPc	1560	1.83 ps	1.8 MHz	58	2.1
Q-Switch	ZnPc	1036	2.2 μs	63 kHz	49	91
Mode-lock	ZnPc	1034	2.6 ps	3.3 MHz	55.7	1.36
Q-Switch	Lawsone	1564	1.7 μs	80 kHz	71	53.7
Mode-lock	Lawsone	1550	1.47 ps	3.4 MHz	71.8	1.5

New material is a promising broadband SA as it showed very comparable performance with other groups of organic material SAs such as P3HT, MEH-PPV, Alq3, and FIrpic reported in terms of the center wavelength, pulse width, repetition rate, pulse energy, and

SNR, see Table 1. Additionally, we did the comparison for this SA to produce mode-locking and Q-switching at 1.5 μm region see table 7.2 and table 7.3 respectively.

Table 7.2. Comparison of different organic group result in QS-EDFL.

	Material	Wavelength Centre (nm)	Pulse Width (μs)	Repetition Rate (kHz)	Pulse Energy (nJ)	SNR (dB)
1	P ₃ HT	1562	3.79	78.63	15.05	49.7
2	MEH-PPV	1564	3.5	78.6	59.54	55.79
3	Alq ₃	1543	2.3	75	38	53
4	Flrpic	1560	3.4	87.4	120	58.3
This work(Lawsone)	New material	1564	1.7	80	30.5	71

Table 7.3. Comparison of different organic group result in ML-EDFL.

	Material	Wavelength Centre (nm)	Pulse Width (Ps)	Repetition Rate (MHz)	Pulse Energy (nJ)	SNR (dB)
1	P ₃ HT	1563	2.62	1.838	1.1	55.23
2	MEH-PPV	1568.5	2.97	1.859	0.8725	55.31
3	Alq ₃	1561.5	1.6	1.8	1.7	41.5
4	Flrpic	1562.57	120,000	3.43	11	38.3
This work(Lawsone)	New material	1550	1.47	3.4	1.5	71.8

7.2 Recommendation for future work

All the proposed objectives have been successfully implemented. However, the demonstration of these organic materials in generating Q-switching and mode-locking pulses can be further explored. Further work should be devoted to enhancing the performance of the proposed fiber laser in terms of shorting the pulse width, increasing the repetition rate, output power and pulse energy. This can be achieved by addressing a shorter cavity length, enhanced cavity gain and improved nonlinear characteristic of the SA. Additionally, a future work should also focus on exploring the developed SAs in other wavelength regions such as 2 μm and 3.0 μm using Thulium-doped fiber (TDF) and ZBLAN EDF, respectively, as the gain medium. Q-switched and mode-locked fiber laser operating in 3.0 μm region will be a very interesting area to investigate. As to the best of

our knowledge, there is no research work have been carried out so far addressing the organic materials-based SA in this wavelength region. On the other hand, developing new set of organic material for fiber laser application will be interesting research as well. As through this research work, we found that these materials have very attractive performance in fiber laser technology.

Universiti Malaya

REFERENCES

- Abdullah, O. G., Aziz, S. B., Omer, K. M., & Salih, Y. M. (2015). Reducing the optical band gap of polyvinyl alcohol (PVA) based nanocomposite. *Journal of Materials Science: Materials in Electronics*, 26(7), 5303-5309.
- Acikbas, Y., Erdogan, M., Capan, R., Ozkaya, C., Baygu, Y., Kabay, N., & Gök, Y. (2021). Preparation of Zinc (II) phthalocyanine-based LB thin film: Experimental characterization, the determination of some optical properties and the investigation of the optical sensing ability. *Optik*, 167661.
- Agrawal, G. (2007). Nonlinear fiber optics and its applications in optical signal processing. *Institute of Optics, University of Rochester, Rocheste, NY, United States*.
- Agrawal, G. P. (2000). Nonlinear fiber optics. In *Nonlinear Science at the Dawn of the 21st Century* (pp. 195-211): Springer.
- Agrawal, G. P. (2007). *Self-phase modulation in optical fiber communications: good or bad?* Paper presented at the 2007 Quantum Electronics and Laser Science Conference.
- Agrawal, G. P., & Dutta, N. K. (1986). Long wavelength semiconductor lasers.
- Ahmad, H., Lee, C., Ismail, M., Ali, Z., Reduan, S., Ruslan, N., . . . Harun, S. W. (2016). Zinc oxide (ZnO) nanoparticles as saturable absorber in passively Q-switched fiber laser. *Optics Communications*, 381, 72-76.
- Ahmad, H. B., Ismail, N. N., Aidit, S. N., Bayang, L., & Yusoff, N. (2020). Q-switched tunable ytterbium-doped fiber laser with molybdenum ditelluride-based saturable absorber. *Optical Engineering*, 59(5), 056110.
- Ahmed, M. H. M., Al-Masoodi, A. H. H., Latiff, A. A., Arof, H., & Harun, S. W. (2017). Mechanically exfoliated 2D nanomaterials as saturable absorber for Q-switched erbium doped fiber laser. *Indian Journal of Physics*, 91(10), 1259-1264.
- Al-Masoodi, A. H., Abdulghafoor, O. B., Alani, I., Ahmed, M., Al Masoodi, A. H., & Harun, S. (2020). Passively Q-switched pulses from ytterbium-doped fiber laser (YDFL) using copper oxide (CuO) nanoparticles as a saturable absorber. *Optical Materials Express*, 10(11), 2896-2908.
- Al-Masoodi, A. H., Ahmad, F., Ahmed, M. H., Arof, H., & Harun, S. W. (2017). Q-switched ytterbium-doped fiber laser with topological insulator-based saturable absorber. *Optical Engineering*, 56(5), 056103.
- Al-Masoodi, A. H. H., Ahmed, M. H. M., Latiff, A. A., Azzuhri, S. R., Arof, H., & Harun, S. W. (2017). Passively mode-locked ytterbium-doped fiber laser operation with few layer MoS₂ PVA saturable absorber. *Optik*, 145, 543-548.

- Alani, I., Ahmad, B. A., Ahmed, M., Latiff, A., Al-Masoodi, A., Lokman, M., & Harun, S. (2019). Nanosecond mode-locked erbium doped fiber laser based on zinc oxide thin film saturable absorber. *Indian Journal of Physics*, 93(1), 93-99.
- Alhazime, A. A., Barakat, M. M. M., Benthami, K., & Nouh, S. A. (2021). Gamma irradiation-induced modifications in the structural, thermal, and optical properties of polyvinyl alcohol-polyethylene glycol/cobalt oxide nanocomposite films. *Journal of Vinyl and Additive Technology*, 27(2), 347-355.
- Alhosseini, S. N., Moztaarzadeh, F., Mozafari, M., Asgari, S., Dodel, M., Samadikuchaksaraei, A., . . . Jalali, N. (2012). Synthesis and characterization of electrospun polyvinyl alcohol nanofibrous scaffolds modified by blending with chitosan for neural tissue engineering. *International journal of nanomedicine*, 7, 25.
- Ares, P., Aguilar-Galindo, F., Rodríguez-San-Miguel, D., Aldave, D. A., Díaz-Tendero, S., Alcami, M., . . . Zamora, F. (2016). Mechanical isolation of highly stable antimonene under ambient conditions. *Advanced Materials*, 28(30), 6332-6336.
- Armenta-Villegas, L., Perez-Martinez, A. L., Navarro, R. E., & Ogawa, T. (2009). Synthesis, characterization and some optical properties of poly (hexa-2, 4-diyne-1, 6-dioxy) dinaphthoates containing polar azo dye. *Designed Monomers and Polymers*, 12(6), 533-541.
- Aziz, S. B., Rasheed, M. A., Saeed, S. R., & Abdullah, O. G. (2017). Synthesis and characterization of CdS nanoparticles grown in a polymer solution using in-situ chemical reduction technique. *Int. J. Electrochem. Sci*, 12(4), 3263-3274.
- Bao, Q., Zhang, H., Wang, Y., Ni, Z., Yan, Y., Shen, Z. X., . . . Tang, D. Y. (2009). Atomic-layer graphene as a saturable absorber for ultrafast pulsed lasers. *Advanced Functional Materials*, 19(19), 3077-3083.
- Barua, P., Sekiya, E., Saito, K., & Ikushima, A. (2008). Influences of Yb³⁺ ion concentration on the spectroscopic properties of silica glass. *Journal of non-crystalline solids*, 354(42-44), 4760-4764.
- Beristain, M. F., Nakamura, M., Nagai, K., & Ogaw, T. (2009). Synthesis and characterization of poly [propargyl (3-methoxy-4-propargyloxy) cinnamate]: a polymer from a natural product. *Designed Monomers and Polymers*, 12(3), 257-263.
- Bhuiyan, M. R., Islam, A., Ali, A., & Islam, M. N. (2017). Color and chemical constitution of natural dye henna (*Lawsonia inermis* L) and its application in the coloration of textiles. *Journal of Cleaner Production*, 167, 14-22.
- Bogachkov, I. V., & Gorlov, N. I. (2016). *Joint testing of optical pulse reflectometers of various types for early diagnostics and detection of "problem" sections in optical fibers*. Paper presented at the 2016 13th International Scientific-Technical Conference on Actual Problems of Electronics Instrument Engineering (APEIE).

- Bonaccorso, F., & Sun, Z. (2014). Solution processing of graphene, topological insulators and other 2d crystals for ultrafast photonics. *Optical Materials Express*, 4(1), 63-78.
- Borade, A. S., Kale, B. N., & Shete, R. V. (2011). A phytopharmacological review on *Lawsonia inermis* (Linn.). *Int J Pharm Life Sci*, 2(1), 536-541.
- Borovkov, N. Y., Odintsova, E., Petrenko, V., & Kolker, A. (2019). Amine-assisted solubilization of unsubstituted zinc phthalocyanine for film deposition purposes. *RSC Advances*, 9(58), 33969-33975.
- Busser, B., Moncayo, S., Coll, J.-L., Sancey, L., & Motto-Ros, V. (2018). Elemental imaging using laser-induced breakdown spectroscopy: A new and promising approach for biological and medical applications. *Coordination Chemistry Reviews*, 358, 70-79.
- Chandrakalavathi, T., Sudha, V., Sindhuja, M., Harinipriya, S., & Jeyalakshmi, R. (2018). Photosonoelectrochemical analysis of *Lawsonia inermis* (henna) and artificial dye used in tattoo and dye industry. *Journal of Photochemistry and Photobiology A: Chemistry*, 360, 44-57.
- Chaudhary, G., Goyal, S., & Poonia, P. (2010). *Lawsonia inermis* Linnaeus: a phytopharmacological review. *International journal of pharmaceutical sciences and drug research*, 2(2), 91-98.
- Chen, B., Zhang, X., Wu, K., Wang, H., Wang, J., & Chen, J. (2015). Q-switched fiber laser based on transition metal dichalcogenides MoS₂, MoSe₂, WS₂, and WSe₂. *Optics express*, 23(20), 26723-26737.
- Chen, Q., Yang, S., Dong, L., Cai, S., Xu, J., & Xu, Z. (2020). Tetraalkyl-substituted zinc phthalocyanines used as anode buffer layers for organic light-emitting diodes. *Chinese Physics B*, 29(1), 017302.
- Chen, Y., Jiang, G., Chen, S., Guo, Z., Yu, X., Zhao, C., . . . Tang, D. (2015). Mechanically exfoliated black phosphorus as a new saturable absorber for both Q-switching and mode-locking laser operation. *Optics express*, 23(10), 12823-12833.
- Chen, Y., Zhao, C., Huang, H., Chen, S., Tang, P., Wang, Z., . . . Tang, D. (2013). Self-assembled topological insulator: Bi₂Se₃ membrane as a passive Q-switcher in an Erbium-doped fiber laser. *Journal of Lightwave Technology*, 31(17), 2857-2863.
- Chernysheva, M., Bednyakova, A., Al Araimi, M., Howe, R. C., Hu, G., Hasan, T., . . . Rozhin, A. (2017). Double-wall carbon nanotube hybrid mode-locker in tm-doped fibre laser: A novel mechanism for robust bound-state solitons generation. *Scientific reports*, 7(1), 1-11.
- Chomean, S., Nantabut, M., Kongtia, W., Saenguthai, K., & Kaset, C. (2019). Evaluation of natural dyes for human spermatozoa morphology assessment. *Acta histochemica*, 121(2), 227-233.

- Chowdhury, S. D., Manna, S., Chatterjee, S., Sen, R., & Pal, M. (2019). Mega-Hertz repetition rate broadband nano-second pulses from an actively mode-locked Yb-fiber laser. *Laser physics*, 29(3), 035102.
- Dananjaya, S., Edussuriya, M., & Dissanayake, A. (2012). Inhibition action of lawsone on the corrosion of mild steel in acidic media. *The Online Journal of Science and Technology*, 2(2), 32-36.
- Davidson, A. (1982). The effect of the metal atom on the absorption spectra of phthalocyanine films. *The Journal of chemical physics*, 77(1), 168-172.
- Diament, P. (1990). *Wave transmission and fiber optics*: Macmillan.
- Ding, J., Liu, J., Wei, X., & Xu, J. (2017). *The SMAT fiber laser for industrial applications*. Paper presented at the Components and Packaging for Laser Systems III.
- Ding, P., Mitryukovskiy, S., Houard, A., Oliva, E., Couairon, A., Mysyrowicz, A., & Liu, Y. (2014). Backward Lasing of Air plasma pumped by Circularly polarized femtosecond pulses for the sake of remote sensing (BLACK). *Optics express*, 22(24), 29964-29977.
- Doran, N., & Wood, D. (1988). Nonlinear-optical loop mirror. *Optics letters*, 13(1), 56-58.
- Dragic, P. D., Cavillon, M., & Ballato, J. (2018). Materials for optical fiber lasers: A review. *Applied Physics Reviews*, 5(4), 041301.
- Du, J., Zhang, M., Guo, Z., Chen, J., Zhu, X., Hu, G., . . . Zhang, H. (2017). Phosphorene quantum dot saturable absorbers for ultrafast fiber lasers. *Scientific reports*, 7(1), 1-10.
- Durteste, Y., Monerie, M., Allain, J., & Poignant, H. (1991). Amplification and lasing at 1.3 μm in praseodymium-doped fluorozirconate fibres. *Electronics Letters*, 27(8), 626-628.
- Elashmawi, I., Hakeem, N., & Selim, M. S. (2009). Optimization and spectroscopic studies of CdS/poly (vinyl alcohol) nanocomposites. *Materials Chemistry and Physics*, 115(1), 132-135.
- Fahad, M., Farooq, Z., Abrar, M., Shah, K. H., Iqbal, T., & Saeed, S. (2018). Elemental analysis of limestone by laser-induced breakdown spectroscopy, scanning electron microscopy coupled with energy dispersive x-ray spectroscopy and electron probe microanalysis. *Laser physics*, 28(12), 125701.
- Farries, M. C., Morkel, P. R., & Townsend, J. E. (1990). *The properties of the samarium fibre laser*. Paper presented at the Fiber Laser Sources and Amplifiers.
- Feldman, D. (2008). Polymer history. *Designed Monomers and Polymers*, 11(1), 1-15.
- García, T., Carreón-Castro, M. d. P., Gelover-Santiago, A., Ponce, P., Romero, M., & Rivera, E. (2012). Synthesis and characterization of novel amphiphilic azo-

- polymers bearing well-defined oligo (ethylene glycol) spacers. *Designed Monomers and Polymers*, 15(2), 159-174.
- Gounden, D., Nombona, N., & van Zyl, W. E. (2020). Recent advances in phthalocyanines for chemical sensor, non-linear optics (NLO) and energy storage applications. *Coordination Chemistry Reviews*, 420, 213359.
- Grelu, P., & Akhmediev, N. (2012). Dissipative solitons for mode-locked lasers. *Nature photonics*, 6(2), 84-92.
- Guo, B., Wang, S.-H., Wu, Z.-X., Wang, Z.-X., Wang, D.-H., Huang, H., . . . Zhang, H. (2018). Sub-200 fs soliton mode-locked fiber laser based on bismuthene saturable absorber. *Optics express*, 26(18), 22750-22760.
- Hamam, K. J., & Alomari, M. I. (2017). A study of the optical band gap of zinc phthalocyanine nanoparticles using UV–Vis spectroscopy and DFT function. *Applied Nanoscience*, 7(5), 261-268.
- Hirschowitz, B. I. (1961). Flexible light transmitting tube. In: Google Patents.
- Hocquet, S., Neauport, J., & Bonod, N. (2011). The role of electric field polarization of the incident laser beam in the short pulse damage mechanism of pulse compression gratings. *Applied Physics Letters*, 99(6), 061101.
- Huang, B., Yi, J., Jiang, G., Miao, L., Hu, W., Zhao, C., & Wen, S. (2017). Passively Q-switched vectorial fiber laser modulated by hybrid organic– inorganic perovskites. *Optical Materials Express*, 7(4), 1220-1227.
- Hussein, M. T., & Kadhim, M. J. H. (2019). *Spectroscopic and structural properties of Zinc-Phthalocyanine prepared by pulsed laser deposition*. Paper presented at the Journal of Physics: Conference Series.
- Ippen, E. P. (1994). Principles of passive mode locking. *Applied Physics B*, 58(3), 159-170.
- Islam, Z. U., Tahir, M., Syed, W. A., Aziz, F., Wahab, F., Said, S. M., . . . Sabri, M. F. M. (2020). Fabrication and photovoltaic properties of organic solar cell based on zinc phthalocyanine. *Energies*, 13(4), 962.
- Jain, V., Shah, D., Sonani, N., Dhakara, S., & Patel, N. (2010). Pharmacognostical and preliminary phytochemical investigation of Lawsonia inermis L. leaf. *Romanian J Biol-Plant Biol*, 55, 127-133.
- Jeong, Y. e., Sahu, J., Payne, D. a., & Nilsson, J. (2004). Ytterbium-doped large-core fiber laser with 1.36 kW continuous-wave output power. *Optics express*, 12(25), 6088-6092.
- Jiang, Y., Liu, Y.-Y., Liu, X., Lin, H., Gao, K., Lai, W.-Y., & Huang, W. (2020). Organic solid-state lasers: a materials view and future development. *Chemical Society Reviews*, 49(16), 5885-5944.

- Kataura, H., Kumazawa, Y., Maniwa, Y., Umezu, I., Suzuki, S., Ohtsuka, Y., & Achiba, Y. (1999). Optical properties of single-wall carbon nanotubes. *Synthetic metals*, 103(1-3), 2555-2558.
- Kelleher, E., Travers, J., Sun, Z., Ferrari, A., Golant, K., Popov, S., & Taylor, J. (2010). Bismuth fiber integrated laser mode-locked by carbon nanotubes. *Laser Physics Letters*, 7(11), 790.
- Keller, U., Weingarten, K. J., Kartner, F. X., Kopf, D., Braun, B., Jung, I. D., . . . Der Au, J. A. (1996). Semiconductor saturable absorber mirrors (SESAM's) for femtosecond to nanosecond pulse generation in solid-state lasers. *IEEE Journal of Selected Topics in Quantum Electronics*, 2(3), 435-453.
- Koester, C. J., & Snitzer, E. (1964). Amplification in a fiber laser. *Applied optics*, 3(10), 1182-1186.
- Koseva, N. S., Novakov, C. P., Rydz, J., Kurcok, P., & Kowalczyk, M. (2010). Synthesis of aPHB-PEG brush co-polymers through ATRP in a macroinitiator-macromonomer feed system and their characterization. *Designed Monomers and Polymers*, 13(6), 579-595.
- Kozlik, M., Paulke, S., Gruenewald, M., Forker, R., & Fritz, T. (2012). Determination of the optical constants of α - and β -zinc (II)-phthalocyanine films. *Organic Electronics*, 13(12), 3291-3295.
- Kruchinin, V., Klyamer, D., Spesivtsev, E., Rykhlytskii, S., & Basova, T. (2018). Optical Properties of Thin Films of Zinc Phthalocyanines Determined by Spectroscopic Ellipsometry. *Optics and Spectroscopy*, 125(6), 1019-1024.
- Kuzyniak, W., Schmidt, J., Glac, W., Berkholz, J., Steinemann, G., Hoffmann, B., . . . Nitzsche, B. (2017). Novel zinc phthalocyanine as a promising photosensitizer for photodynamic treatment of esophageal cancer. *International journal of oncology*, 50(3), 953-963.
- Li, D., Castillo, A. E. D. R., Jussila, H., Ye, G., Ren, Z., Bai, J., . . . Bonaccorso, F. (2016). Black phosphorus polycarbonate polymer composite for pulsed fibre lasers. *Applied Materials Today*, 4, 17-23.
- Li, H., Xia, H., Lan, C., Li, C., Zhang, X., Li, J., & Liu, Y. (2014). Passively Q-switched erbium-doped fiber laser based on few-layer MoS₂ saturable absorber. *IEEE Photonics Technology Letters*, 27(1), 69-72.
- Li, J., Luo, H., He, Y., Liu, Y., Zhang, L., Zhou, K., . . . Turistyn, S. (2014). Semiconductor saturable absorber mirror passively Q-switched 2.97 μ m fluoride fiber laser. *Laser Physics Letters*, 11(6), 065102.
- Li, Q., Wei, C., Chi, H., Zhou, L., Zhang, H., Huang, H., & Liu, Y. (2019). Au nanocages saturable absorber for 3- μ m mid-infrared pulsed fiber laser with a wide wavelength tuning range. *Optics express*, 27(21), 30350-30359.
- Li, W., Yu, A., Higgins, D. C., Llanos, B. G., & Chen, Z. (2010). Biologically inspired highly durable iron phthalocyanine catalysts for oxygen reduction reaction in

polymer electrolyte membrane fuel cells. *Journal of the American Chemical Society*, 132(48), 17056-17058.

- Li, X., Peng, X.-H., Zheng, B.-D., Tang, J., Zhao, Y., Zheng, B.-Y., . . . Huang, J.-D. (2018). New application of phthalocyanine molecules: from photodynamic therapy to photothermal therapy by means of structural regulation rather than formation of aggregates. *Chemical science*, 9(8), 2098-2104.
- Liu, W., Liu, M., Liu, X., Wang, X., Deng, H. X., Lei, M., . . . Wei, Z. (2020). 2D Materials for Fiber Lasers: Recent Advances of 2D Materials in Nonlinear Photonics and Fiber Lasers (Advanced Optical Materials 8/2020). *Advanced Optical Materials*, 8(8), 2070031.
- Liu, W., Liu, M., OuYang, Y., Hou, H., Lei, M., & Wei, Z. (2018). CVD-grown MoSe₂ with high modulation depth for ultrafast mode-locked erbium-doped fiber laser. *Nanotechnology*, 29(39), 394002.
- Liu, Z., Zhang, Z. F., Tam, H.-Y., & Tao, X. (2019). *Multifunctional smart optical fibers: Materials, fabrication, and sensing applications*. Paper presented at the Photonics.
- Louazri, L., Amine, A., Bouzzine, S., Hamidi, M., & Bouachrine, M. (2016). Photovoltaic properties of Zn-complexed-phthalocyanine and derivatives for DSSCs application. *J. Mater. Environ. Sci.*, 7, 2305-2313.
- Luo, Z., Huang, Y., Weng, J., Cheng, H., Lin, Z., Xu, B., . . . Xu, H. (2013). 1.06 μm Q-switched ytterbium-doped fiber laser using few-layer topological insulator Bi₂Se₃ as a saturable absorber. *Optics express*, 21(24), 29516-29522.
- Luo, Z., Huang, Y., Zhong, M., Li, Y., Wu, J., Xu, B., . . . Weng, J. (2014). 1-, 1.5-, and 2- μm fiber lasers Q-switched by a broadband few-layer MoS₂ saturable absorber. *Journal of Lightwave Technology*, 32(24), 4077-4084.
- Mahkam, M., Kafshboran, H. R., & Nabati, M. (2014). Synthesis and characterization of novel colored polymers based on lawsone natural compound. *Designed Monomers and Polymers*, 17(8), 784-794.
- Mahkam, M., Nabati, M., Latifpour, A., & Aboudi, J. (2014). Synthesis and characterization of new nitrogen-rich polymers as candidates for energetic applications. *Designed Monomers and Polymers*, 17(5), 453-457.
- Maiman, T. (2010). 1960. Stimulated optical radiation in ruby. In *A Century of Nature* (pp. 113-114): University of Chicago Press.
- Makhija, I. K., Dhananjaya, D., Kumar, V. S., Devkar, R., Khamar, D., Manglani, N., & Chandrakar, S. (2011). Lawsonia inermis—from traditional use to scientific assessment. *African journal of pharmaceutical sciences and pharmacy*, 2(1).
- Malinauskas, M., Žukauskas, A., Hasegawa, S., Hayasaki, Y., Mizeikis, V., Buividas, R., & Juodkazis, S. (2016). Ultrafast laser processing of materials: from science to industry. *Light: Science & Applications*, 5(8), e16133-e16133.

- Mao, D., She, X., Du, B., Yang, D., Zhang, W., Song, K., . . . Zhao, J. (2016). Erbium-doped fiber laser passively mode locked with few-layer WSe₂/MoSe₂ nanosheets. *Scientific reports*, 6(1), 1-9.
- Margulis, V. A., & Sizikova, T. (1998). Theoretical study of third-order nonlinear optical response of semiconductor carbon nanotubes. *Physica B: Condensed Matter*, 245(2), 173-189.
- Markom, A., Latiff, A., Muhammad, A., Ahmad, M., Yusoff, Z., Paul, M. C., . . . Harun, S. (2020). Q-switched Zirconia-Yttria-Aluminium-Erbium-doped pulsed fiber laser with a pencil-core of graphene as saturable absorber. *Optoelectronics and Advanced Materials-Rapid Communications*, 14(1-2), 1-5.
- Martinez-Diaz, M. V., de la Torre, G., & Torres, T. (2010). Lighting porphyrins and phthalocyanines for molecular photovoltaics. *Chemical Communications*, 46(38), 7090-7108.
- Matsuo, Y., Ogumi, K., Jeon, I., Wang, H., & Nakagawa, T. (2020). Recent progress in porphyrin-and phthalocyanine-containing perovskite solar cells. *RSC Advances*, 10(54), 32678-32689.
- Maxwell, J. C. (1865). VIII. A dynamical theory of the electromagnetic field. *Philosophical transactions of the Royal Society of London*(155), 459-512.
- McKearney, D., Choua, S., Zhou, W., Ganga-Sah, Y., Ruppert, R., Wytko, J. A., . . . Leznoff, D. B. (2018). Ring-Oxidized Zinc (II) Phthalocyanine Cations: Structure, Spectroscopy, and Decomposition Behavior. *Inorganic chemistry*, 57(16), 9644-9655.
- Mgidlana, S. (2019). Effect of substituents on the photophysical properties and nonlinear optical properties of asymmetrical zinc (II) phthalocyanine when conjugated to semiconductor quantum dots.
- Milam, D. (1998). Review and assessment of measured values of the nonlinear refractive-index coefficient of fused silica. *Applied optics*, 37(3), 546-550.
- Miya, T., Terunuma, Y., Hosaka, T., & Miyashita, T. (1979). Ultimate low-loss single-mode fibre at 1.55 μm . *Electronics Letters*, 15(4), 106-108.
- Mocker, H. W., & Collins, R. (1965). Mode competition and self-locking effects in aq-switched ruby laser. *Applied Physics Letters*, 7(10), 270-273.
- Muhammad, H., & Muhammad, S. (2005). The use of Lawsonia inermis Linn.(henna) in the management of burn wound infections. *African Journal of Biotechnology*, 4(9).
- Nakazawa, M., Yoshida, E., & Kimura, Y. (1991). Low threshold, 290 fs erbium-doped fiber laser with a nonlinear amplifying loop mirror pumped by InGaAsP laser diodes. *Applied Physics Letters*, 59(17), 2073-2075.
- Ngo, N. Q. (2018). *Ultra-fast fiber lasers: principles and applications with MATLAB® models*: CRC Press.

- Niemz, M. H. (2019). Medical applications of lasers. In *Laser-Tissue Interactions* (pp. 153-249): Springer.
- Nizamani, B., Jafry, A. A. A., Khudus, M. A., Memon, F. A., Shuhaimi, A., Kasim, N., . . . Harun, S. W. (2020). Indium tin oxide coated D-shape fiber as saturable absorber for passively Q-switched erbium-doped fiber laser. *Optics & Laser Technology, 124*, 105998.
- Nizamani, B., Salam, S., Jafry, A., Zahir, N., Jurami, N., Khudus, M. A., . . . Harun, S. (2020). Indium tin oxide coated D-shape fiber as a saturable absorber for generating a dark pulse mode-locked laser. *Chinese Physics Letters, 37*(5), 054202.
- Novotny, M., Bulir, J., Bensalah-Ledoux, A., Guy, S., Fitl, P., Vrnata, M., . . . Moine, B. (2014). Optical properties of zinc phthalocyanine thin films prepared by pulsed laser deposition. *Applied Physics A, 117*(1), 377-381.
- Novotný, M., Šebera, J., Bensalah-Ledoux, A., Guy, S., Bulíř, J., Fitl, P., . . . Hubík, P. (2016). The growth of zinc phthalocyanine thin films by pulsed laser deposition. *Journal of Materials Research, 31*(1), 163-172.
- Okamoto, K., & Marcatili, E. (1989). Chromatic dispersion characteristics of fibers with optical Kerr-effect nonlinearity. *Journal of Lightwave Technology, 7*(12), 1988-1994.
- Okhotnikov, O., Grudinin, A., & Pessa, M. (2004). Ultra-fast fibre laser systems based on SESAM technology: new horizons and applications. *New journal of physics, 6*(1), 177.
- Osellame, R., Cerullo, G., & Ramponi, R. (2012). *Femtosecond laser micromachining: photonic and microfluidic devices in transparent materials* (Vol. 123): Springer Science & Business Media.
- Ouedraogo, S., Meunier-Prest, R., Kumar, A., Bayo-Bangoura, M., & Bouvet, M. (2020). Modulating the electrical properties of organic heterojunction devices based on phthalocyanines for ambipolar sensors. *ACS sensors, 5*(6), 1849-1857.
- Pillai, C. (2010). Challenges for natural monomers and polymers: novel design strategies and engineering to develop advanced polymers. *Designed Monomers and Polymers, 13*(2), 87-121.
- Piovella, N., & Volpe, L. (2021). A Review of High-Gain Free-Electron Laser Theory. *Atoms, 9*(2), 28.
- Plamann, K., Aptel, F., Arnold, C., Courjaud, A., Crotti, C., Deloison, F., . . . Legeais, J.-M. (2010). Ultrashort pulse laser surgery of the cornea and the sclera. *Journal of Optics, 12*(8), 084002.
- Popa, D., Sun, Z., Hasan, T., Torrisi, F., Wang, F., & Ferrari, A. C. (2011). Graphene Q-switched, tunable fiber laser. *Applied Physics Letters, 98*(7), 073106.

- Qiao, Y., Wen, L., Wu, B., Ren, J., Chen, D., & Qiu, J. (2008). Preparation and spectroscopic properties of Yb-doped and Yb–Al-codoped high silica glasses. *Materials Chemistry and Physics*, *107*(2-3), 488-491.
- Radnatarov, D., Khripunov, S., Kobtsev, S., Ivanenko, A., & Kukarin, S. (2013). Automatic electronic-controlled mode locking self-start in fibre lasers with non-linear polarisation evolution. *Optics express*, *21*(18), 20626-20631.
- Roy, D., Das, N. M., Shakti, N., & Gupta, P. (2014). Comparative study of optical, structural and electrical properties of zinc phthalocyanine Langmuir–Blodgett thin film on annealing. *RSC Advances*, *4*(80), 42514-42522.
- Rui, X., Zhu, J., Sim, D., Xu, C., Zeng, Y., Hng, H. H., . . . Yan, Q. (2011). Reduced graphene oxide supported highly porous V₂O₅ spheres as a high-power cathode material for lithium ion batteries. *Nanoscale*, *3*(11), 4752-4758.
- Rusdi, M., Latiff, A., Ahmad, M., Rahman, M., Rosol, A., Harun, S., & Ahmad, H. (2019). *Nickel Oxide as a Q-switcher for Short Pulsed Thulium Doped Fiber Laser Generation*. Paper presented at the Journal of Physics: Conference Series.
- Saadaoui, S., Youssef, M. A. B., Karoui, M. B., Gharbi, R., Smecca, E., Strano, V., . . . Puglisi, R. A. (2017). Performance of natural-dye-sensitized solar cells by ZnO nanorod and nanowall enhanced photoelectrodes. *Beilstein journal of nanotechnology*, *8*(1), 287-295.
- Safie, N. E., Ludin, N. A., Su'ait, M. S., Hamid, N. H., Sepeai, S., Ibrahim, M. A., & Teridi, M. A. M. (2015). Preliminary study of natural pigments photochemical properties of curcuma longa l. and lawsonia inermis l. as tio₂ photoelectrode sensitizer. *Malaysian Journal of Analytical Sciences*, *19*(6), 1243-1249.
- Şahin, Z., Meunier-Prest, R., Dumoulin, F., Kumar, A., Isci, Ü., & Bouvet, M. (2021). Tuning of organic heterojunction conductivity by the substituents' electronic effects in phthalocyanines for ambipolar gas sensors. *Sensors and Actuators B: Chemical*, *332*, 129505.
- Salam, S., Al-Masoodi, A., Al-Hiti, A. S., Al-Masoodi, A. H., Wang, P., Wong, W. R., & Harun, S. W. (2019). FIRpic thin film as saturable absorber for passively Q-switched and mode-locked erbium-doped fiber laser. *Optical Fiber Technology*, *50*, 256-262.
- Salam, S., Harun, S. W., Al-Masoodi, A. H., Ahmed, M. H., Al-Masoodi, A. H., Alani, I. A., . . . Yasin, M. (2019). Tris-(8-hydroxyquinoline) aluminium thin film as saturable absorber for passively Q-switched erbium-doped fibre laser. *IET Optoelectronics*, *13*(5), 247-253.
- Salim, M. A. M., Azzuhri, S. R., Khudus, M. A., Razak, M. Z. A., Nasir, N., & Amiri, I. S. (2018). Generation of dual-wavelength ytterbium-doped fibre laser using a highly nonlinear fibre. *Laser physics*, *28*(11), 115107.
- Samanta, A. K., Awwad, N., & Algarni, H. M. (2020). *Chemistry and Technology of Natural and Synthetic Dyes and Pigments: BoD–Books on Demand*.

- Sandoval, H. P., Donnenfeld, E. D., Kohnen, T., Lindstrom, R. L., Potvin, R., Tremblay, D. M., & Solomon, K. D. (2016). Modern laser in situ keratomileusis outcomes. *Journal of Cataract & Refractive Surgery*, 42(8), 1224-1234.
- Sathiyar, S., Velmurugan, V., Senthilnathan, K., Babu, P. R., & Sivabalan, S. (2016). All-normal dispersion passively mode-locked Yb-doped fiber laser using MoS₂-PVA saturable absorber. *Laser physics*, 26(5), 055103.
- Saxena, K. K., Qian, J., & Reynaerts, D. (2020). A tool-based hybrid laser-electrochemical micromachining process: Experimental investigations and synergistic effects. *International Journal of Machine Tools and Manufacture*, 155, 103569.
- Schmidt, A., Rivier, S., Steinmeyer, G., Yim, J. H., Cho, W. B., Lee, S., . . . Aguiló, M. (2008). Passive mode locking of Yb: KLuW using a single-walled carbon nanotube saturable absorber. *Optics letters*, 33(7), 729-731.
- Serres, J. M., Loiko, P., Mateos, X., Yumashev, K., Griebner, U., Petrov, V., . . . Díaz, F. (2015). Tm: KLu (WO 4) 2 microchip laser Q-switched by a graphene-based saturable absorber. *Optics express*, 23(11), 14108-14113.
- Set, S. Y., Yaguchi, H., Tanaka, Y., & Jablonski, M. (2004). Laser mode locking using a saturable absorber incorporating carbon nanotubes. *Journal of Lightwave Technology*, 22(1), 51.
- Shinomoto, R., Ito, Y., Kizaki, T., Tatsukoshi, K., Fukasawa, Y., Nagato, K., . . . Mitsuishi, M. (2016). Experimental analysis of glass drilling with ultrashort pulse lasers. *International Journal of Automation Technology*, 10(6), 863-873.
- Singh, R., Jain, A., Panwar, S., Gupta, D., & Khare, S. (2005). Antimicrobial activity of some natural dyes. *Dyes and pigments*, 66(2), 99-102.
- Snitzer, E., & Woodcock, R. (1966). 9C8-Saturable absorption of color centers in Nd³⁺ and Nd³⁺-Yb³⁺ laser glass. *IEEE Journal of Quantum Electronics*, 2(9), 627-632.
- Soboh, R. S., Al-Masoodi, A. H., Erman, F. N., Al-Masoodi, A. H., Nizamani, B., Arof, H., . . . Harun, S. (2021). Lawson dye material as potential saturable absorber for Q-switched erbium doped fiber laser. *Optical Fiber Technology*, 64, 102537.
- Soboh, R. S., Al-Masoodi, A. H., Erman, F. N., Al-Masoodi, A. H., Yasin, M., & Harun, S. W. (2021). Passively Q-switched Ytterbium-doped fiber laser using zinc phthalocyanine thin film as saturable absorber. *Optik*, 228, 165736.
- Soboh, R. S., Al-Masoodi, A. H. H., Erman, F. N., Al-Masoodi, A. H., Arof, H., Yasin, M., & Harun, S. W. (2020). Zinc phthalocyanine thin film as saturable absorber for Q-switched pulse generation. *Optical Fiber Technology*, 57, 102235.
- Socol, M., Preda, N., Stanculescu, A., Stanculescu, F., & Socol, G. (2017). Heterostructures Based on Porphyrin/Phthalocyanine Thin Films for Organic Device Applications. In *Phthalocyanines and Some Current Applications: IntechOpen*.

- Song, Y., Liang, Z., Jiang, X., Chen, Y., Li, Z., Lu, L., . . . Lu, S. (2017). Few-layer antimonene decorated microfiber: ultra-short pulse generation and all-optical thresholding with enhanced long term stability. *2D Materials*, *4*(4), 045010.
- Sotor, J., Pasternak, I., Krajewska, A., Strupinski, W., & Sobon, G. (2015). Sub-90 fs a stretched-pulse mode-locked fiber laser based on a graphene saturable absorber. *Optics express*, *23*(21), 27503-27508.
- Sotor, J., Sobon, G., & Abramski, K. M. (2014). Sub-130 fs mode-locked Er-doped fiber laser based on topological insulator. *Optics express*, *22*(11), 13244-13249.
- Sotor, J., Sobon, G., Macherzynski, W., Paletko, P., & Abramski, K. M. (2015). Black phosphorus saturable absorber for ultrashort pulse generation. *Applied Physics Letters*, *107*(5), 051108.
- Stetser, D., & DeMaria, A. (1966). Optical spectra of ultrashort optical pulses generated by mode-locked glass: Nd lasers. *Applied Physics Letters*, *9*(3), 118-120.
- Su, Z., Li, N., Frankis, H. C., Magden, E. S., Adam, T. N., Leake, G., . . . Watts, M. R. (2018). High-Q-factor Al₂O₃ micro-trench cavities integrated with silicon nitride waveguides on silicon. *Optics express*, *26*(9), 11161-11170.
- Sun, Z., Hasan, T., Torrisi, F., Popa, D., Privitera, G., Wang, F., . . . Ferrari, A. C. (2010). Graphene mode-locked ultrafast laser. *ACS nano*, *4*(2), 803-810.
- Tian, B., Fernandez-Bravo, A., Najafiaghdam, H., Torquato, N. A., Altoe, M. V. P., Teitelboim, A., . . . Barnard, E. S. (2018). Low irradiance multiphoton imaging with alloyed lanthanide nanocrystals. *Nature communications*, *9*(1), 1-8.
- Tian, X., Luo, H., Wei, R., Zhu, C., Guo, Q., Yang, D., . . . Qiu, J. (2018). An ultrabroadband Mid-infrared pulsed optical switch employing solution-processed bismuth oxyselenide. *Advanced Materials*, *30*(31), 1801021.
- Tran, V., Soklaski, R., Liang, Y., & Yang, L. (2014). Layer-controlled band gap and anisotropic excitons in few-layer black phosphorus. *Physical Review B*, *89*(23), 235319.
- Tritschler, T., Mücke, O., & Wegener, M. (2003). Extreme nonlinear optics of two-level systems. *Physical Review A*, *68*(3), 033404.
- Uehara, H., Tokita, S., Kawanaka, J., Konishi, D., Murakami, M., & Yasuhara, R. (2019). A passively Q-switched compact Er: Lu₂O₃ ceramics laser at 2.8 μm with a graphene saturable absorber. *Applied Physics Express*, *12*(2), 022002.
- Ushenko, Y. A., Koval, G. D., Ushenko, A. G., Dubolazov, O. V., Ushenko, V. A., & Novakovskaia, O. Y. (2016). Mueller-matrix of laser-induced autofluorescence of polycrystalline films of dried peritoneal fluid in diagnostics of endometriosis. *Journal of Biomedical Optics*, *21*(7), 071116.
- Valli, F., Vior, M. C. G., Roguin, L. P., & Marino, J. (2020). Crosstalk between oxidative stress-induced apoptotic and autophagic signaling pathways in Zn (II)

phthalocyanine photodynamic therapy of melanoma. *Free Radical Biology and Medicine*, 152, 743-754.

- Wang, A., Li, C., Zhang, J., Chen, X., Cheng, L., & Zhu, W. (2019). Graphene-oxide-supported covalent organic polymers based on zinc phthalocyanine for efficient optical limiting and hydrogen evolution. *Journal of colloid and interface science*, 556, 159-171.
- Wang, J., Wang, Y., Chen, Z., Yang, X., & Lv, R. (2019). CH₃NH₃PbI₃ perovskite thin films as a saturable absorber for a passively Q-switched Nd: YAG laser. *Journal of Materials Chemistry C*, 7(17), 5047-5050.
- Wang, K., Wang, J., Fan, J., Lotya, M., O'Neill, A., Fox, D., . . . Zhao, Q. (2013). Ultrafast saturable absorption of two-dimensional MoS₂ nanosheets. *ACS nano*, 7(10), 9260-9267.
- Wang, M., Chen, C., Huang, C., & Chen, H. (2014). Passively Q-switched Er-doped fiber laser using a semiconductor saturable absorber mirror. *Optik*, 125(9), 2154-2156.
- Wang, S., Yu, H., Zhang, H., Wang, A., Zhao, M., Chen, Y., . . . Wang, J. (2014). Broadband few-layer MoS₂ saturable absorbers. *Advanced Materials*, 26(21), 3538-3544.
- Weber, M., Lynch, J., Blackburn, D., & Cronin, D. (1983). Dependence of the stimulated emission cross section of Yb³⁺ on host glass composition. *IEEE Journal of Quantum Electronics*, 19(10), 1600-1608.
- Woodward, R., Kelleher, E., Howe, R., Hu, G., Torrisi, F., Hasan, T., . . . Taylor, J. (2014). Tunable Q-switched fiber laser based on saturable edge-state absorption in few-layer molybdenum disulfide (MoS₂). *Optics express*, 22(25), 31113-31122.
- Woodward, R. I., & Kelleher, E. J. (2015). 2D saturable absorbers for fibre lasers. *Applied Sciences*, 5(4), 1440-1456.
- Wu, K., Zhang, X., Wang, J., Li, X., & Chen, J. (2015). WS₂ as a saturable absorber for ultrafast photonic applications of mode-locked and Q-switched lasers. *Optics express*, 23(9), 11453-11461.
- Xia, F., Wang, H., & Jia, Y. (2014). Rediscovering black phosphorus as an anisotropic layered material for optoelectronics and electronics. *Nature communications*, 5(1), 1-6.
- Yang, M., Wang, D., Liu, X., & Feng, Q. (2018). Properties of copper phthalocyanine thin film transistors fabricated in vertical structures. In *Electronic Engineering* (pp. 39-42): CRC Press.
- Yang, S., Sheng, X., Zhao, G., & Li, S. (2019). Simple birefringent terahertz fiber based on elliptical hollow core. *Optical Fiber Technology*, 53, 102064.

- Yao, S., Ren, P., Song, R., Liu, Y., Huang, Q., Dong, J., . . . Zhu, Y. (2020). Nanomaterial-enabled flexible and stretchable sensing systems: processing, integration, and applications. *Advanced Materials*, 32(15), 1902343.
- Ye, Y., Yang, B., Wang, P., Zeng, L., Xi, X., Shi, C., . . . Xu, X. (2021). Industrial 6 kW high-stability single-stage all-fiber laser oscillator based on conventional large mode area ytterbium-doped fiber. *Laser physics*, 31(3), 035104.
- Yi, X., Li, Z., & Liu, Z. (2015). Underwater optical communication performance for laser beam propagation through weak oceanic turbulence. *Applied optics*, 54(6), 1273-1278.
- Yusoff, R., Kasim, N., Jafry, A., Munajat, Y., Harun, S., & Suliman, M. (2019). *Q-Switched dual-wavelength erbium-doped fiber laser using graphene as a saturable absorber*. Paper presented at the Journal of Physics: Conference Series.
- Zhang, B., Liu, J., Wang, C., Yang, K., Lee, C., Zhang, H., & He, J. (2020). Recent progress in 2D material-based saturable absorbers for all solid-state pulsed bulk lasers. *Laser & Photonics Reviews*, 14(2), 1900240.
- Zhang, H., Lu, S., Zheng, J.-l., Du, J., Wen, S., Tang, D., & Loh, K. (2014). Molybdenum disulfide (MoS₂) as a broadband saturable absorber for ultra-fast photonics. *Optics express*, 22(6), 7249-7260.
- Zhang, H., Xia, W., Song, P., Wang, J., & Li, X. (2018). *Theoretical and experimental study of a laser-diode-pumped actively Q-switched Yb: NaY (WO₄)₂ laser with acoustic-optic modulator*. Paper presented at the Young Scientists Forum 2017.
- Zhao, C., Zhang, H., Qi, X., Chen, Y., Wang, Z., Wen, S., & Tang, D. (2012). Ultra-short pulse generation by a topological insulator based saturable absorber. *Applied Physics Letters*, 101(21), 211106.
- Zhou, D.-P., Wei, L., Dong, B., & Liu, W.-K. (2009). Tunable passively Q-switched erbium-doped fiber laser with carbon nanotubes as a saturable absorber. *IEEE Photonics Technology Letters*, 22(1), 9-11.
- Zolotovskaya, S., Savitski, V., Gaponenko, M., Malyarevich, A., Yumashev, K., Demchuk, M., . . . Nejezhleb, K. (2006). Nd: KGd (WO₄)₂ laser at 1.35 μm passively Q-switched with V³⁺: YAG crystal and PbS-doped glass. *Optical Materials*, 28(8-9), 919-924.